Dynamic Analysis of the Tower Crane

Hamid Nalbandian Abhar

DISSERTATION SUBMITTED TO THE FACULTY OF ENGINEERING,

UNIVERSITY OF MALAYA IN PARTIAL FULFILLMENT OF THE

REQUIREMENT FOR THE DEGREE OF MASTER OF MECHANICAL

ENGINEERING

UNIVERSITI MALAYA

ORIGINAL LITERARY WORK DECLARATION

Name of Candidate: **HAMID NALBANDIAN ABHAR** (I.C/Passport No:)

Registration/Matric No: **KGH080022**

Name of Degree: **Master of Engineering**

Title of Project Paper/Research Report/Dissertation/Thesis ("this Work"):

"Dynamic Analysis of the Tower Crane"

Field of Study: Mechanics

I do solemnly and sincerely declare that:

(1)   I am the sole author/writer of this Work;

(2)   This Work is original;

(3)   Any use of any work in which copyright exists was done by way of fair dealing and for permitted purposes and any excerpt or extract from, or reference to or reproduction of any copyright work has been disclosed expressly and sufficiently and the title of the Work and its authorship have been acknowledged in this Work;

(4)   I do not have any actual knowledge nor do I ought reasonably to know that the making of this work constitutes an infringement of any copyright work;

(5)   I hereby assign all and every rights in the copyright to this Work to the University of Malaya ("UM"), who henceforth shall be owner of the copyright in this Work and that any reproduction or use in any form or by any means whatsoever is prohibited without the written consent of UM having been first had and obtained;

(6)   I am fully aware that if in the course of making this Work I have infringed any copyright whether intentionally or otherwise, I may be subject to legal action or any other action as may be determined by UM.

Candidate's Signature   Date

Subscribed and solemnly declared before,

Witness's Signature   Date

Name:
Designation:

This dissertation is dedicated to my father.

ACKNOWLEDGEMENTS

ABSTRACT

Tower cranes are amongst the most important machines used in industrial activities; therefore, understanding the natural frequency of these structures for optimal performance remains an essential field of study.

Vibration, from an origin such as 'Swing of the payload', creates a dynamic load on the tower crane structure which may result in fatigue, weakness and ultimately collapse of the crane. The purpose of this thesis is to identify the dynamic behavior of planar model tower cranes under the pendulum motions of the payload. By doing this, hypotheses will be generated that may aid in improving the performance and safety of the crane.

In this thesis, Pendulation motion equations, after adjusting for cable stiffness along the crane's jib, will be defined based on the Lagrange Equations and solved using the numerical method based on the Runge-Kutta fifth order.

The crane will be modeled and analysed using finite element software (FEM), and the first few natural frequencies of the complex planar model will be compared by analytical methods in order to verify the data. Continued load effects will be determined by the numerical solution of differential equations, and these will be entered into the finite element software for the purpose of analysis. Research results will present any changes in the effect of vibration, such as stress and deformation, when the payload is placed at different positions along the crane's jib and body

ABSTRAK

Kren menara adalah antara mesin yang paling penting yang digunakan dalam aktiviti-aktiviti perindustrian, oleh itu, memahami frekuensi semulajadi struktur ini untuk prestasi optimum kekal sebagai bidang penting dalam kajian.

Getaran, daripada sumber yang seperti 'Swing daripada muatan', mewujudkan beban dinamik pada struktur kren menara yang boleh mengakibatkan keletihan, kelemahan dan akhirnya kejatuhan kren. Tujuan projek ini adalah untuk mengenal pasti tingkah laku yang dinamik satah kren menara model di bawah usul bandul muatan. Dengan cara ini, hipotesis akan dijana yang boleh membantu dalam meningkatkan prestasi dan keselamatan kren.

Dalam tesis ini, persamaan gerakan Pendulation, selepas pelarasan untuk ketegangan kabel sepanjang jib kren, akan ditakrifkan berdasarkan Persamaan Lagrange dan diselesaikan menggunakan kaedah berangka berdasarkan perintah kelima Runge-Kutta.

Kren akan dimodelkan dan dianalisis menggunakan perisian unsur terhingga (FEM), dan yang pertama frekuensi semula jadi beberapa model satah kompleks akan dibandingkan dengan kaedah analisis untuk mengesahkan data. Kesan beban berterusan akan ditentukan oleh penyelesaian berangka persamaan pembezaan, dan ini akan dimasukkan ke dalam perisian unsur terhingga bagi tujuan analisis. Hasil kajian akan membentangkan apa-apa perubahan dalam kesan getaran, seperti tekanan dan ubah bentuk, apabila muatan itu diletakkan pada kedudukan yang berbeza di sepanjang jib kren dan badan

iv

Table of Contents

List of Tables

List of Figures

CHAPTER 1:   INTRODUCTION

1.1. Background of Study

Cranes are useful and frequently used equipment which have a wide, global application. The construction of large and tall structures is impossible without the use of a crane. In most building construction, tower cranes are used to lift and move payloads. Payloads always have a tendency to sway about the vertical position under excitations. This sway results in a payload pendulum motion which leads to vibrations and an unwanted dynamic load on the crane body. In turn, this shortens the life time of the crane. As stress, strain and fatigue are all factors which can damage the structure of a crane, these all need to be fully understood and studied carefully and methodically before a crane is designed.

An in depth understanding of the physical nature of the crane will assist the engineer in re-designing the crane structure where necessary; it will also ensure a safe and stable system.

To date, most of the analysis carried out on cranes has only into account the simple pendulum motion of the payload, whist ignoring cable flexibilities (Kim & Hong, 2009; Oguamanam et al., 2001). In this project a 2-D crane was analyzed whilst taking both the pendulum motion of the payload, the cable flexibility, and wide angle for pendulation into consideration.

1.2. Objective of Study

The study objectives are outlined below:

- Derive the non-simplified Pendulum Equation of motion based on the Lagrange Equation and Rayleigh's dissipation function and solve it numerically based on the Runge-Kutta method.
- Modal analyses the mathematically model of the 2-D tower crane based on the "System linked by two coordinates" approach and find the first four natural frequencies.
- Create and modal analysis of the soft model of tower crane and verification of the modal result with mathematical model, using the obtain data of the equation and run the dynamic response of the crane by Ansys Workbench.

1.3. Scope of Study

To determine the effects of vibrations on a tower crane, using a model of 2-D crane while taking into consideration both the pendulum motion of the payload and the flexibility of the cable. Pendular motion of the payload with an elastic cable causes transverse and longitudinal vibration that has a detrimental effect on the crane (Lahres et al., 2000). The purpose of this study is to show the effects of this vibration on the tower crane body when the payload is attached to different points on the Jib.

1.4. Gap of Knowledge

After reviewing the research into this area, it became evident that several parameters of the tower crane had not been studied simultaneously. Up to know research

into this field has only analyzed the simple pendulum motion of the payload and has ignored cable flexibilities and wide pendulation angle. Because of this gap of knowledge, this study plans to take these factors into consideration.

1.5. Significance of this Study

Up to now, the dynamic analysis of the tower crane is composed of a collection of assumptions that have neglected to investigate certain important aspects, or to combine the research. There are several strengths to this study: the actual dimensions for the crane soft model have been taken into consideration, in addition to the non-rigid cable, wide angle and several attachment points along the jib simultaneously. Further to this, three software combine in order to analysis (Ansys Workbench, MATLAB and AutoCAD) and a mathematical model of the tower crane has been formulated.

CHAPTER 2:   LITERATURE REVIEW

2.1. Introduction

Tower cranes are one of the intricate pieces of machinery constructed and they exhibit complex dynamic behaviours (Neitzel et al., 2001). Their design has to take into account the diverse and varied environmental conditions they may operate in, such as on land or at sea, or in adverse weather conditions with winds up to 36 m/s (Ju & Choo, 2003). The cranes system has been studied theoretically, along with its optimized control factors and non-linear dynamics behaviour. Most of the research to date has limited itself to several assumptions regarding the crane, such as it has a rigid structure or boom, and a simple beam (Kiliçslan et al., 1999).

2.2. Mathematical Model for Pendulum Motion

2.2.1. Lagrange Equations and Pendulum Motions

Lagrange's Equations have been derived from Newton's laws. They are in fact a restatement of Newton's laws written out in term of appropriate variables that allow constraint forces to be eliminated from consideration.(José & Saletan, 1998)

Lagrangian formulation is easier to apply to dynamical system other than the simplest. It brings out the connection between conservation laws and important symmetry properties of dynamical system. The properties of the system that determine the choice are geometric: they are the number of freedoms and the shape, in which the system is free to move.

Since the early nineteen- nineties many methods have been created to control the pendulum motion of the payload. One method, described by Golafshani and Aplevich (2002) to decrease the swing of the load in the tower crane, is the 'Time-Optimal Trajectory' method. This method, when applied to the crane model, had five degrees of freedom and a mathematical model that was based on Lagrange Equations. In this model the tower crane was divided into two parts: the rotating boom with moveable trolley and the suspended load from the trolley. Assumptions for this model included: a rigid crane body; a hook, load and trolley which were considered as point masses, a frictionless model, a weightless and rigid rope and; no air resistance. In addition, to decrease the swing of the load the 'sub-optimal' method was proposed. The results, after solving the equations and taking into account the simulation, gave proof of the efficiency of this method; however it should be noted that the model was theoretical in nature and had never been tested on an actual tower crane.

The degree of pendulation in the crane system is directly affected by the length of the cable. Because of this, adjusting the length of the cable, in order to control the pendulation, and so reduce the vibration of the load, can be used as a solution. This was demonstrated by Abdel-Rahman and Nayfeh (2002). In both, a 2-D and 3-D model, with the assumptions that there was a point mass and rigid cable. 2-D and 3-D models of this pendulum were formed by Euler–Lagrange Equations. After comparison of the pendulation, the weakness of the 2-D model for analyzing and predicting the system was evident. Although this system had no force damping, except for the natural one, it was found that changing the cable length was extremely effective in the manipulation and control of pendulation.

Dynamic load causes vibration in cranes which results in such detrimental side effects as fatigue. Jerman et al. (2004) illustrate this in a study they carried out to examine the slewing motion of a suspended load from the jib. They did this by building an actual model of a crane, and then comparing the results of this model to the acquired results of the mathematical model that was based on the Lagrange Equation of motions. The investigators tested the accelerating and decelerating forces and their effect on the load sway using different input data. In this study the mass of the jib, crab and payload were all considered as a point mass, the rope and mass connection were weightless, and the rope's stiffness, damping and moment of friction were all taken into account. Another factor, air resistance, was also present and acting on the point masses. The mathematical model was validated by measurements of the physical model and results were almost similar. Considering the good initial condition and assumption in the mathematical model caused the similarity at results in compare with the physical model measurements.

Mobile cranes are very important tools in industrial areas because of their versatility and movement ability. Several approaches for controlling the slewing action of the load in tower cranes have been established. Kosiski (2005) suggested a method to control and minimize the sway of the pay load using the slewing motion at the end point in the mobile crane and created a mathematical and physical model to demonstrate this. In addition to this, a hydraulic system was modeled based on the mathematical equations. This consisted of a system for minimizing the tangential component of the payload swing movement vector (SMV) and a system for controlling the angular position of the hydraulic motor drive shaft (SAC), along with a block completed by a proportional integral derivative (PID) controller. This model was effective for controlling swing and luffing motions under maximal permissible velocity movements. The following assumptions were made during the crane mathematical modeling analysis: the crane and boom had a rigid body;

there were six degrees of freedom; rotation of boom crane occurred around the vertical axis only; payload was considered as a mass point and; the rope was both weightless and rigid. In an additional frictionless model without a damping part, linear elastic deflection was also assumed. Experimental and simulation results demonstrated the ability of this design to effectively control the slewing motion of the crane.

One of the biggest human challenges when dealing with load transferring of the tower crane is oscillation of the payload, and how best to manipulate it safely, quickly and accurately. If the mass of the hook is greater than the mass of the payload, then a second mode of these two masses will appear which results in a phenomenon known as double-pendulation (Lacarbonara et al., 2001). To address this issue, a control system with the ability to decrease the effects of double-pendulation was designed (Singhose & Kim, 2007). This method was developed for two modes of frequency only, with the following assumptions: there is no air resistance on the mass point of the hook and load, and; the length of the cable and rigging does not have an influence on the lifting process. In this investigation, as the tower crane body had no effect on what was being studied, it was not included in the model. The final experimental results from the model showed the efficiency of this controller in decreasing the number of collisions.

Terashima et al. (2007). presented a method to control the sway of the load by using 'straight transfer transformation' (STT) (Y. Shen et al., 2003). This method allows the controller to transfer the load in a straight line by changing the rope length and luffing. When using the STT mode as three movements of the crane are combined (rotation, luffing and changing the rope length), the three dimensional movement is converted into a two dimensional one, thereby eliminating the centrifugal force. In addition, this controller has the ability to decrease the transfer time. In this model the crane body and

weightless rope were considered to be rigid structures, and the reaction time of the boom and crane, as well as the friction of the rotary torque, were neglected. The advantages to this are that the calculation of the proposed approach using the STT model is faster and cheaper compared to other similar methods because there are fewer sensors required. Comparison between the simulation and experimental data from this model showed the efficiency and accuracy of this controller when using the STT model.

When double-pendulation does not occur, mobile boom cranes are a good choice. The analysis of double-pendulum in the mobile boom crane has been presented by Fujioka et al. (2009). In this model, the crane consisted of a thin plate which acted as a cart, with four springs and dampers instead of wheels. It contained a boom, a weightless but rigid rope, a frictionless crane body and a simple or double-pendulum attached to the tip of the boom. The investigators considered three stages in their stability analysis: static, semi dynamic and fully dynamic stability, and compared the results from the three stages with each other. In conclusion, the researchers found the semi dynamic analysis to be the most simple and useful method for determining stability in mobile cranes which have double-pendulation effects.

Ahmad (2009) investigated the anti-sway angle system in gantry cranes using a fuzzy logic controller in 2-D space. Gantry cranes consist of simple pendulum attached to the moveable cart. For the purpose of this study MATLAB and Simulink were used to simulate this controller and the Lagrange method was used to derive the Equation of motion. Both the delayed feedback signal system and proportional-derivative type fuzzy logic were used as controllers. The assumptions of this investigation were: the point mass of the cart and payload, weightless and rigid rope, no friction on the sliding of the cart

and no air resistance. The simulation results for this system demonstrated the performance of the controller in terms of sway angle suppression and disturbances cancellation.

2.2.2. Generalised Coordinates

In analytical mechanics especially for dynamics system, a system should be described by parameters; these parameters must be unique and define the configuration of the system, which is called generalized coordinates (Ginsberg, 1998). Suppose that a system is subject to geometrical constraints only. Then the position vector (r_i) of its particle are not independent variables, but are related to each other by those constrains. A possible 'position' of such system is called a configuration. A set of values for the position vectors (r_i) that is consist with the geometrical constraint is a configuration of the system(Gregory, 2006).

To select the new coordinates, they must be independent of each other, but are still sufficient to specify the configuration of the system. Those new coordinates are called generalised coordinates. When it is said the generalised coordination must be independent variables, that means there must be no functional relation connecting them. If there were, one of the coordination could be removed and remaining $(n-1)$ coordinates would still determine the configuration of the system. The set of generalized coordinates must not be reducible in this way (Gregory, 2006).

Generalised coordinates $q_1, ..., q_n$ determined the configuration of the system S, it means, when the value of the coordinates $(q_1, ..., q_n)$ are given, the position of every

particle of S is determined. In the other words, the position vectors (r_i) of the particle must be known functions of the independent variables $q_1,...,q_n$ (Scheck, 1999), that is:

$$r_i = r_i(q_1,...,q_n), \ (i=1,...,N)$$ (2.1)

Generalised coordinates are remarkably easy to use. They are chosen to be displacements or angles that appear naturally in the problem.(Gregory, 2006)

2.2.3. Lagrange's Equations

To derive the dynamic equations of motion for the planar pendulum in the crane system, total energy needs to be computed using the Lagrangian approach (Fowles & Cassiday, 1999). After which the Euler-Lagrange formulation should be considered to characterize the dynamic behavior of the system.

Lagrangian Equation of motion for a conservative system with the generalised coordinates q is written in terms of the kinetic and potential energy (Fowles & Cassiday, 1999),

$$T = T(q,\dot{q})$$ (2.2)

$$V = V(q)$$ (2.3)

In any motion of the system, the coordinates $q(t)$ have to satisfy the system of the Equations (Gregory, 2006),

$$\frac{d}{dt}\left(\frac{\partial T}{\partial \dot{q}_i}\right) - \frac{\partial T}{\partial q_i} = -\frac{\partial V}{\partial q_i}, \quad \left(1 \le i \le n\right)$$ (2.4)

These are Lagrangian's Equations for the conservative system. Kinetic and potential Equations can be expressed as single function,

$$L = T - V$$ (2.5)

That is called the Lagrangian function (José & Saletan, 1998) or in simple terms, Lagrangian. If $\partial V / \partial \dot{q}_i = 0$, then the Equation (2.4) can be written into the new form,

$$\frac{d}{dt}\left(\frac{\partial T}{\partial \dot{q}_i}\right) - \frac{\partial T}{\partial q_i} = \frac{d}{dt}\left(\frac{\partial V}{\partial \dot{q}_i}\right) - \frac{\partial V}{\partial q_i}, \quad \left(1 \le i \le n\right)$$ (2.6)

If $L = T - V$ is substituted into the Equation, another form called the Lagrangian Equation (Fowles & Cassiday, 1999) is derived,

$$\frac{d}{dt}\left(\frac{\partial L}{\partial \dot{q}_i}\right) - \frac{\partial L}{\partial q_i} = 0, \quad \left(i = 1, 2, 3, ..., n\right)$$ (2.7)

2.2.4. Dissipative System

A general Lagrange Equation for conservative system has been expressed (Chapter 2.2.3). However, in some systems where friction or air resistance dissipate energy and make the system non-conservative, Lagrange Equations should be adapted. For non-conservative force, generalized force (Fowles & Cassiday, 1999) is calculated by:

$$Q_i = \sum_j F_j \bullet \left(\partial r_j / \partial q_i \right) \tag{2.8}$$

Then the Lagrange's Equations can be written as:

$$\frac{d}{dt}\left(\frac{\partial L}{\partial \dot{q}_i} \right) - \frac{\partial L}{\partial q_i} = Q_i, \quad \left(i = 1, 2, 3, ..., n \right) \tag{2.9}$$

Rayleigh's (Baruh, 1999) suggested a modification for Lagrange's Equation, which is known as Rayleigh's Dissipation Function (Fowles & Cassiday, 1999).

$$D = \frac{1}{2} \sum_{i=1}^{N} \left(c_{xi} \dot{x}_i^2 + c_{yi} \dot{y}_i^2 + c_{zi} \dot{z}_i^2 \right) \tag{2.10}$$

Dissipative generalized forces (Török, 2000) are derive from the D function, hence,

$$\delta W = \sum_{i=1}^{n} Q_i^{nc} \delta q_i$$
$$= -\sum_{i=1}^{n} \frac{\partial D}{\partial \dot{q}_i} \delta q_i \tag{2.11}$$

With the Rayleigh's Dissipation function D (Török, 2000), the corresponding generalized force is given by:

$$Q_i = \sum_j \vec{F}_{fj} \bullet \frac{\partial \vec{r}_j}{\partial q_i} = -\sum \nabla_v D \bullet \frac{\partial \vec{r}_j}{\partial q_i} = -\sum \nabla_v D \bullet \frac{\partial \dot{\vec{r}}_j}{\partial \dot{q}_i} = -\frac{\partial D}{\partial \dot{q}_i} \tag{2.12}$$

Lagrange modification by using the Rayleigh's function (Török, 2000) is written as,

$$\frac{d}{dt}\left(\frac{\partial L}{\partial \dot{q}_i} \right) - \frac{\partial L}{\partial q_i} = -\frac{\partial D}{\partial \dot{q}_i}, \quad \left(i = 1, 2, 3, ..., n \right) \tag{2.13}$$

2.2.5. Numerical Method for Differential Equation

Some of the general differential Equations can be solved analytically, however, when there is no analytical solution a numerical approach is often used by engineers and physicists to solve the Equations. Several methods for numerical computation of partial differential Equations exist, such as the Taylor series, Euler and Runge-Kutta approach (Riley et al., 1999).

The general form of the ordinary differential Equation is:

$$\frac{dy}{dx} = f(x, y) \tag{2.14}$$

Numerical methods for solving this Equation can be written in another general form:

$$new\ value = old\ value + slope \times step\ size \tag{2.15}$$

A mathematical term of the expression (Equation (2.15)) is:

$$y_{i+1} = y_i + \phi h \tag{2.16}$$

Based on the Equation (2.16), a slope estimate of (ϕ) is used to extrapolate from an old value (y_i) to a new value (y_{i+1}) over a distance (h). This Equation can be applied step by step to compute all the required values.

The higher-order of classical Runge-Kutta is still one of the more accurate methods for differential Equations. In addition, Runge-Kutta is stable which means that small errors aren't amplified (Arfken et al., 2005). The fifth-order of Runge-Kutta, also known

as the Butcher method, is slightly superior in comparison to the classical method. The Runge-Kutta fifth-order approach Equation (Chapra & Canale, 1998) is expressed as:

$$y_{i+1} = y_i + \frac{1}{90}\left(7k_1 + 32k_3 + 12k_4 + 32k_5 + 7k_6\right)h \qquad (2.17)$$

Where

$$k_1 = f\left(x_i + y_i\right) \qquad (2.18)$$

$$k_2 = f\left(x_i + \frac{1}{4}h, y_i + \frac{1}{4}k_1h\right) \qquad (2.19)$$

$$k_3 = f\left(x_i + \frac{1}{4}h, y_i + \frac{1}{8}k_1h + \frac{1}{8}k_2h\right) \qquad (2.20)$$

$$k_4 = f\left(x_i + \frac{1}{2}h, y_i - \frac{1}{2}k_2h + k_3h\right) \qquad (2.21)$$

$$k_5 = f\left(x_i + \frac{3}{4}h, y_i + \frac{3}{16}k_1h + \frac{9}{16}k_4h\right) \qquad (2.22)$$

$$k_6 = f\left(x_i + h, y_i - \frac{3}{7}k_1h + \frac{2}{7}k_2h + \frac{12}{7}k_3h - \frac{12}{7}k_4h + \frac{8}{7}k_5h\right) \qquad (2.23)$$

Where $f\left(x_i + y_i\right)$ is the differential Equation evaluated at (x_i) and (y_i) and (h) is step size.

System of Equations

Many practical problems in engineering and science require the solution of a system of simultaneous ordinary differential Equations, rather than a single Equation. In general, such systems (Chapra & Canale, 1998) may be represented as:

14

$$\frac{dy_1}{dx} = f_1\left(x, y_1, y_2, ..., y_n\right)$$

$$\frac{dy_2}{dx} = f_1\left(x, y_1, y_2, ..., y_n\right)$$

.

.   (2.24)

.

$$\frac{dy_n}{dx} = f_1\left(x, y_1, y_2, ..., y_n\right)$$

The general solution of such a system requires that an initial condition must be known at the starting value of (x).

2.3. Mathematical Approach, Natural Frequency of the Crane

2.3.1. Crane Analytical Model

The use of cranes is not restricted to the ground; they are widely used on the ocean. Witz (1995) carried out a general investigation to look at the relationship between sea vessels and crane dynamics. In it, he analyzed the parametric excitation of the crane on vessels in an intermediate sea state, applying the numerical solution of the Equation for motion models. He used six degrees of freedom for modeling purposes and applied the Pierson-Moskowitx spectral formulation (Pierson Jr & Moskowitz, 1964) for random force on a vessel. Although many parameters, such as the vessel body and how it is attached to the crane, the structure of the crane, damping, friction, and lifting were not defined in this paper, the investigation was strengthened by the application of the Pierson-Moskowitx method (Pierson Jr & Moskowitz, 1964).

Crane lifting can be modeled as a simple pendulum with variable mass. An investigation of this model was presented by Cveticanin (1995). Influence of reactive

force which appeared because of mass variation on the system was studied and the fundamental assumptions in this study were: a constant rate of relative mass and length variation; variation in damping and; wind force. According to this investigation, the vibrations of the load decrease when the damping coefficient is equal to, or greater than, the relative mass variation rate (Cveticanin, 1995); this demonstrates the influence of the damping coefficient. The findings from this study showed that when the mass separation velocity is set at zero, the system acts like a constant mass system. A mathematical model of the simple pendulum under special conditions was also studied analytically from this and it was concluded that when the relative mass variation rate is fixed, the absolute velocity of unloading and damping has a vital effect.

Cranes are dynamic, nonlinear systems with infinite modes. A non-linear control system was designed by Tabata et al. (2003) in order to convert a nonlinear system into a linear one. To simplify the crane construction, the crane body and rope were considered to be rigid objects and the mass of the rope was ignored. In addition, the crane angle and rope length were constants and the effects of the joints and friction were not taken into consideration. This system provides a simple method to analyze and control the load sway in crane rotations.

Transferring goods in a harbor is one application for a mobile crane, but because of the nonlinearity in dynamic behaviors and the difficulties encountered in measuring the rope angle, there are few existing approaches to control mobile cranes (Schaub, 2008). To address this, an anti-sway system that uses the boom crane to control the sway through a decentralized trajectory tracking control approach has been proposed by Matthews and DeCarlo (1988) and Sawodny et al. (2002). This system has been applied to LIEBHERR LHM 400 harbor mobile cranes with a capacity of 104 tons. The investigators used

Lagrange Equations to describe the luffing movement system that consists of a jib with mass and moment, a weightless rope and point mass payload. In addition, the investigators modeled and analyzed a hydraulic cylinder with Equations derived from the standard model. To address the difficulty of measuring rope angles, two gyroscopes were used in the crane hook. This controller used an actual boom crane and the results showed the ability of anti-sway system based on the decentralized trajectory tracking (CHEN & JIA, 2008).

The telescopic mobile crane is another type of crane which has the ability to change the length of the boom. Maczynski and Wojciech (2003) carried out an investigation to study the optimization of the slewing motion and dynamics of the telescopic mobile crane by using a 3-D model of the crane. One of the goals of their research was to address the safety aspects involved in transferring the load with the minimum oscillations. The crane structure was modeled at six degree of freedom, and Lagrange second order Equations are the basis of all derived formulas. Kinematic and potential energy methods were used for the vehicle chassis and all the jacks and the upper part of the crane was modeled as a supporting beam with a variable cross-section(Maczynski & Wojciech, 2003). Massless rope and servo-motor has been modeled as simple spring and damper, and also effect of servo-motor kinetic energy on the system has been neglected. Servo-motor parts with its flexibility and damping by neglecting the kinematic energy of its motors, weightless rope with flexibility and contact of the load with ground have been considered.

Analysis of the telescopic mobile crane is difficult because of the nonlinearity in the system. Sa irli et al. (2003) took this into account when modeling their telescopic rotary crane which has been modeled based on the 4GO45L45 manufactured by Gelisim Automotive, ISTANBUL, for study purposes. In addition, they considered the elasticity

of the boom and the hydraulic system, and calculated the effective force with the aid of Bond Graph techniques. In this research a mathematical model of an actual crane was built and the Equation of motion to improve the model was derived by assuming that the main telescopic boom was an elastic structure, whereas all other parts, such as supports, chassis and the main body, were rigid. This model was able to rotate in both vertical and horizontal plane. In addition to this, the hydraulic system with its compressible fluid was modeled. In this model, a rigid and weightless rope connected the point of mass load to the boom. Rotational damping was ignored and vertically damping used as overall on tip of the boom.

Controlling the rotary boom crane that solely rotates around the vertical axis has proven impossible, to date, with a smooth controller. Kondo and Shimahara (2005) examined changes in system stabilization for this rotation using different controls: an energy control, an open-loop control and a feedback control. Assumptions in this paper were formed on the basis that the crane only rotates about the vertical axis and not about the horizontal axis. The crane model used in this study was similar to a simple pendulum and thus, neither the boom mass nor air resistance had any effect on this system. Simulations on that rotary crane has verified the stabilization method via switching control.

Controlling the sway of dangerous and heavy loads that transfer with Gantry cranes in industrial areas was the basis of a study carried out by Omar and Nayfeh (2005). The investigators used the feedback controller method to control sway whilst taking into account the friction of the parts. Mathematical models based on Lagrange Equation were derived. The crane model consisted of a simple pendulum that attached to a moveable trolley. For estimation of friction in the crane parts a standard model of a DC motor with

a known friction coefficient was used. A crane with a closed loop controller with variable rope lengths and masses formed the basis of this study. Experimental and numerical results were compared; this outcome demonstrated the efficiency of this controller which reduced the load oscillation during the load transferring.

Crane slewing motion induces the horizontal inertial force on the suspended payload (Jerman & Kramar, 2008). For this research, they used previous mathematical crane models which included factors such as nonlinearity and deformability. Equations of motion were derived from second order Lagrange Equations, and by using the appropriate values they were able to make their model more comparable to standard and linear crane motions. In this paper, environmental effects, such as air resistance, were considered in Equations and the point force masses of the crane and payload were shown as a point mass and moment of inertia. Rope mass was neglected and the mean damping coefficient and stiffness were used instead of structure damping and stiffness. In addition, moment of friction was used to represent slewing ring friction.

2.3.2. Analytical System Linked By Two Coordinates (an Approach for Crane Mathematical Model)

The Receptance

The receptance method has been proposed to find the natural frequencies and vibration modes of combined structures (Hayashi et al., 1964). For the vibrating system which has n degree of freedom or assemblies composed (R. E. D. Bishop & Johnson, 2011), there will be n simultaneous Equations of motion. These can usually be set up most conveniently by the method of Lagrange. The Equations may be solved by trial solution

in which all the displacements vary harmonically at the disturbing frequency. This theory (Hayashi et al., 1964) has existed for many years.
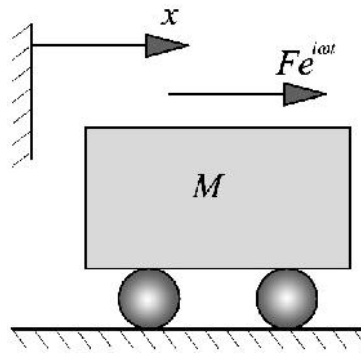
Figure 2-1, Displacement of the rigid mass under the harmonic force

Let a harmonic force $Fe^{i\omega t}$ act at some points of a dynamical system so that the system takes up a steady motion with the same frequency (ω), such that the point of the application of the force has the displacement (R. E. D. Bishop & Johnson, 2011):

$$x = Xe^{i\omega t} \tag{2.25}$$

Then, if the Equations of motion are linear, this may be written (R. E. D. Bishop & Johnson, 2011), (Huang & Chen, 2007):

$$x = \alpha F e^{i\omega t} \tag{2.26}$$

Where (α) depends upon the nature of the system and the frequency (ω) but not upon the amplitude (F) of the force. The quantity (α) is termed "the direct receptance at (x)".

If on the other hand (x) is displacement at some point of the system other than that at which the force is applied, then Equation (2.26) defines a cross receptance α.

The displacement (x) of the rigid mass (M) of the **Figure 2-1** is given (R. E. D. Bishop & Johnson, 2011) by:

$$M\ddot{x} = Fe^{i\omega t} \tag{2.27}$$

So that, if the displacement varies sinusoidally, then it is possible to write $x = Xe^{i\omega t}$ and it then follows that (R. E. D. Bishop & Johnson, 2011),

$$-M\omega^2 X = F \tag{2.28}$$

That is to say

$$\alpha = -\frac{1}{M\omega^2} \tag{2.29}$$

Which is the direct receptance at (x).

By virtue of certain simple properties of the receptances, it is often possible to break down a complex system into simple parts in which the receptances are known, and then to analyze it. After simplifying the system, the receptances, the principal modes, and the frequency Equation of the complex system can then be calculated using this information. This method often saves much of the time and effort that is required for the determination of receptances by direct substitution into Equations of motion (R. Bishop & Johnson, 1960). The (α) symbol is used for the whole system receptances. The simple parts of the system can also be denoted by symbols: (β) and (γ) are used for each simple part.

For finding the two block system reaccceptance as in Figure 2-2 is presented:
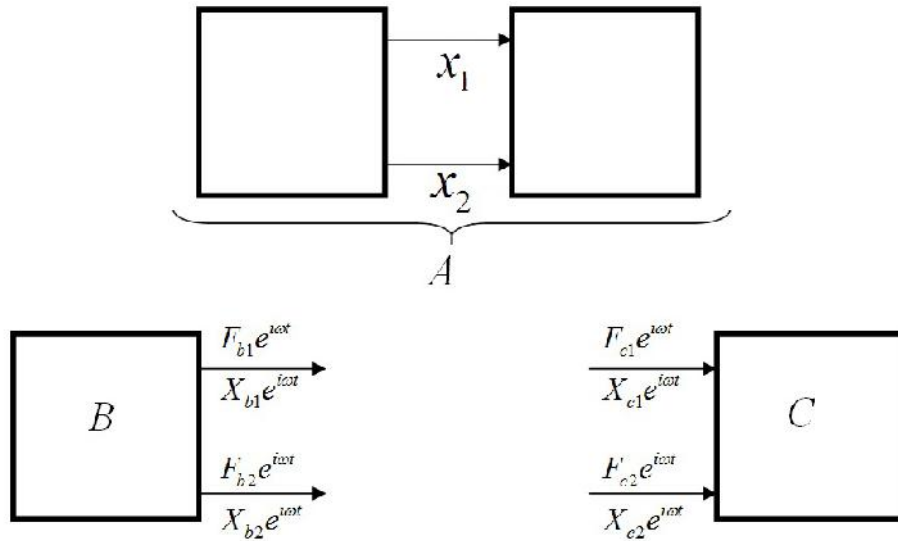
Figure 2-2, System Block Diagram

Using the notation shown (R. E. D. Bishop & Johnson, 2011), we have

$$\left.\begin{array}{l} X_{b1} = \beta_{11}F_{b1} + \beta_{12}F_{b2} \\ X_{b2} = \beta_{21}F_{b1} + \beta_{22}F_{b2} \end{array}\right\} \tag{2.30}$$

And

$$\left.\begin{array}{l} X_{c1} = \gamma_{11}F_{c1} + \gamma_{12}F_{c2} \\ X_{c2} = \gamma_{21}F_{c1} + \gamma_{22}F_{c2} \end{array}\right\} \tag{2.31}$$

The applied forces are $F_1 e^{i\omega t}$ and $F_2 e^{i\omega t}$, where:

$$\left.\begin{array}{l} F_1 = F_{b1} + F_{c1} \\ F_2 = F_{b2} + F_{c2} \end{array}\right\} \tag{2.32}$$

Since the systems are linked

$$\left.\begin{array}{l} X_1 = X_{b1} = X_{c1} \\ X_2 = X_{b2} = X_{c2} \end{array}\right\} \tag{2.33}$$

If $F_2=0$ so that excitation is applied at (x_1) only (R. E. D. Bishop & Johnson, 2011), then it may be shown from the Equations that

$$\alpha_{11} = \frac{X_1}{F_1} = \frac{\beta_{11}\left(\gamma_{11}\gamma_{22} - \gamma_{12}^2\right) + \gamma_{11}\left(\beta_{11}\beta_{22} + \beta_{12}^2\right)}{\left(\beta_{11} + \gamma_{11}\right)\left(\beta_{22} + \gamma_{22}\right) - \left(\beta_{12} + \gamma_{12}\right)^2}$$ (2.34)

And

$$\alpha_{21} = \frac{X_2}{F_1} = \frac{\beta_{12}\left(\gamma_{11}\gamma_{22} - \beta_{12}\gamma_{12}\right) + \gamma_{12}\left(\beta_{11}\beta_{22} + \beta_{12}\gamma_{12}\right)}{\left(\beta_{11} + \gamma_{11}\right)\left(\beta_{22} + \gamma_{22}\right) - \left(\beta_{12} + \gamma_{12}\right)^2}$$ (2.35)

Again, assume that the subscripts of the cross-receptances may be interchanged. Also, if ($F_1=0$), so that excitation is applied at (x_2) only, then (α_{12}) is found to be given by the above (R. E. D. Bishop & Johnson, 2011) expression for (α_{12}) and

$$\alpha_{22} = \frac{X_2}{F_2} = \frac{\beta_{22}\left(\gamma_{11}\gamma_{22} - \gamma_{12}^2\right) + \gamma_{22}\left(\beta_{11}\beta_{22} - \beta_{12}^2\right)}{\left(\beta_{11} + \gamma_{11}\right)\left(\beta_{22} + \gamma_{22}\right) - \left(\beta_{12} + \gamma_{12}\right)^2}$$ (2.36)

The frequency Equation for the composite system is obtained, as usual, from the resonance condition at which all the receptances become infinite (R. E. D. Bishop & Johnson, 2011). This is when

$$\left(\beta_{11} + \gamma_{11}\right)\left(\beta_{22} + \gamma_{22}\right) - \left(\beta_{12} + \gamma_{12}\right)^2 = 0$$ (2.37)

2.4. Finite Element Method for Cranes

Okubo et al. (1997) carried out a study to examine how a system controls the vibration of a girder and the containers concurrently in a container crane. In their study,

the container crane was modeled as a mass and spring damper, with a trolley and sheave masses. rope as spring and load mass were define for this model. Load positions for this controller were detected by a CCD camera (Charge Coupled Device), and through this it was observed that the vibration of the girder had an effect on the container. Numerical simulation and experimental data on the actual model demonstrated the ability of the controller to decrease the vibrations on the trolley and also increased the speed and effectiveness of load carrying. During the crane operation, this controller was able to decrease the maximum vibration on the girder by 50% and increase the damping constant by up to 11.5 times, with no residual vibration remaining in the system.

Mobile cranes which stand on the ground with their jacks have been defined as rigid structures. The stability of these cranes was examined by Towarek (1998) in an investigation that took into account the effect of soil dynamics during the boom rotation. In this investigation, six degrees of freedom was used for modeling purposes, an elastic rope attached the point mass load to the boom, and the crane body and boom were considered to be rigid structures. 12 weightless springs were used to hold the crane body onto the ground and soil dynamics were described by Duhamel integral (Kreyszig, 2007). Simulation results for each crane support in both states of soil (with and without deformation) were calculated and compared to each other; results indicated that due to the dynamic behavior of the soil there was a real possibility of danger if this effect was not taken into consideration.

Operators usually control cranes. Human commands are the input data for systems, but this can be a weakness as it is not linear data. An investigation of the nonlinear input that is executed by an operator was carried out by Parker et al. (2002). This method depicted real-time control to prevent the sway of the payload in a ship boom crane. A

model of an actual Navy crane with a scale of 1/16 was designed. This model had the ability to reduce the oscillation of the payload and thus increase the safety and efficiency of the crane. Under specific terms which are the low speeds of crane operation, this linear filter can be applied directly to operator's commands. The shapes or forms of the cranes which were used for the investigation consisted of a point mass that attached to the boom, with a weightless rope and a varying lift-line length. One of the weaknesses of this design was the linear filter which had difficulty working within small ranges of crane speeds.

One method to control sway in rotary cranes is the addition of a straight transfer transformation (STT). Y Shen et al. (2003) built a model of a crane and derived the geometric parameters. The investigators used the optimization method of Davidon-Fletcher-Powell (DFP) (Fletcher & Powell, 1963) to eliminate the sway at the end point of transfer. The experimental results from their simulations indicate that the centrifugal force in the STT mode (2-D) was ignored. In addition, the time of optimization was seen to be slower in the 2-D model than it was in three-dimensional (3-D) space. In this study, most of the parameters were considered with the exception of friction in the torque mechanism, elongation and mass of the rope and environmental effects. Experimental result verified the simulation result of STT model.

As the experience of an operator is a strong influencing factor, a highly experienced operator is necessary to control the boom crane. Based on this knowledge, Arnold et al. (2003) have proposed a method to optimally control the sway in the boom crane in order to let those with lower levels of experience function as crane operators. In order to achieve their objective, the researchers applied the Newton-Euler method for non-linear dynamic systems, and solved the optimal control issue with the numerical method in the 9th order of ODE (Ordinary Differential Equation). Luffing and slewing of the crane was extended

to the hydraulic drives. The actual data which demonstrates this method of control was taken from the LIEBHERR LHM 400. The small difference that was found between the final luffing angle and minute sway of this model could be improved by tuning. This model assumed a point mass of payload with no air resistance, a weightless rope, a moveable boom with moment of mass, and a hydraulic system for luffing. This system was mounted on an actual crane and comparison between the simulation and experimental data have shown its ability, and reliability.

To complete their previous research Sun et al. (2005) used a new method, the Timoshenko beam element (Davis et al., 1972) method, for the finite element calculation of a boom crane. In this study, a hydraulic system was used for a secondary hoisting system. Hoisting system was described in three elements types which were drum rope, hoisting rope and pulley-rope; then the Equation of system dynamics was established according to these three assumptions. The speed of hoisting and braking was used for the input data and the output data included the dynamic response and control. In this model, other parameters, such as oil flow, stability and motor output, were studied simultaneously. Technically, data for the mathematical model in simulation was taken from the actual crane. This paper focused on three elements of the hoisting system, created a mathematical model of each of them and solved these Equations simultaneously. The final analysis of the paper included three areas: a) hoisting, which was divided in three parts: the hoisting drum, the rope and the pulley; b) the crane steel structure like jib and boom and; c) the hydraulic system.

There are three main motions of the mobile crane that can define the position of the load: the rotation of boom in the horizontal, the vertical plane and finally the change in rope length. The operator can control the position, but not the swing of the load, by using

these movements. Neupert et al. (2010) examined the relationship between operator commands and swing control of a load in a mobile harbor crane. The focus of the controller was on a semi-automatic model which consisted of two sub-controller: 1/ disturbance observers; 2/ a model predictive trajectory generation module (Neupert et al., 2010). Input data in the mathematical model and control approach consisted of Linearized Operator commands. Assumptions of the model included a weightless and rigid rope, a rigid crane body and a mass pointed load with a small swing angle. In addition, mixed sway of the load was neglected and rope length was considered a constant due to the slow hoisting speed. The hydraulic system and its oil flow, which is responsible for luffing, was also modeled and disturbance of centrifugal effects was added to the radial controller. Encoders were used for measuring the crane position, and two gyroscopes were employed to correct for angular velocity and radial direction. This controller was executed on a real harbor mobile crane (LIEBHERR LHM 400), experimental results demonstrated the efficiency of the controller.

CHAPTER 3:   METHODOLOGY

3.1. Introduction

Tower cranes are widely used for moving loads in construction, industry and transportation. Load swinging imparts the forces to the support point, and this can be considered as vibrations. Typically, the payload is modeled as a point mass suspended from a rigid cable that is moving in a horizontal plane.(Ghigliazza & Holmes, 2002). Aim of present research is to investigate the 2-D tower crane dynamics under the planar pendulation motions of the payload including the elastic cable. The method of calculation is carefully built upon stages ranging from Lagrange equations and mass force relation from Newton's law. For the first stage, Lagrange principal is used to derive the dynamic model of the pendulum systems as partial differential Equations. A wide displacement of approximately 10 m and elastic cable is considered in the calculation. The Newton's second law is used to treat forces induced by the swinging gain in the cable. MATLAB software is used to solve the set of the partial differentials Equations. Numerical calculations give the results of the force reaction at the base. In addition, all real structures potentially have an infinite number of displacements. Therefore, the most critical phase of a structural analysis is to create a computer model with a finite number of members and a finite number of node (joint) displacements that will simulate the behavior of the real structure(Wilson, 1996).

Real structure has an infinite numbers of displacements. Therefore dynamic analysis can be done by the computer with finite members of the elements. Soft model of

the tower crane is created by AutoCAD, the final result will be used for dynamic analysis of the tower crane under the pendulation motion of the load by Ansys Workbench.

Firstly, to demonstrate the software accuracy, a simple model of the crane was analysed using the Modal technique, in addition to a mathematical model. By comparing the results of the mathematical and software model, the accuracy of the analysis could be verified and confirmed.

3.2. Mathematical Model of Pendulum Motion

3.2.1. Pendulation Motion Based on the Lagrange's Equation

To obtain the Lagrangian Equations for pendulum system (**Figure 3-1**), kinetic and potential energy, and consequently Lagrangian function (L) are written in terms of the generalised coordinate as expressed in Chapter 2.2.3, Equations (2.2) and (2.3).

Pendulum consists of a mass which hang by a rope or cable from a fixed point. For the purpose of simple calculation, most of the pendulums are simplified, and a rigid cable ($dr/dt = 0$) (Yi et al., 2003) as well as a small displacement ($\sin\theta \approx \theta$) (Cho & Lee, 2000) are the most common assumptions. After taking this into account the whole equation can be written as one parameter, (θ). In this study non-simplified pendulum was taken into consideration and a large displacement $\left(\sin\theta \neq \theta\right)$ and non-rigid cable $\left(dr/dt \neq 0\right)$ were assumed. Generalized coordinates for the pendulum (**Figure 3-1**) were defined as: (r) and (θ), or cable length and cable angle between the resting and current position respectively.
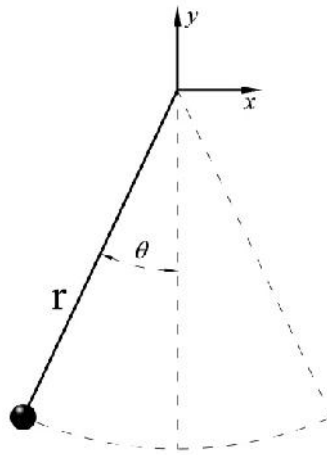
Figure 3-1, Pendulum swinging in the x-y plane

Generalised coordinates (Chapter 2.2.2) have been set based on the polar coordinates (r,θ) for the pendulum motion. Potential and Kinetics Equations based on two generalized coordinates (r,θ) are obtained by the Lagrange's Equations of motion (Ferreira & Ewins, 1996) are:

$$T = \frac{1}{2} m \dot{\vec{r}}^2 \tag{3.1}$$

$$V = \frac{1}{2} k \Delta r^2 + mg\vec{r} \tag{3.2}$$

And also:

$$\ddot{\vec{r}} = \ddot{r} - r\dot{\theta}^2 \tag{3.3}$$

Where (m), (k) and (g) are payload mass, cable stiffness and gravity acceleration, respectively.

Lagrangian function of the system (**Figure 3-1**) based on Equation (2.5) is $L = T - V$. By substituting the potential and kinetic energy into the Lagrangian function, we got:

$$L = T - V$$

$$L = \frac{1}{2}m\dot{\bar{r}}^2 - \left(\frac{1}{2}k\Delta r^2 + mg\bar{r}\right)$$

$$L = \frac{1}{2}m\left\{\dot{r}^2 + \left(r\dot{\theta}\right)^2\right\} - \left\{\frac{1}{2}k\left(r - r_0\right)^2 - mgr\cos\left(\theta\right)\right\} \tag{3.4}$$

Air resistance has been taken account which makes this system non-conservative, as another assumption for pendulum Equation of motion.

The Rayleigh's dissipation function (Chapter 2.2.4) associated with the air resistance is then based on the Equation (2.11) and it is possible to get:

$$D = \frac{1}{2}c\dot{q}^2 \tag{3.5}$$

Air resistance is based on the dissipation function in polar coordinates and can be written along with the coordinates,

$$D = \frac{1}{2}c\left(\dot{r}\right)^2 + \frac{1}{2}\left(r\dot{\theta}\right)^2 \tag{3.6}$$

Two generalized coordinate can create two set of the Lagrange's Equations, where

$$\begin{cases} \dfrac{d}{dt}\left(\dfrac{\partial L}{\partial \dot{r}}\right) - \dfrac{\partial L}{\partial r} = -\dfrac{\partial D}{\partial \dot{r}} \\[2mm] \dfrac{d}{dt}\left(\dfrac{\partial L}{\partial \dot{\theta}}\right) - \dfrac{\partial L}{\partial \theta} = -\dfrac{\partial D}{\partial \dot{\theta}} \end{cases} \tag{3.7}$$

Each part of the Lagrange is found, and then after taking derivations based on the (r) the formula is:

$$\frac{d}{dt}\left(\frac{\partial L}{\partial \dot{r}}\right) = m\ddot{r}$$

$$\frac{\partial L}{\partial r} = mr\dot{\theta}^2 - k\left(r - r_0\right) + mg\cos\left(\theta\right)$$

$$\frac{\partial D}{\partial \dot{r}} = c\dot{r}$$

Whereat the derivation based on the variable (θ) gives:

$$\frac{d}{dt}\left(\frac{\partial L}{\partial \dot{\theta}}\right) = 2mr\dot{r}\dot{\theta} + mr^2\ddot{\theta}$$

$$\frac{\partial L}{\partial \theta} = -mg\sin\left(\theta\right)$$

$$\frac{\partial D}{\partial \dot{\theta}} = cr^2\dot{\theta}$$

Substituting the derivations inside the Lagrange's Equations, yield,

$$\begin{cases} m\ddot{r} - mr\dot{\theta}^2 + k\left(r - r_0\right) - mg\cos\left(\theta\right) = -c\dot{r} \\ \\ mr^2\ddot{\theta} + 2mr\dot{r}\dot{\theta} + mg\sin\left(\theta\right) = -cr^2\dot{\theta} \end{cases} \qquad (3.8)$$

By rearranging the parameters, two set of final Equations (3.8) are denoted as Equation (3.9):

$$\begin{cases} \ddot{r} - r\dot{\theta}^2 + \dfrac{k}{m}\left(r - r_0\right) + \dfrac{c}{m}\dot{r} - g\cos\left(\theta\right) = 0 \\ \\ \ddot{\theta} + \dfrac{2}{r}\dot{r}\dot{\theta} + \dfrac{c}{m}r\dot{\theta} + \dfrac{g}{r}\sin\left(\theta\right) = 0 \end{cases} \qquad (3.9)$$

The differential Equation of pendulation motion (Equation(3.9)) is shown in its general form, therefore to compute using that Equation initial conditions are required.**Table 3-1** and **Table 3-2** give the specification such as stiffness (Torkar & Arzenek, 2002) and initial condition of the payload.

Table 3-1, Payload and Cable Properties

Specification	symbol	unit
Payload mass	m	1000 (*kg*)
Cable stiffness	k	1 (*MN*)

Table 3-2, Pendulum Initial Condition

Initial specification	symbol	unit
Initial angle of the cable	θ_0	0 (*Rad*)
Initial rope length	r_0	30 (*m*)
Initial incitation	ω_0	0.05 (*Rad/sec*)

Two set of partial differential Equations are the result of the Lagrange's Equations which then have to be solved simultaneously. If there is no analytical solution for these

sets of Equations, then numerical methods must be utilized in order to solve the Equations.

3.2.2. Numerical Differential Equation by Using MATLAB

Equations (3.9) define the position of the payload during the time in the (X-Y) plane. As there is no analytical answer for these sets of Equations, the numerical method will be used to define the answer. The Runge-Kutta approach is one of the methods for governing the optimized answer, and MATLAB software has been employed to solve that Equations numerically based on the Runge-Kutta method (Chapter 2.2.5, Equation (2.17) based on the Equation(2.24)). MATLAB code is written as several functions which are expressed in Appendix A.

3.2.3. Dynamics of the Forces

All real structures behave dynamically when subjected to displacements or loads (Wilson, 1996). Second law of Newton's dictates that a change of motion is proportional to the applied force and takes place in the direction of the straight line along which that force acts (Scheck, 1999)
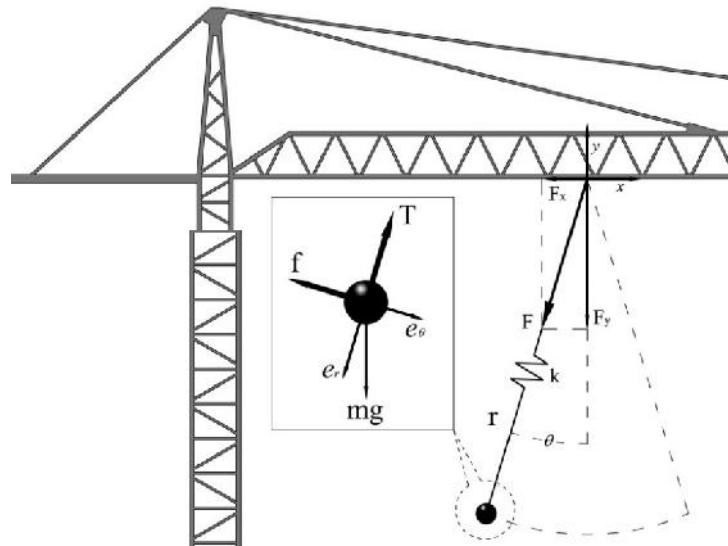
Figure 3-2, Pendulum force reaction on the tower crane

To state the Newton's second law for objects, a free diagram of the applicable forces is required to show the direction and components of these forces. For simplification, Pendulum can be assumed as a mass point and a cable with stiffness, **Figure 3-2** illustrates the state of the pendulum. In addition, Cartesian coordinates have been placed on the pendulum base and Polar coordinates on the mass.

Newton's second law is written in terms of velocity and acceleration, expressed in Polar coordinates (McGill & King, 1995). Acceleration of the swinging mass can be divided into two components (Meriam & Kraige, 2006), which have been placed on the diagram as polar coordinates (r, θ),

$$\vec{F} = m\ddot{\vec{r}} \tag{3.10}$$

Where:

$$\ddot{\vec{r}} = \ddot{r} - r\dot{\theta}^2 \tag{3.11}$$

The second law of Newton's is written along the *r* direction. The reason is, the force can act only along this coordinates (Hibbeler, 2002), This is written by:

$$F = m\left(\ddot{r} - \dot{r}\dot{\theta}^2\right)$$

(3.12)

Simplification of the Equation (Groesberg, 1968) yield:

$$F = -k\left(r - r_0\right) + mg\cos\theta$$

(3.13)

Where cable stiffness (*k*) (Beer & Johnston, 2011) is expressed as:

$$k = \frac{EA}{r}$$

(3.14)

Where (*E*), (*A*) and (*r_0*) are the Young's modulus, cable cross area sectional and free length of cable respectively (Chaplin, 1995; Torkar & Arzenek, 2002). (*r*) and (*θ*) are the variable parameters and their approximate value is calculated using a numerical solution derived from the values which resulted from the set of Partial Differential Equations (3.9)
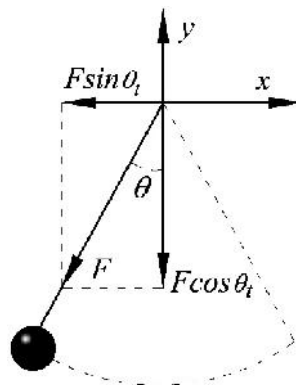
Figure 3-3, Components of the Force Reaction of Pendulum

Force reaction on the jib can be expressed as two components along the (x) and (y)

axis (**Figure 3-3**); thus,

$$F_x = F \sin \theta_t \qquad\qquad (3.15)$$

$$F_y = F \cos \theta_t \qquad\qquad (3.16)$$

Solving the Equations (3.15) and (3.16) based on the obtained (r) and (θ), gives the

force reaction components. According to **Figure 3-2**, (T) and (F) are the same in value

but their figures lie in opposite directions.

3.3. Mathematical Approach for Modal Analysis of the Tower Crane

The tower Crane complex body can be simplified and modeled as a frame which is

composed of two uniform segments, and can be found by using the receptances of the

separate segments. In the following diagram **Figure 3-4**, the frame is shown as two joint

beams at right angles:
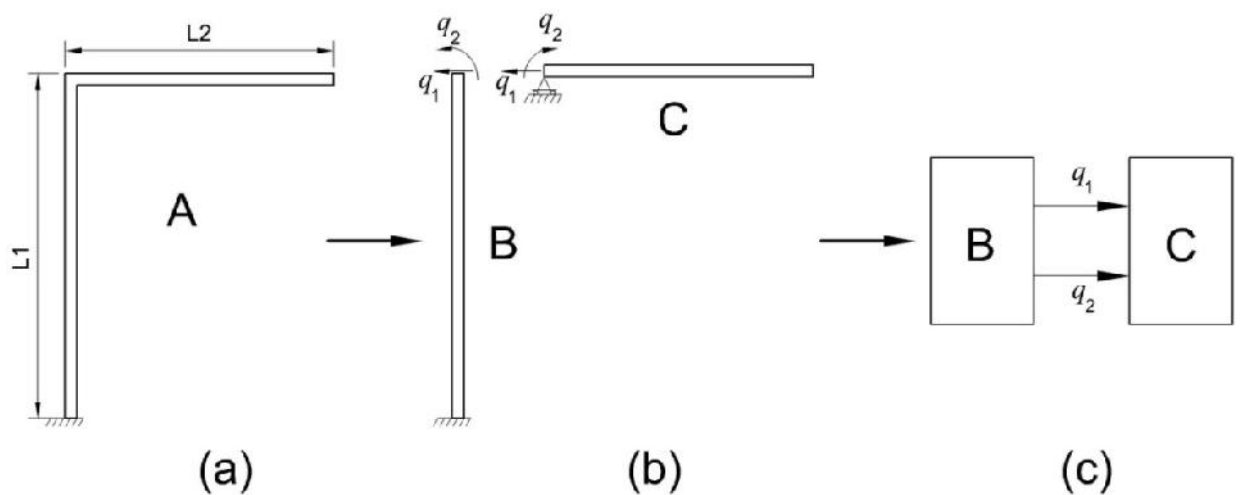
Figure 3-4, Crane System and its Related Block Diagram

Before discussing the calculations for this system, it should be noted that the arrangement shown in Figure 3-4(a) also represents the first step involved in the construction of other types of systems which originate from straight members, and that there is no limit to the complexity of such a system

However, although this is the case, there are also several practical limitations on the extent to which our methods of analysis may be applied to a system that has a large number of members. In particular, it should be kept in mind that as the number of members increase, and the number of ways in which they may be oriented relative to each other also increase, new terms have to be included in the Equations of motion. Thus, when going from the straight beam to the bent cantilever, the additional effect must be included in the longitudinal motion of the member that is remote from the clamp; even if the discussion is confined to vibration in the plane of the cantilever. If the vibrations out of that plane are to be examined, then the torsional characteristic of the clamped member must be taken into account.

Furthermore, when analyzing the motion of a cantilever which is built up from three uniform beams, it is helpful to keep in mind that, in general, all applied methods may involve torsion, in addition to bending if the bars are not co-planar. If a system is examined in which the uniform members are sufficient in number to be arranged to form closed polygons, as in the two-story portal frame or in space frames, then torsional and flexural motion of all the members should be allowed for. However, despite the differences, the process of setting up the Equations is not fundamentally altered.

For the purposes of calculation, the strip may be divided into the two subsystems shown in **Figure 3-4**(b), so that (B) is a clamped-free beam and (C) is a free-pinned beam which is capable of longitudinal motion. The motion in the latter beam may be treated as

rigid body motion, as it is assumed that the natural frequencies which we are concerned with are much lower than the natural frequencies that result from the longitudinal vibration of the bar (C). The linking coordinates, (q_1) and (q_2), are illustrated in **Figure 3-4**(b) and the complete system is shown in block form in **Figure 3-4**(c).

The frequency Equation for the composite system has been derived from (2.37) and the relevant receptances (R. E. D. Bishop & Johnson, 2011), (Huang & Chen, 2007) are:

$$\beta_{11} = \frac{-F_5}{EI\lambda^3 F_4} \tag{3.17}$$

$$\beta_{22} = \frac{F_6}{EI\lambda F_4} \tag{3.18}$$

$$\beta_{12} = \frac{F_1}{EI\lambda^2 F_4} \tag{3.19}$$

$$\gamma_{11} = \frac{-1}{A\rho l \omega^2} \tag{3.20}$$

$$\gamma_{22} = \frac{F_4}{EI\lambda F_5} \tag{3.21}$$

$$\gamma_{12} = 0 \tag{3.22}$$

In which:

$$F_1 = (\sin \lambda l)(\sinh \lambda l) \tag{3.23}$$

$$F_2 = (\cos \lambda l)(\cosh \lambda l) \tag{3.24}$$

$$F_3 = (\cos \lambda l)(\cosh \lambda l) - 1 \tag{3.25}$$

$$F_4 = (\cos \lambda l)(\cosh \lambda l) + 1 \tag{3.26}$$

$$F_5 = (\cos \lambda l)(\sinh \lambda l) - (\sin \lambda l)(\cosh \lambda l) \tag{3.27}$$

$$F_6 = (\cos \lambda l)(\sinh \lambda l) + (\sin \lambda l)(\cosh \lambda l) \tag{3.28}$$

$$F_7 = (\sin \lambda l) + (\sinh \lambda l) \tag{3.29}$$

$$F_8 = \left(\sin \lambda l\right) - \left(\sinh \lambda l\right) \tag{3.30}$$

$$F_9 = \left(\cos \lambda l\right) + \left(\cosh \lambda l\right) \tag{3.31}$$

$$F_{10} = \left(\cos \lambda l\right) - \left(\cosh \lambda l\right) \tag{3.32}$$

In writing these expressions, no distinguishing suffixes have been added to (A), (E), (I), (l), (λ) and (ρ) because all these quantities are the same for the two beams. Further to this, since the argument (λl) of the functions (F) is the same for each beam, these too, carry no letter subscripts. When the receptances have been substituted into Equation (2.37) the resulting Equation may be simplified by multiplying throughout by ($EI\lambda^4$). This gives (R. E. D. Bishop & Johnson, 2011):

$$\left(\frac{F_5}{F_4} + \frac{1}{\lambda l}\right)\left(\frac{F_6}{F_4} + \frac{F_4}{F_5}\right) + \left(\frac{F_1}{F_4}\right)^2 = 0 \tag{3.33}$$

Substituting Equations (3.23) to (3.32) into (3.33) yields,

$$\left(\frac{\left(\cos \lambda l\right)\left(\sinh \lambda l\right) - \left(\sin \lambda l\right)\left(\cosh \lambda l\right)}{\left(\cos \lambda l\right)\left(\cosh \lambda l\right) + 1} + \frac{1}{\lambda l}\right)\left(\frac{\left(\cos \lambda l\right)\left(\sinh \lambda l\right) + \left(\sin \lambda l\right)\left(\cosh \lambda l\right)}{\left(\cos \lambda l\right)\left(\cosh \lambda l\right) + 1} + \right.$$

$$\left. \frac{\left(\cos \lambda l\right)\left(\cosh \lambda l\right) + 1}{\left(\cos \lambda l\right)\left(\sinh \lambda l\right) - \left(\sin \lambda l\right)\left(\cosh \lambda l\right)}\right) + \left(\frac{\left(\sin \lambda l\right)\left(\sinh \lambda l\right)}{\left(\cos \lambda l\right)\left(\cosh \lambda l\right) + 1}\right)^2 = 0$$

$$\tag{3.34}$$

Solving the Equation for the values of (λl) can be used for finding the natural frequency. Natural frequency can be expressed as,

$$\omega_n = \frac{(\lambda_n l)^2}{l^2} \sqrt{\left(\frac{EI}{A\rho}\right)} \qquad (3.35)$$

Natural frequencies are gained by several parameters (Room & Hall, 2012) which those parameters are defined at **Table 3-3**.

Table 3-3, Properties of mathematical crane model

|		
Young Modulus	E	210 *Gpa*
Density	p	7688 *kg/m³*
Moment of Inertia	I	0.01
Cross Sectional Area	A	0.02 *m²*
Stripe Length	l	54.20 *m*

When Equation (3.34) has been solved and the first four roots have been found, then Equation (3.35) is used to calculate the natural frequency of the simple model of the tower crane.

3.4. Modal Analysis and Dynamic Response of the Tower Crane Using the Ansys Workbench

FEA (finite element analysis) include three main steps which are: pre-processing, solution and post-processing phase. Ansys Workbench is a kind of finite elements analysis software. Those three main steps divide into several steps which are:

41

- Modelling

- Material selection

- Meshing

- Apply Constrain

- Apply Load (Dynamics or Statics)

- Solving the problem

- Print out the result

Analysis steps which have implemented at this thesis are expressed concisely. Application of pendulation Equation of motion and Mathematical approach for modal analysis (Chapter 3.2 and Chapter 3.3) based on the FEA sequences is presented at **Figure 3-5**.
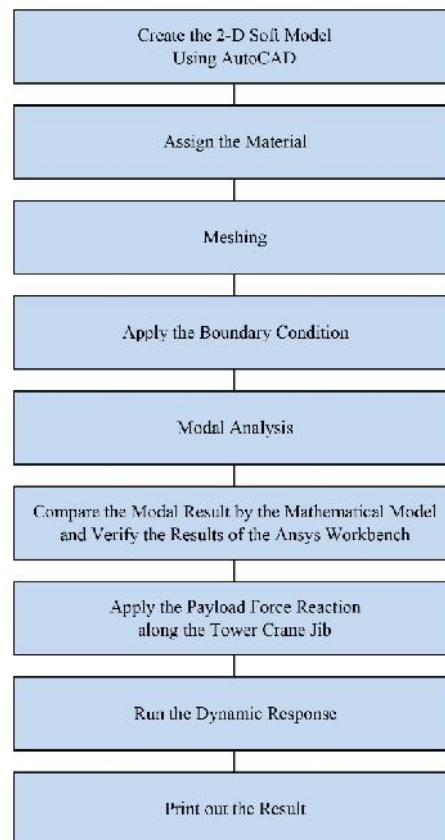
Figure 3-5, Ansys Workbench sequences for the current problem

3.4.1. Tower Crane Modelling

AutoCAD software was used to create the soft model of the tower crane based on the actual dimensions (LIEBHERR 132 HC, Appendix C); **Figure 3-6** shows the feature of the program and design.
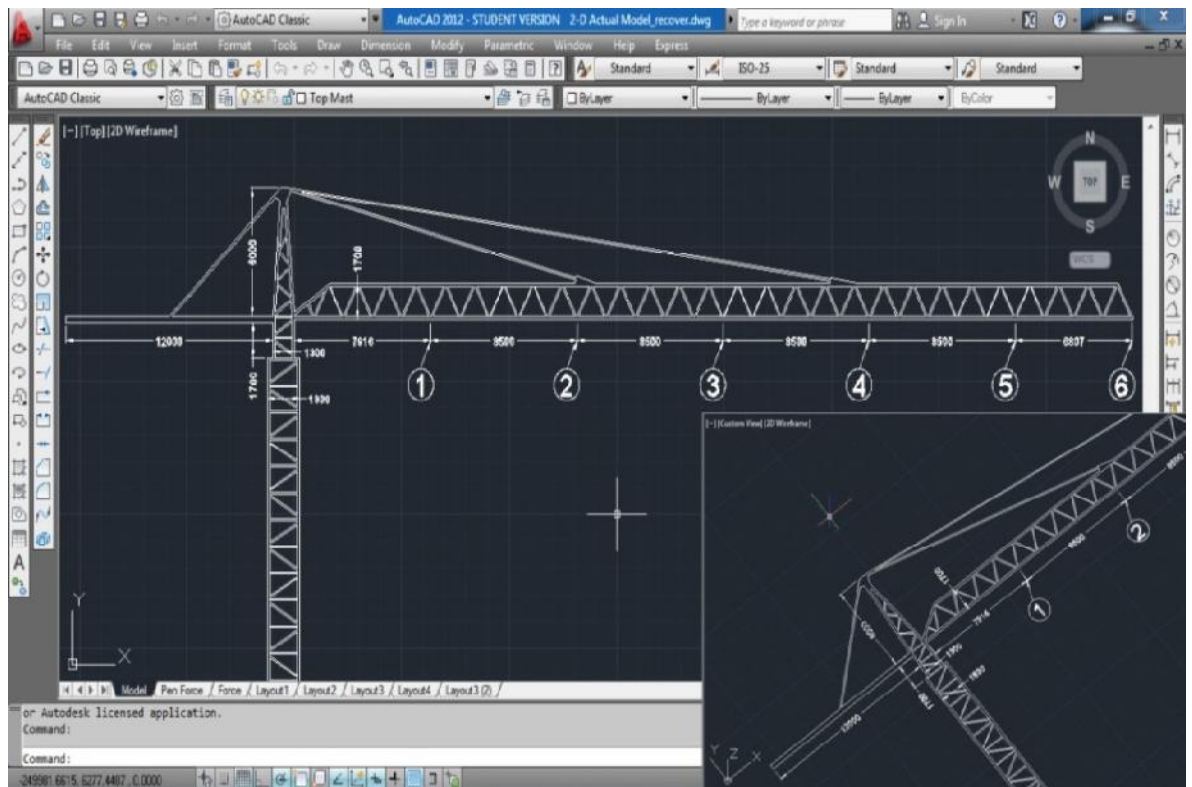
Figure 3-6, Tower Crane in AutoCAD

Figure 3-7 shows the dimensions of several parts of the tower crane. This model is rigid and was exported to the Ansys Workbench for modal and dynamic analysis.
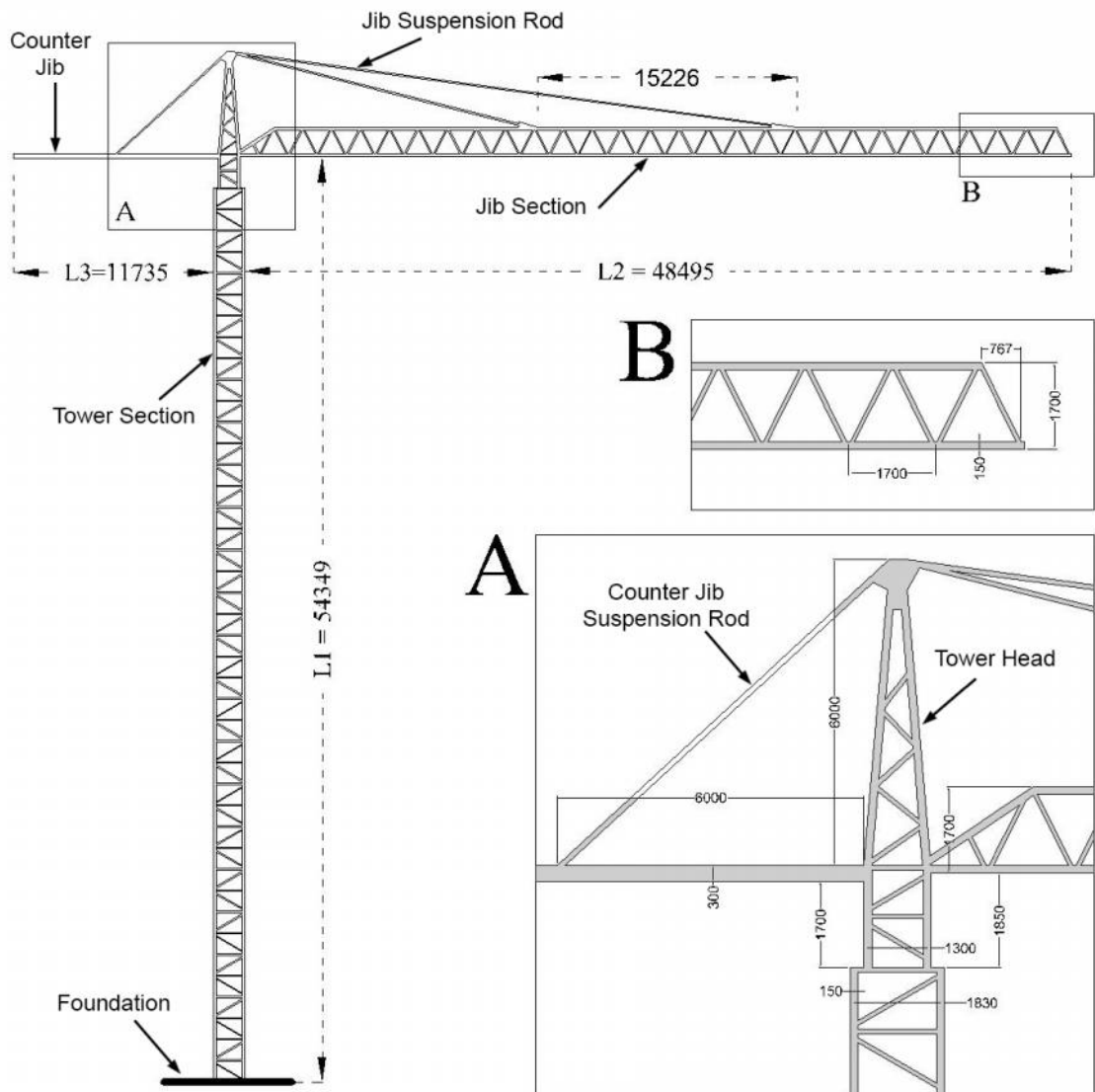
Figure 3-7, Crane Dimensions Detail

3.4.2. Material Selection

Material selection is great step towards getting the good result of the analysis, all the materials are defined by some properties such as Density, Young's modulus, Poisson's ratio and so on. **Table 3-4** shows the crane material specification for this case of the study (Hibbeler & Fan, 2004).

Table 3-4, Tower Crane Material Properties

|		
Young's Modulus (Pa)	E	2e+11
Poisson's Ration	υ	0.3
Density (kg/m3)	ρ	7850
Tensile Strength (Pa)		2.5e+8
Compressive Yield Strength (Pa)		2.5e+8
Tensile Ultimate Strength (Pa)		4.6e+8

3.4.3. Meshing

An essential and complex pre-process step at finite element software is Meshing. Meshing system consist of points (Node) which make a grid (Mesh). At meshing step the geometry model divide into elements. Mesh contains the material and structure properties. Density is assigned to the Nodes and high stress regions usually have more node density than the little or no stress. Mesh behaviour is as same as spider web which formed by node. Material properties are carried by this web of vector.

Software use two method of meshing: manual and automatic. Manual meshing is happened just by taking a long time. The other way which is automatic meshing, which is done by the system algorithm and it is common way of the meshing. Auto-mesh has been used for this tower crane.

3.4.4. Load and Constrain

Payload dynamic behavior during the swinging motion has been calculated from the Equations (Chapter 3.2.3). Data from other Equations were used to calculate the effects of the force on the reaction at the base point of the payload. Force reaction data is required in the analysis of the tower crane dynamic response when using the Ansys Workbench. In order to analyze the cranes behavior under the pendulation motion, six points along the jib will be considered. **Figure 3-8** shows the dimension and position of those six points.
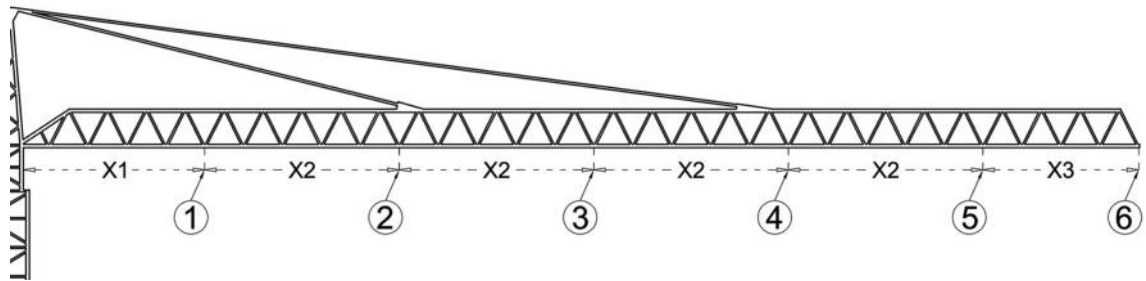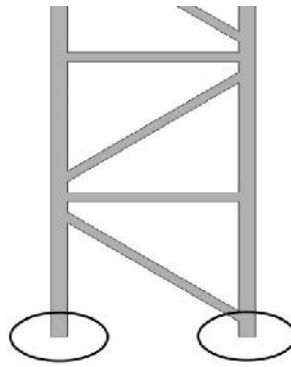

Figure 3-8, Pay Load Positions along the Jib

Where,

$$\begin{cases} X1 = 7916 \ (mm) \\ X2 = 8500 \ (mm) \\ X3 = 6807 \ (mm) \end{cases}$$

Based on the real situation, cranes are fixed at the ground to avoid collapsing during the operation. This tower crane supposed attached to the ground then tow line (Nodes and Grids) at the base of the crane has been chosen as fixed and non-moveable support (**Figure 3-9**).

46

Figure 3-9, Apply the constrain at the base of the tower crane

3.4.5. Solving the Problem and Result

Load and constrain have been defined. Dynamic load is applied at each point (six point totally) and solving bottom is pressed. Analysis of the each point presented by the digits which those information give the crane reaction under the payload excitation. **Figure 3-10** shows the feature of the Ansys Workbench and how the loads attached along the jib.
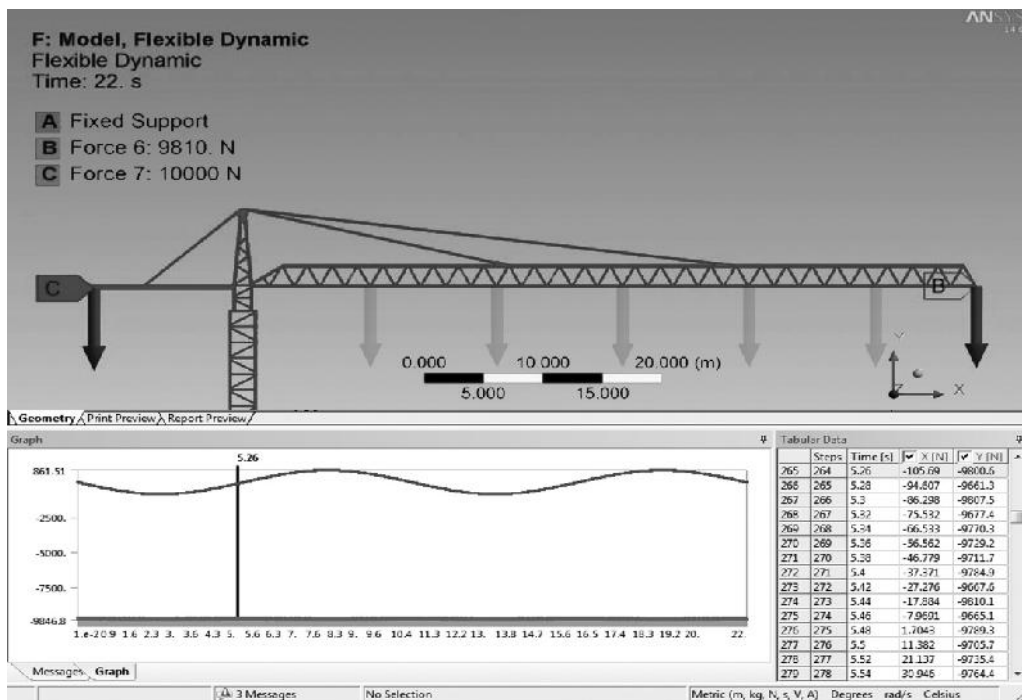

Figure 3-10, Attaching the Force along the Jib at Workbench

CHAPTER 4:   RESULT AND DISCUSTION

4.1. Pendulation Equation of Motion Output

Based on the previous chapters (Chapters (2.2) and (3.2)), the pendulum differential Equation (Equation (3.9)) was derived, and MATLAB code (Appendix A) was applied in order to obtain the results. **Figure 4-1** and **Figure 4-2** show the (r) and (θ) over a time span of 22 seconds.
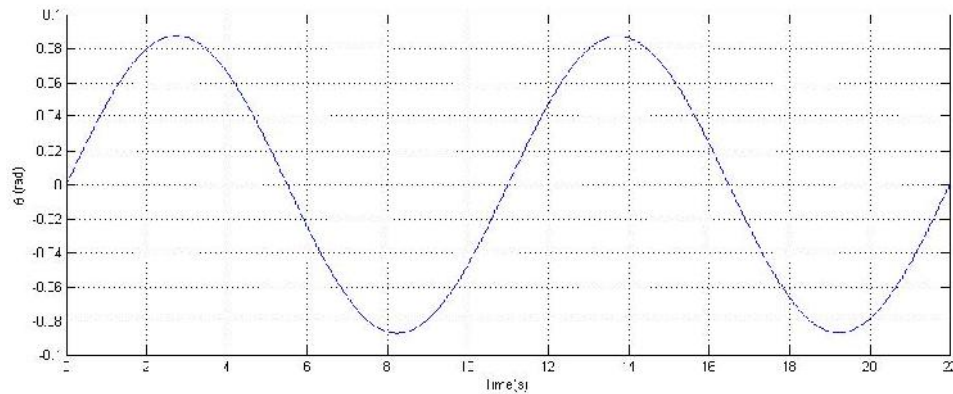
**Figure 4-1**, θ variations in 22 seconds

As both the cable and the mass have pendulation motion, then the angle between the resting and the current position will also change. **Figure 4-1** shows the change over a 22 second period (2 cycles).
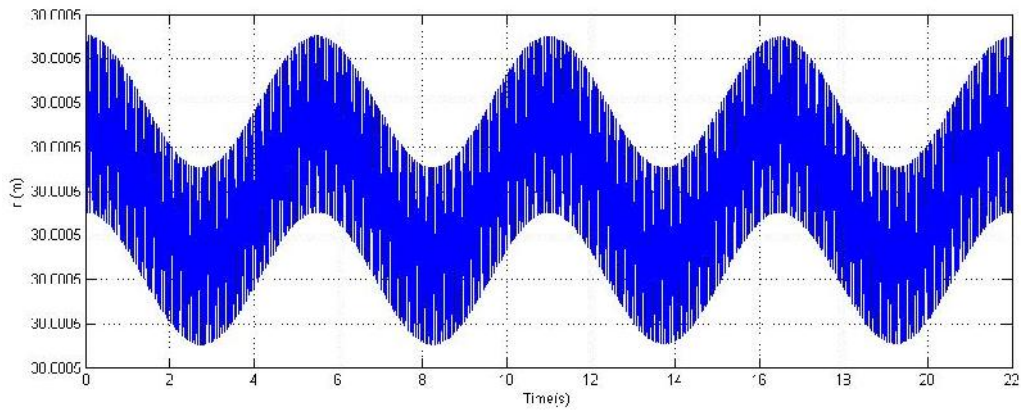
Figure 4-2, Cable length variations in 22 seconds

In **Figure 4-2** the band of the variation of the cable length illustrates that the cable length changes extremely fast during the cycles.

Figure 4-3 gives a more focused snapshot of a 0.3 second portion of the 22 second time, while displaying a clearer picture of the wide band seen in **Figure 4-2**. As it shown, the rope change is about 0.008 mm with high frequency (0.045 Hz) at longitudinal vibration.
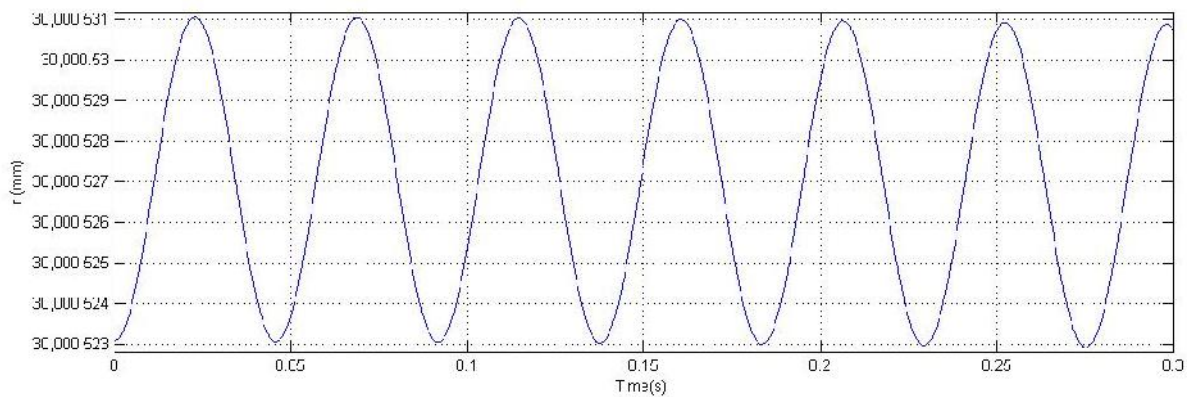

Figure 4-3, Cable length variation in 0.3 second

Variation of (r) and (θ) were shown at **Figure 4-1** and **Figure 4-2**. These data use for calculation of the force reactions on the base of the pendulum (Based on Chapter3.2.3 and Equations (3.13), (3.15) and (3.16)).

Figure 4-4 and **Figure 4-5** were plotted to show the F_x and F_y variation based on (r) and (θ). From this, it becomes obvious that the high longitudinal vibration along the cable has influence on the force reaction, mostly F_y. Small change at the cable length ($\approx$0.008 mm) made the force reaction in both directions (x-y) nonlinear, especially, F_y has change about 150N.
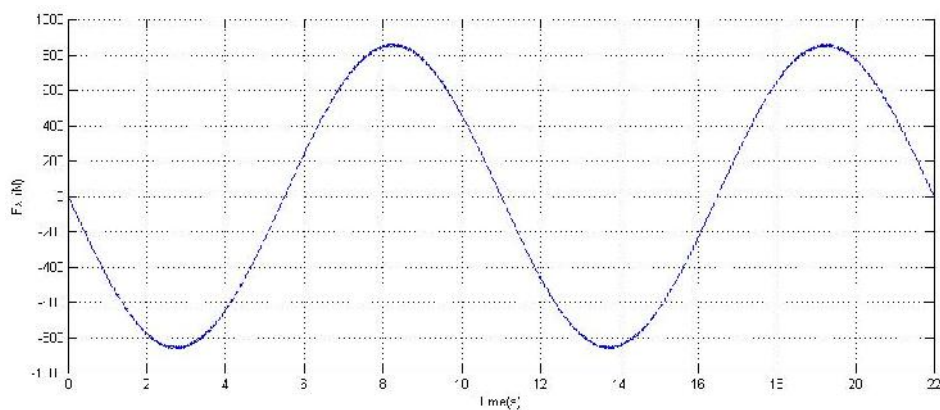
Figure 4-4, Variations of the F_x in time
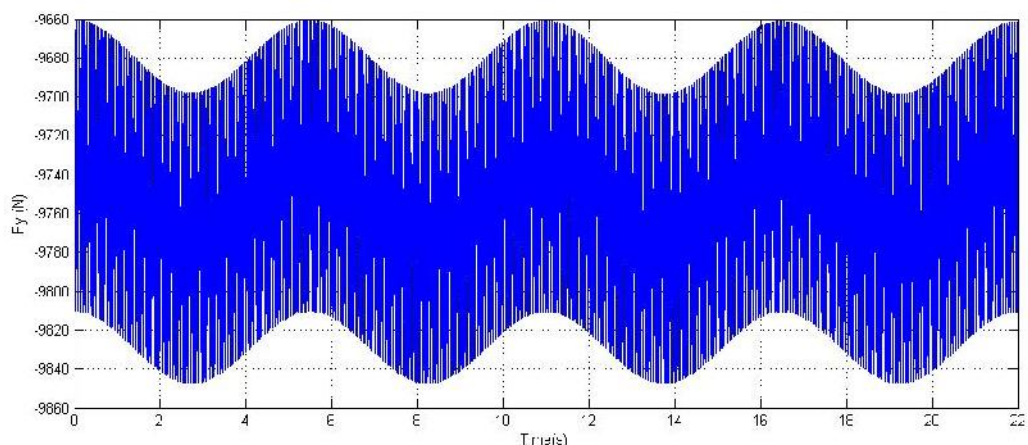
Figure 4-5, Variations of the F_y in time

To show the portion of the F_y variation (**Figure 4-5**), **Figure 4-6** has been plotted over a 0.3 second period.
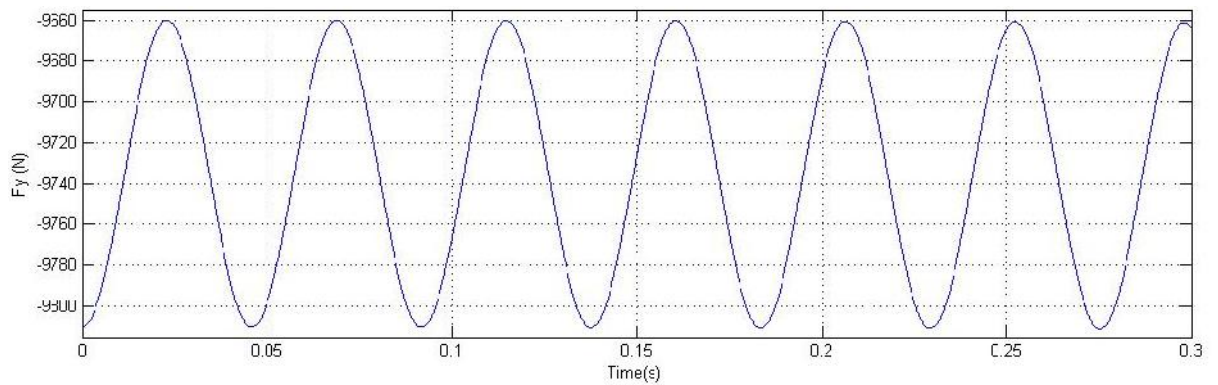
Figure 4-6, F_y variation in 0.3 second

4.2. Mathematical Model of the Tower Crane

Mathematical modal analysis for the simple 2-D tower crane has been explained in previous chapters (Chapter 2.3.2 and Chapter 0). Solving the Equation (3.34) and finding the first four roots yields,

$$\lambda_1 l = 1.2165$$

$$\lambda_2 l = 1.2479$$

$$\lambda_3 l = 3.1399$$

$$\lambda_4 l = 3.1416$$

Based on the Equation (3.35), $\lambda_n l$ and **Table 3-3** the first four natural frequencies (ω_n) can be calculated as:

$$\omega_1 = \frac{(\lambda_1 l)^2}{l^2}\sqrt{\left(\frac{EI}{A\rho}\right)} = \frac{1.2165^2 \times 3235}{54.2^2} = 1.39\,(rad/\sec) \rightarrow 0.22\,(Hz)$$

$$\omega_2 = \frac{(\lambda_2 l)^2}{l^2}\sqrt{\left(\frac{EI}{A\rho}\right)} = \frac{1.2479^2 \times 3235}{54.2^2} = 1.46\,(rad/\sec) \rightarrow 0.23\,(Hz)$$

$$\omega_3 = \frac{(\lambda_3 l)^2}{l^2}\sqrt{\left(\frac{EI}{A\rho}\right)} = \frac{3.1399^2 \times 3235}{54.2^2} = 9.27\,(rad/\sec) \rightarrow 1.47\,(Hz)$$

$$\omega_4 = \frac{(\lambda_4 l)^2}{l^2}\sqrt{\left(\frac{EI}{A\rho}\right)} = \frac{3.1416^2 \times 3235}{54.2^2} = 9.28\,(rad/\sec) \rightarrow 1.48\,(Hz)$$

Table 4-1 shows the analytical calculations of the first four natural frequencies of the simple mathematical model of the 2-D tower crane. This table is presented for verification of the output data from the software.

Table 4-1, First Four Natural Frequencies of Analytical Method

Mode	Frequency (Hz)
1st	0.22
2nd	0.23
3rd	1.47
4th	1.48

4.3. Dynamic Analysing of the Tower Crane

Equation (3.9) was solved as part of this experiment. As one of the factors that was defined during the oscillation was time (θ_t), this allowed for Equations (3.15) and (3.16) to also be solved, based on the (θ_t). For the purpose of this investigation, time duration was divided into small segments (0.1s) and all the force components were defined in these segments; these were also used in the finite element software calculations. **Table 4-2** shows some of the force components at play in each time segment.

Table 4-2, Variations of the (F_x) and (F_y) during a 22 second time period

T (s)	0	0.1	0.2	0.3	…	21.7	21.8	21.9	22
F_x (N)	-851.7	-850.4	-846.3	-839.6	…	-841.5	-847.6	-851	-851.7
F_y (N)	9735.5	9736	9737.4	9739.8	…	9739.1	9737	9735.8	9735.5

In order to calculate the dynamic behavior of the tower crane during the specified time period, the jib was divided into 6 semi equal parts. The results of the force components **Table 4-2** were also used as input data for the software calculations.

4.3.1. Modal Analysis of the Tower Crane

Modal analysis of the tower crane, by using the Ansys Workbench, yields both the mode shapes and the related frequencies. **Table 4-3** shows the first four modes analyzed.

<div align="center">**Table 4-3**, First Four Mode of the Tower Crane</div>

Mode	Frequency (Hz)
1st	0.20
2nd	0.51
3rd	0.59
4th	1.51

These four natural frequencies illustrate the critical frequency of the tower crane. When comparing these data with both the software and analytical method data **Table 4-4**, the accuracy of the finite elements software, as well as that of the analytic data, is verified.

<div align="center">**Table 4-4**, Comparison between the Analytical and software modal frequencies</div>

Mode	Analytical Frequency (Hz)	Software Frequency (Hz)
1	0.22	0.20
2	0.23	0.51
3	1.47	0.59
4	1.48	1.51

First and fourth modes of vibrations (ω_1 and ω_4) are on the crane body (Tower and Jib) that's why Mathematical and software method had almost same result (2% and 10% error), but second and third modes (ω_2 and ω_3) are on the crane suspensions rod and showed the error on simplified and complex model.

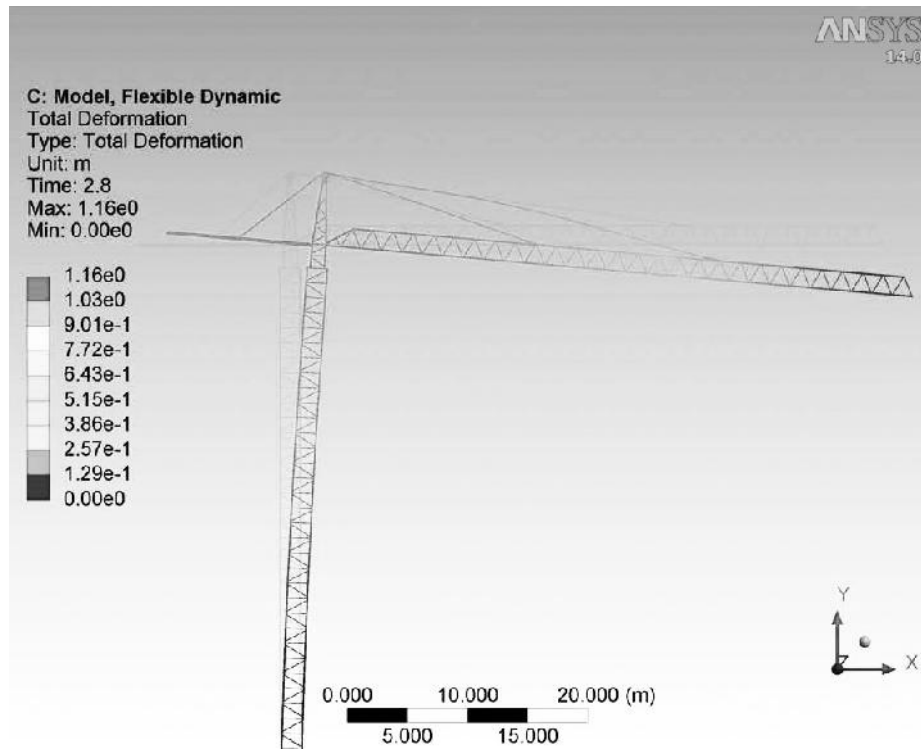**Figure 4-7**, Tower Crane Deformation (Scale 4.3x)
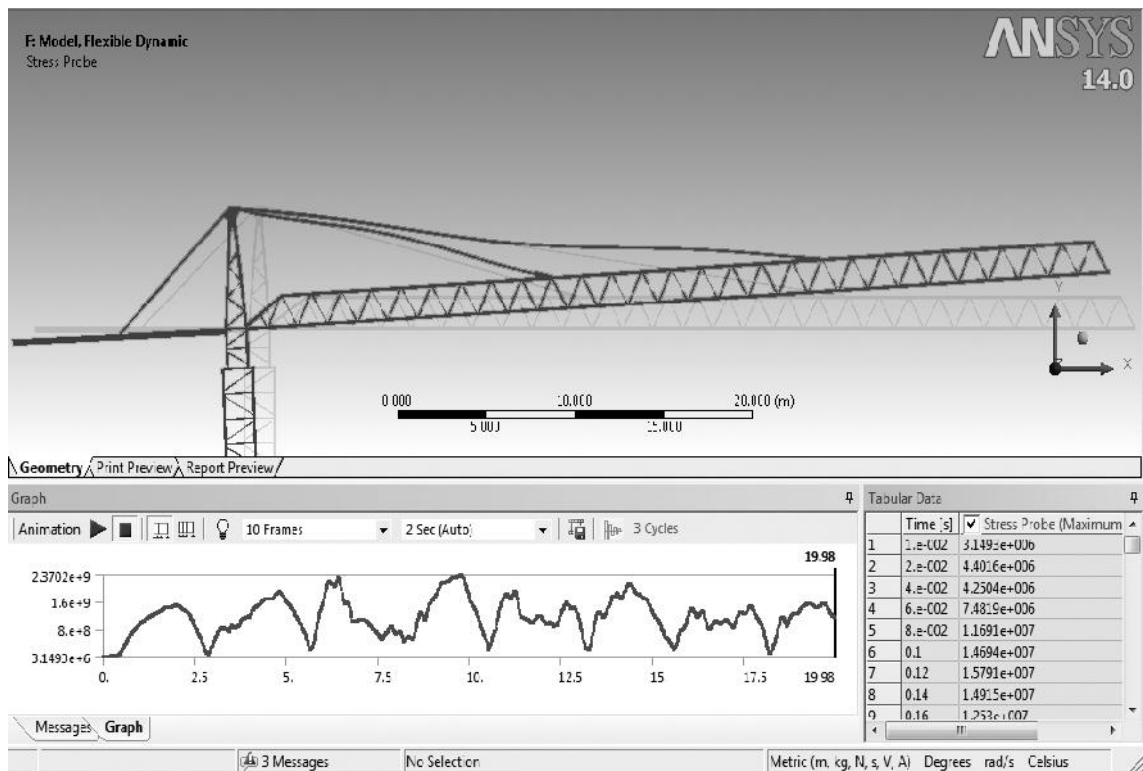
Figure 4-8, Workbench Feature of the Modal Flexible Dynamics Analysis

4.3.2. Result of the Six Points along the Jib

For showing the reaction of the tower crane under the swinging of the payload, all of six points (Chapter 3.4.4 and **Figure 3-8**) have been analyzed. Results are shown in the figures and clarify the effect of the distance under the same load excitation (**Figure 4-4** and **Figure 4-5**).
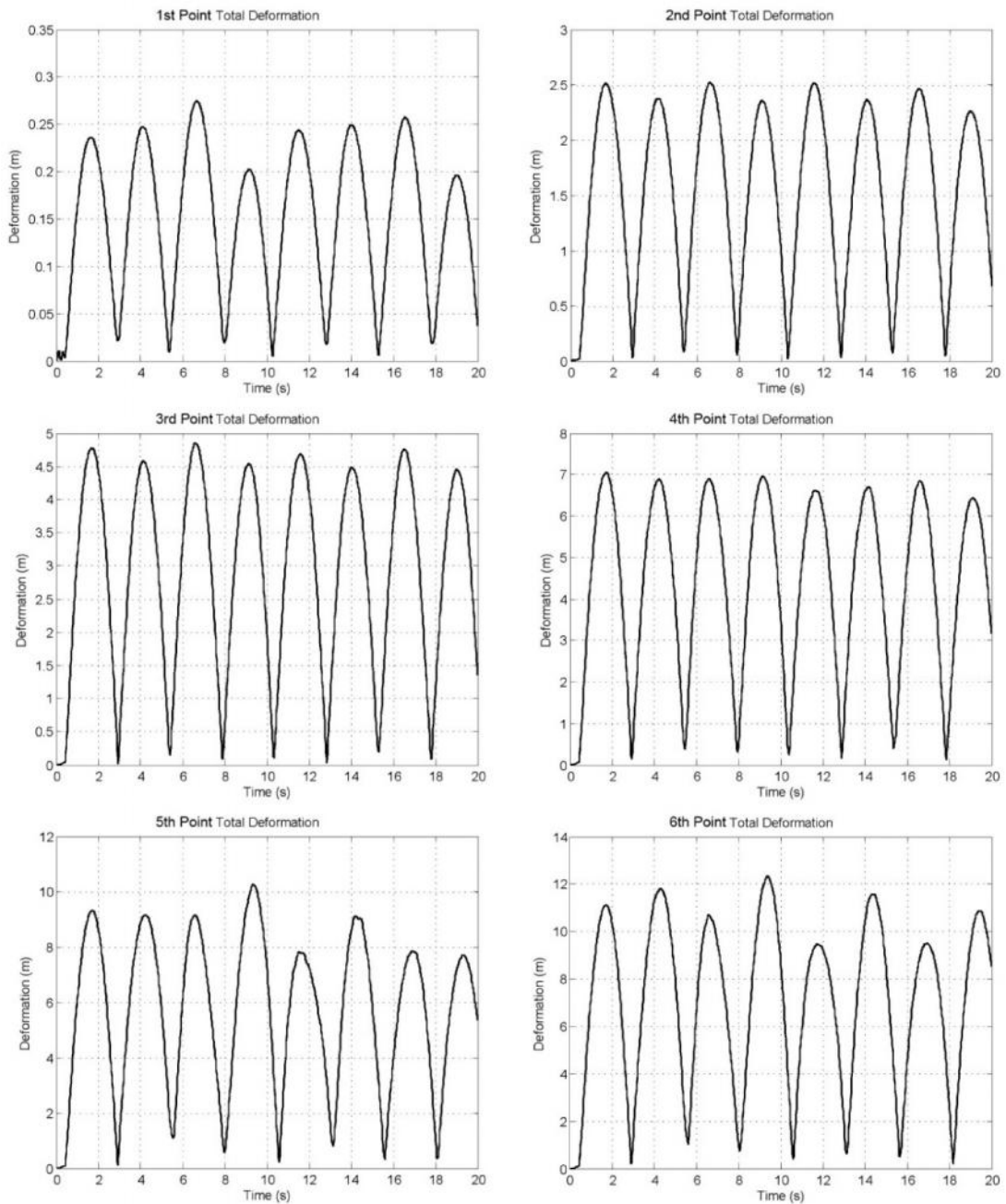
Figure 4-9, Total Deformation Effects of the Crane Body

Figure 4-9 shows the total deformation of the tower crane from the original position under the same swinging payload force at different position. To illustrate the effects of the load position and compare them together **Figure 4-10** has been printed.
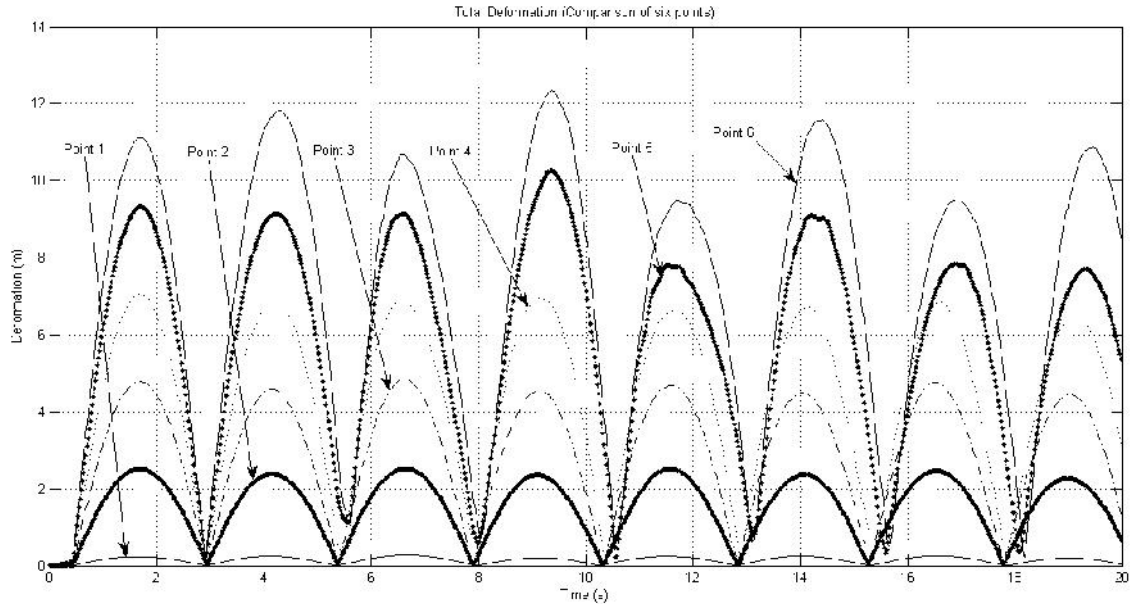
Figure 4-10, Total deformation effects on the tower crane under the same excitation but different positions of payload
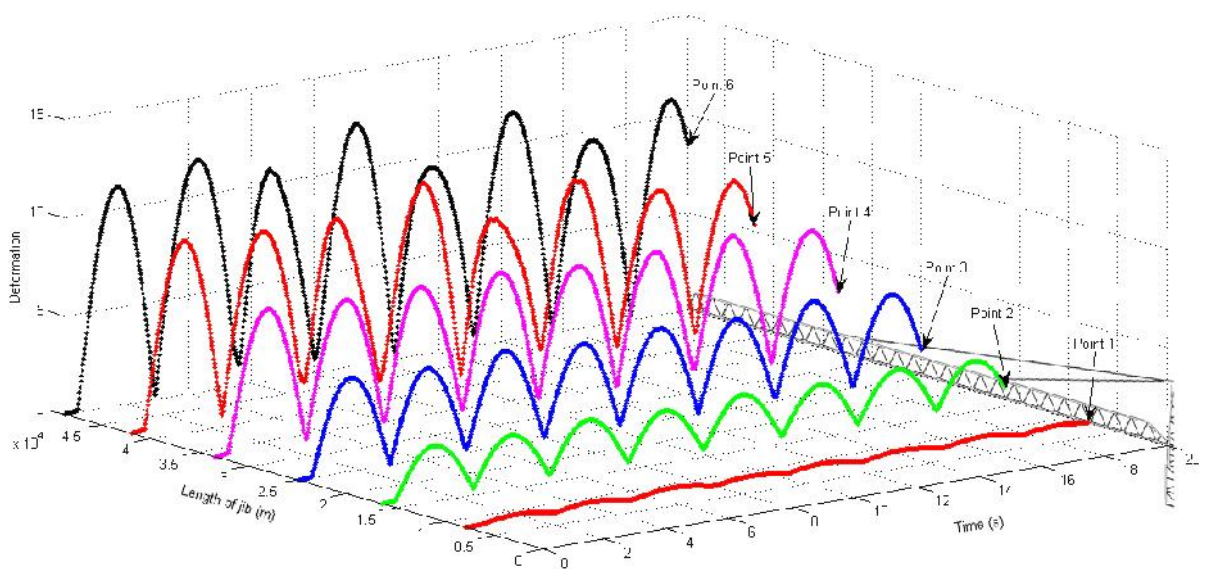
Figure 4-11, Comparison of total deformation effects based on the length of jib length

57
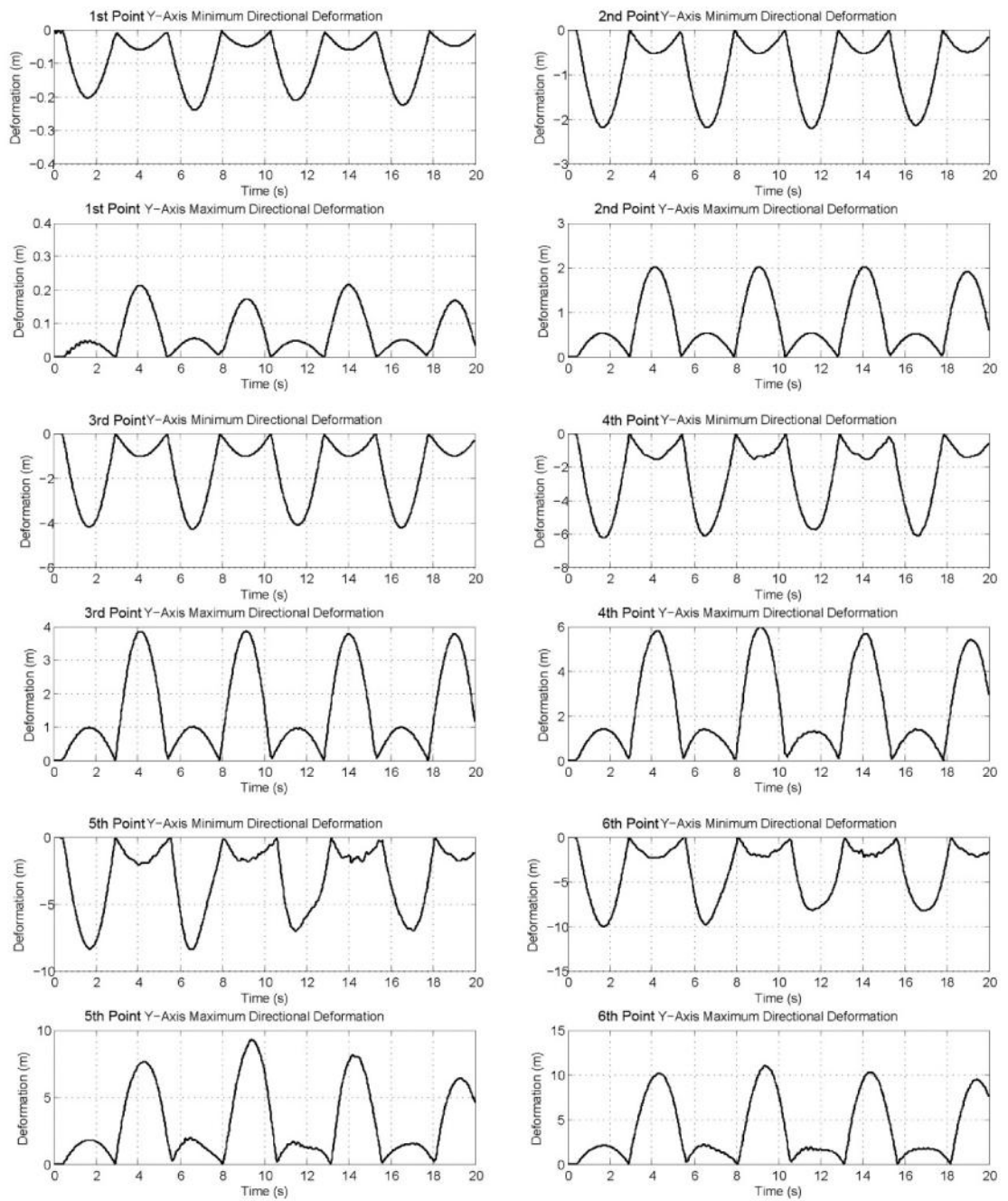
Figure 4-12, Y-Axis Direction Deformation Reaction of the Crane
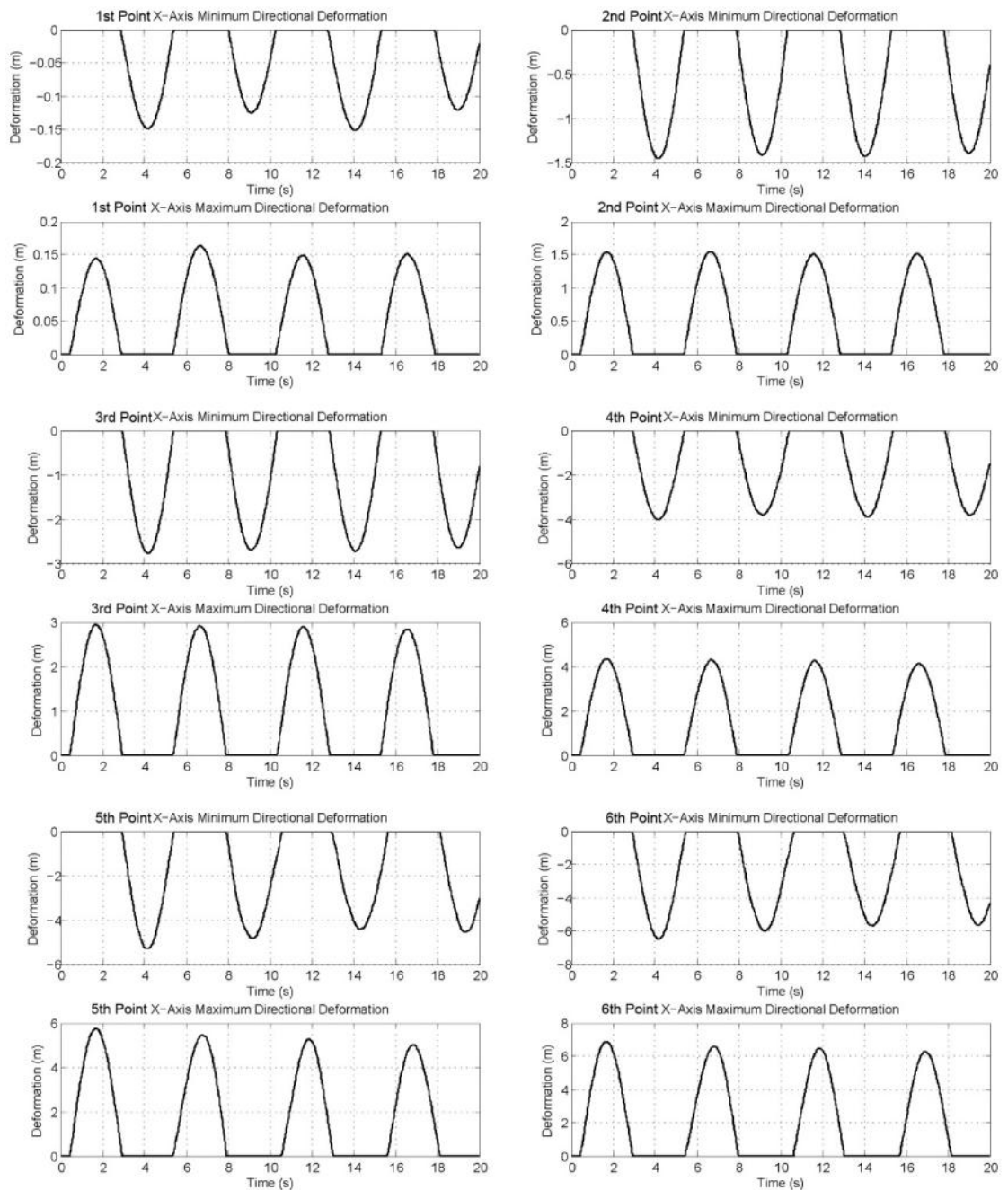
Figure 4-13, X -Axis Direction Deformation Reaction of the Crane

Figure 4-9 showed the overall total deformation from original point but **Figure 4-12** and **Figure 4-13** show the maximum and minimum deformations at (*x*) and (y) directions which clarify the effects of distance and time at each coordinates.
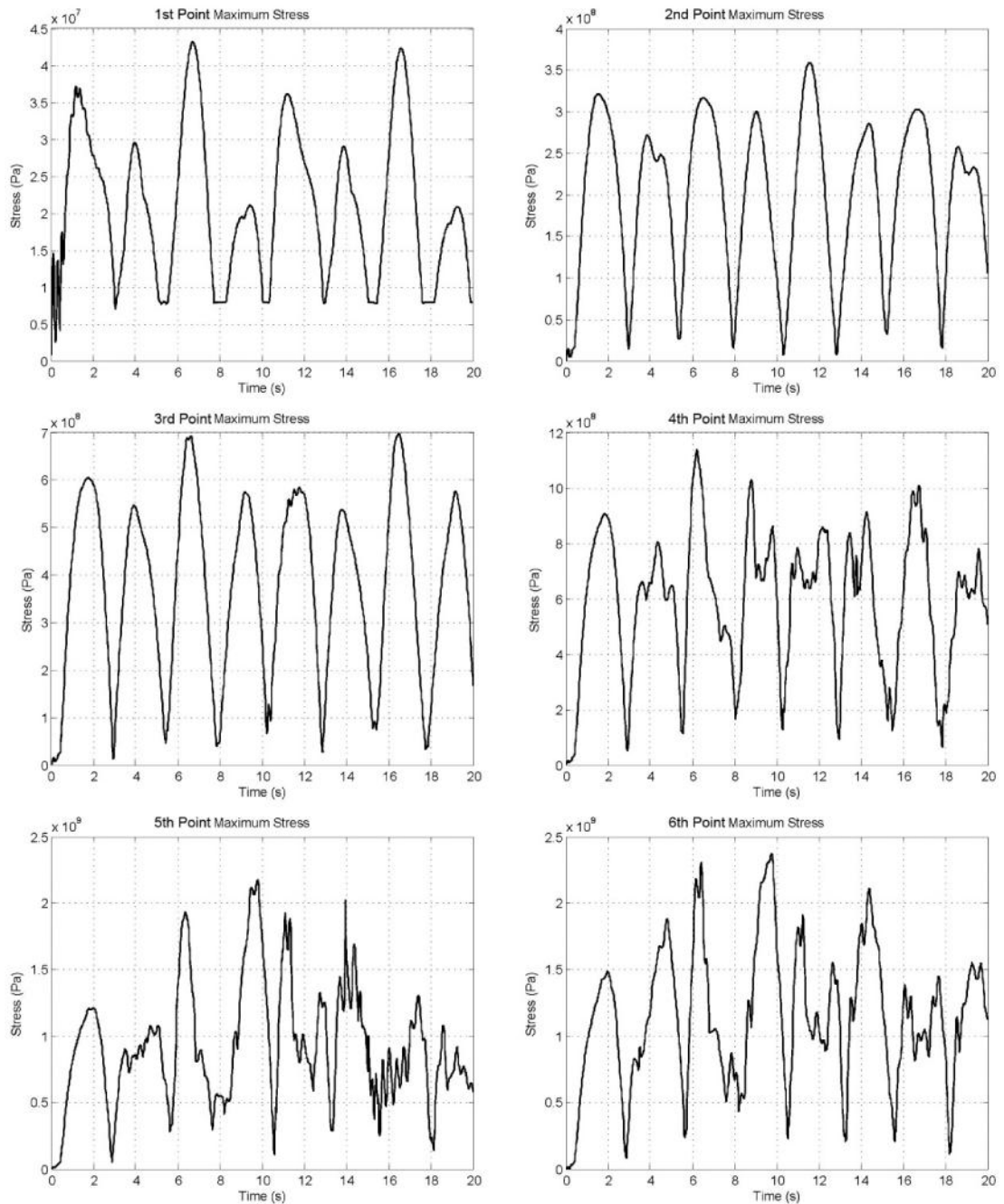
Figure 4-14, Stress of Crane Base (Based on the Maximum Principal

Stress is most important parameter for designer. Overload and high stresses are a danger and can collapse the structure which can kill people, waist the time and money. That's why; first option which is considered by designer is stress. Payload motion effects also appear as stress on the crane body. **Figure 4-14** shows the stress during the swing motion of the payload and its effect on the base of the tower crane. **Figure 4-15**

60

illuminates all six point stresses at one figure. This figure also clarifies, the points which are near the tip of the Jib, have critical condition.
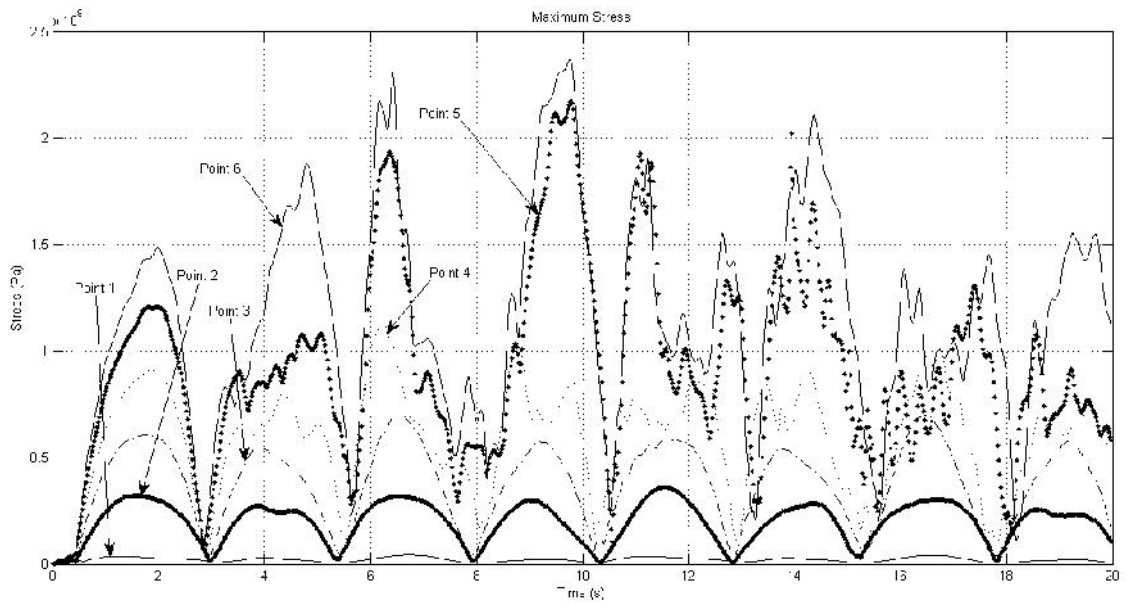

Figure 4-15, Stress effects on the base of tower crane under the same excitation but different positions of payload
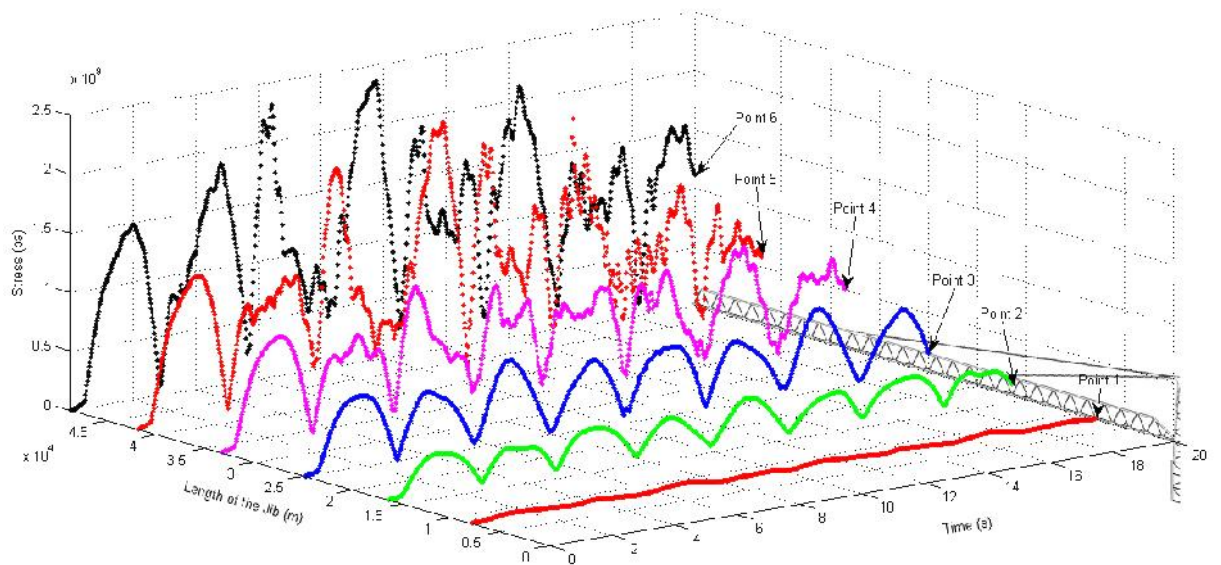
**Figure 4-16**, Comparison of the stress effects based on the jib dimension

If material deformation exceed over the elastic limit, it cannot go back to the original shape; then plastic deformation happens (Wang et al., 2010). To avoid the plastic deformation elastic strain should be under its limitations. **Figure 4-17** has been plotted to illuminate the strain of the crane body under the payload dynamics load.
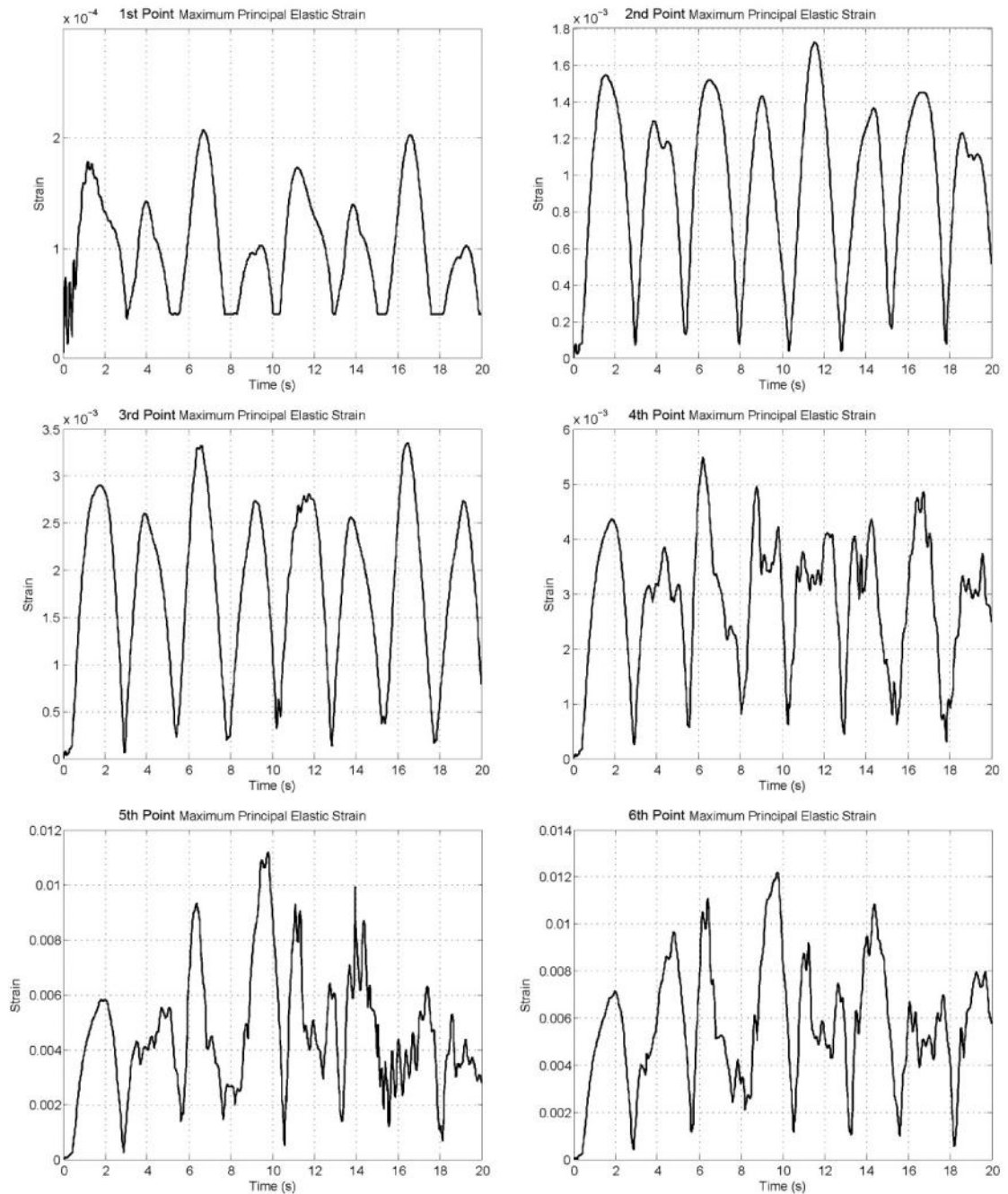
Figure 4-17, Elastic Stain of Crane Base (Based on the Maximum Principal)
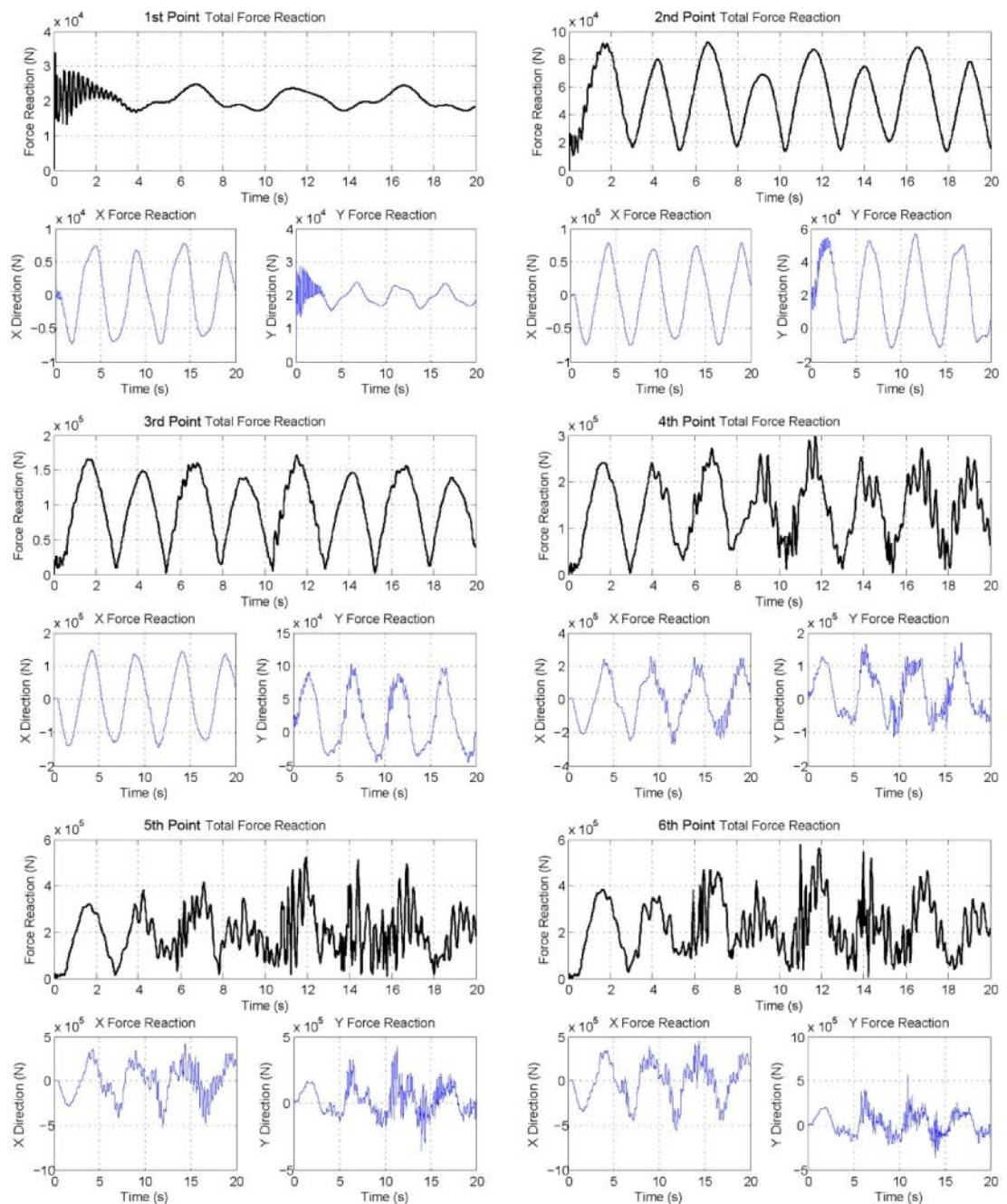
Figure 4-18, Total, X and Y Directional Force Reaction of the Crane

One of the useful information in the crane analysis is Force Reaction. **Figure 4-18** shows that reaction at the fixed support (base of the crane) and its variation during the time. Knowing about the reaction at the base will help to design the safe structures such as Crane. Total force is summation of two components. **Figure 4-18** also shows the force reaction components in (x) and (y) directions.

CHAPTER 5: CONCLUSIONS

For the purpose of this investigation a model of a tower crane was constructed, and results were analysed and compared using Mathematical and FEM software (**Table 4-1** and **Table 4-3**). The first four natural frequencies (ω_n, $n : 1, 2, 3, 4$) of the two methods (Mathematical and FEM model) were compared, and the accuracy of the FEA software was demonstrated (**Table 4-4**). Results, using the Payload Equation of motion, showed that cable stiffness is an important factor to consider as, not only did it cause small changes in the cable length ($\approx$0.008mm) but, at each fluctuation, it also generated nonlinear force variation ($\approx$150N) at the base of the cable where it attached to the jib. In addition, it caused high frequency ($\approx$22.21Hz) vibration which appeared as force along the cable. Six analyses were executed using the FEA software for the six different points where the payload was attached to the jib. Initial condition and force reactions were kept at the same value for each point analysed (**Table 3-1** and **Table 3-2**). Based on the acquired results, the length difference between the first and the sixth point was approximately 6.15 times, whereas the crane deformation showed an increase of approximately 62 times. In addition, the stress at the crane base, which was induced by the pendulum vibration, was also seen to increase by approximately 8.8 times between point 1 and point 6. These observations demonstrate the important and influential role of position of the load along the jib. Further to this, the swinging effect of the payload on the tower crane body was studied. The results (**Figure 4-9** to **Figure 4-18**) provided insight into the importance of this factor, and offered information that may prove useful to enhance the safety of future tower crane designs.

In summary, this investigation found that during high wind or storm conditions, when a tower crane was operating under a heavy load which was attached near the tip of

the jib, the swinging of the load put it at a higher risk for collapse. This risk was seen to decrease as the position of the load moved away from the tip. Inevitably, as collapse could lead to workplace injuries and fatalities, this is an important finding requiring further consideration.

Future Work

After critically analysing the steps in this investigation and considering the results from it, I plan to build on the findings and take the study a step further, by creating a 3D model of the tower crane with the actual elements, shapes and sizes. Only through the analysis of payload effects using a 3D model can the real reaction of the tower crane be explored.

REFERENCES

Abdel-Rahman, EM, & Nayfeh, AH. (2002). Pendulation reduction in boom cranes using cable length manipulation. *Nonlinear Dynamics, 27*(3), 255-269.

Ahmad, MA. (2009). Sway Reduction on Gantry Crane System using Delayed Feedback Signal and PD-type Fuzzy Logic Controller: A Comparative Assessment. *International Journal of Computer Systems Science and Engineering, 4*(3).

Arfken, G.B., Weber, H.J., & Harris, F.E. (2005). *Mathematical Methods For Physicists International Student Edition*: Academic press.

Arnold, E, Sawodny, O, Hildebrandt, A, & Schneider, K. (2003). *Anti-sway system for boom cranes based on an optimal control approach*.

Baruh, H. (1999). *Analytical dynamics*: WCB/McGraw-Hill.

Beer, F.P., & Johnston, E.R. (2011). *Statics and mechanics of materials*: McGraw-Hill.

Bishop, R.E.D., & Johnson, D.C. (2011). *The mechanics of vibration*: Cambridge University Press.

Bishop, RED, & Johnson, DC. (1960). The mechanics of vibration 1960: Cambridge University Press.

Chaplin, CR. (1995). Failure mechanisms in wire ropes. *Engineering Failure Analysis, 2*(1), 45-57.

Chapra, SC, & Canale, RP. (1998). Numerical Method for Engineers [M J. USA: the McGraw—Hil Companies: Inc.

CHEN, G.D., & JIA, P.F. (2008). Robust decentralized trajectory tracking control of robot manipulators based on extended state observer. *Acta Automatica Sinica, 34*(7), 828-832.

Cho, S.K., & Lee, H.H. (2000). *An anti-swing control of a 3-dimensional overhead crane*.

Cveticanin, L. (1995). Dynamic behavior of the lifting crane mechanism* 1. *Mechanism and machine theory, 30*(1), 141-151.

Davis, R., Henshell, RD, & Warburton, GB. (1972). A Timoshenko beam element. *Journal of Sound and Vibration, 22*(4), 475-487.

Ferreira, JV, & Ewins, DJ. (1996). *Nonlinear receptance coupling approach based on describing functions*.

Fletcher, R., & Powell, M.J.D. (1963). A rapidly convergent descent method for minimization. *The Computer Journal, 6*(2), 163-168.

Fowles, G.R., & Cassiday, G.L. (1999). *Analytical mechanics*: Saunders College Pub.

Fujioka, DD, Rauch, A, Singhose, WE, & Jones, T. (2009). *Tip-over stability analysis of mobile boom cranes with double-pendulum payloads*.

Ghigliazza, RM, & Holmes, P. (2002). On the dynamics of cranes, or spherical pendula with moving supports. *International journal of non-linear mechanics, 37*(7), 1211-1221.

Ginsberg, J.H. (1998). *Advanced engineering dynamics*: Cambridge University Press.

Golafshani, AR, & Aplevich, JD. (2002). *Computation of time-optimal trajectories for tower cranes*.

Gregory, R.D. (2006). *Classical mechanics: an undergraduate text*: Cambridge Univ Pr.

Groesberg, S.W. (1968). Groesberg (1968) Advanced mechanics.

Hayashi, C., Shepard, S., Winkler, I., Glenn, S., Harris, E., Quaid, D., Hershey, B., Kaufman, P., Chartoff, R., & Wolfe, T. (1964). *Nonlinear oscillations in physical systems* (Vol. 33): McGraw-Hill New York.

Hibbeler, R.C. (2002). *Engineering mechanics*: Pearson Education.

Hibbeler, R.C., & Fan, SC. (2004). *Statics and mechanics of materials* (Vol. 2): Prentice Hall.

Huang, D.T., & Chen, DK. (2007). Dynamic characteristics of a structure with multiple attachments: A receptance approach. *Journal of Sound and Vibration, 307*(3), 941-952.

Jerman, B, & Kramar, J. (2008). A study of the horizontal inertial forces acting on the suspended load of slewing cranes. *International Journal of Mechanical Sciences, 50*(3), 490-500.

Jerman, B, Podraj, P, & Kramar, J. (2004). An investigation of slewing-crane dynamics during slewing motion--development and verification of a mathematical model. *International Journal of Mechanical Sciences, 46*(5), 729-750.

José, J.V., & Saletan, E.J. (1998). *Classical dynamics: a contemporary approach*: Cambridge Univ Pr.

Ju, F., & Choo, YS. (2003). *Dynamics Characteristic of Tower Cranes*.

Kiliçslan, S., Balkan, T., & Ider, SK. (1999). Tipping loads of mobile cranes with flexible booms. *Journal of Sound and Vibration, 223*(4), 645-657.

Kim, C.S., & Hong, K.S. (2009). Boundary control of container cranes from the perspective of controlling an axially moving string system. *International Journal of Control, Automation and Systems, 7*(3), 437-445.

Kondo, R, & Shimahara, S. (2005). *Anti-sway control of a rotary crane via switching feedback control*.

Kosiski, J. (2005). Swing-free stop control of the slewing motion of a mobile crane. *Control Engineering Practice, 13*(4), 451-460.

Kreyszig, E. (2007). *Advanced engineering mathematics*: John Wiley & Sons.

Lacarbonara, W., Soper, R.R., Nayfeh, A.H., & Mook, D.T. (2001). A nonclassical vibration absorber for pendulation reduction. *Journal of Vibration and Control, 7*(3), 365-393.

Lahres, S., Aschemann, H., Sawodny, O., & Hofer, E.P. (2000). *Crane automation by decoupling control of a double pendulum using two translational actuators*. Paper presented at the American Control Conference, 2000. Proceedings of the 2000.

Maczynski, A, & Wojciech, S. (2003). Dynamics of a Mobile Crane and Optimisation of the Slewing Motion of Its Upper Structure. *Nonlinear Dynamics, 32*(3), 259-290.

Matthews, G.P., & DeCarlo, R.A. (1988). Decentralized tracking for a class of interconnected nonlinear systems using variable structure control. *Automatica, 24*(2), 187-193.

McGill, D.J., & King, W.W. (1995). *Engineering mechanics*: Pws-Kent.

Meriam, J.L., & Kraige, L.G. (2006). *Engineering Mechanic (Vol. 2) Dynamics 5Th Ed*: Wiley-India.

Neitzel, R.L., Seixas, N.S., & Ren, K.K. (2001). A review of crane safety in the construction industry. *Applied Occupational and Environmental Hygiene, 16*(12), 1106-1117.

Neupert, J, Arnold, E, Schneider, K, & Sawodny, O. (2010). Tracking and anti-sway control for boom cranes. *Control Engineering Practice, 18*(1), 31-44.

Oguamanam, DCD, Hansen, JS, & Heppler, GR. (2001). Dynamics of a three-dimensional overhead crane system. *Journal of Sound and Vibration, 242*(3), 411-426.

Okubo, Y, Fujii, T, Kono, S, Monzen, T, & Uchida, K. (1997). Development of Vibration Control System on Container Crane Girder. *MITSUBISHI JUKO GIHO, 34*, 50-53.

Omar, HM, & Nayfeh, AH. (2005). Gantry cranes gain scheduling feedback control with friction compensation. *Journal of Sound and Vibration, 281*(1-2), 1-20.

Parker, GG, Groom, K, Hurtado, J, Robinett, RD, & Leban, F. (2002). *Command shaping boom crane control system with nonlinear inputs*.

Pierson Jr, W.J., & Moskowitz, L. (1964). A proposed spectral form for fully developed wind seas based on the similarity theory of SA Kitaigorodskii. *Journal of geophysical research, 69*(24), 5181-5190.

Riley, KF, Hobson, MP, Bence, SJ, & Spector, D. (1999). Mathematical methods for physics and engineering. *American Journal of Physics, 67*, 165.

Room, WH, & Hall, W. (2012). Advanced mechanics of materials.

Sa irli, A, Bo oçlu, ME, & Ömürlü, VE. (2003). Modeling the Dynamics and Kinematics of a Telescopic Rotary Crane by the Bond Graph Method: Part I. *Nonlinear Dynamics, 33*(4), 337-351.

Sawodny, O, Aschemann, H, Kumpel, J, Tarin, C, & Schneider, K. (2002). *Anti-sway control for boom cranes*.

Schaub, H. (2008). Rate-based ship-mounted crane payload pendulation control system. *Control Engineering Practice, 16*(1), 132-145.

Scheck, F. (1999). Mechanics: from Newton's laws to deterministic chaos.

Shen, Y, Yano, K, & Terashima, K. (2003). *Sway control of rotary crane using straight transfer transformation method considering the variation of rope length*.

Shen, Y., Terashima, K., & Yano, K. (2003). Optimal Control of Rotary Crane Using the Straight Transfer Transformation Method to Eliminate Residual Vibration. DAGGER. *Transactions, 39*(9), 817-826.

Singhose, W, & Kim, D. (2007). *Manipulation with tower cranes exhibiting double-pendulum oscillations*.

Sun, G, Kleeberger, M, & Liu, J. (2005). Complete dynamic calculation of lattice mobile crane during hoisting motion. *Mechanism and machine theory, 40*(4), 447-466.

Tabata, Y, Ichise, K, Ouchi, S, & Liu, KZ. (2003). *Anti-sway control system of a rotational crane using a nonlinear controller*.

Terashima, K, Shen, Y, & Yano, K. (2007). Modeling and optimal control of a rotary crane using the straight transfer transformation method. *Control Engineering Practice, 15*(9), 1179-1192.

Torkar, M, & Arzenek, B. (2002). Failure of crane wire rope. *Engineering Failure Analysis, 9*(2), 227-233.

Török, J.S. (2000). *Analytical mechanics: With an introduction to dynamical systems*: Wiley.

Towarek, Z. (1998). The dynamic stability of a crane standing on soil during the rotation of the boom. *International Journal of Mechanical Sciences, 40*(6), 557-574.

Wang, H., Wu, PD, Tomé, CN, & Huang, Y. (2010). A finite strain elastic–viscoplastic self-consistent model for polycrystalline materials. *Journal of the Mechanics and Physics of Solids, 58*(4), 594-612.

Wilson, E.L. (1996). Three-Dimensional Static and Dynamic Analysis of Structures. *Computers and Structures, Inc., Berkeley, CA*.

Witz, JA. (1995). Parametric excitation of crane loads in moderate sea states. *Ocean Engineering, 22*(4), 411-420.

Yi, J., Yubazaki, N., & Hirota, K. (2003). Anti-swing and positioning control of overhead traveling crane. *Information Sciences, 155*(1), 19-42.

Appendix

A.1. MATLAB Functions

In Chapter 3.2 a pendulum differential Equation of motion was derived. As an exact solution for that differential Equation does not exist, then the Runge-Kutta fifth-order (Butcher) was used as a numerical method (Chapter 2.2.5) to solve this set of multi variable differential Equations. In addition, MATLAB software was used to evaluate the answer

$$
\begin{cases}
\ddot{r} - r\dot{\theta}^2 + \dfrac{k}{m}(r - r_0) + \dfrac{c}{m}\dot{r} - g\cos\theta = 0 \\[3mm]
\ddot{\theta} + \dfrac{2}{r}\dot{r}\dot{\theta} + \dfrac{c}{m}r\dot{\theta} + \dfrac{g}{r}\sin\theta = 0
\end{cases}
$$

Definition of two parameters (r) and (θ), and also their derivations ($\dot{r}$) and ($\dot{\theta}$).

$$y(1) = r \,;$$

$$y(2) = \theta \,;$$

$$y(3) = \dot{r} \,;$$

$$y(4) = \dot{\theta} \,;$$

Replacement of the functions based on the software methods.

$$y_1' = F(1) = y(3);$$

$$y_2' = F(2) = y(4);$$

$$y_3' = F(3) = y(1)*y(4)^2 - (k/m)*(y(1)-r) - g*cos(y(2));$$

$$y_4' = F(4) = -2/(y(1))*y(3)*y(4) - (c/m)*y(4) - (g/y(1))*sin(y(2));$$

A.1.1. Equation of Motion Function:

function F = fex7_5(x,y)

F = zeros(1,2);

g=9.81;

r=30;

c=10;

m=1000;

k=100000;

F(1)=y(3);

F(2)=y(4);

*F(3)=y(1)*y(4)^2-(k/m)*(y(1)-r)-g*cos(y(2));*

*F(4)=-2/(y(1))*y(3)*y(4)-(c/m)*y(4)-(g/y(1))*sin(y(2));*

A.1.2. Butcher Function:

function [xSol,ySol] = Butcher(dEqs,x,y,xStop,h)

if size(y,1) > 1 ; y = y'; end % y must be row vector

xSol = zeros(2,1); ySol = zeros(2,length(y));

xSol(1) = x; ySol(1,:) = y;

i = 1;

while x < xStop

i = i + 1;

h = min(h,xStop - x);

K1 = h*feval(dEqs,x,y);

K2 = h*feval(dEqs,x + h/4, y + K1/4);

K3 = h*feval(dEqs,x + h/4, y + K1/8 + K2/8);

K4 = h*feval(dEqs,x + h/2, y - K2/2 + K3);

K5 = h*feval(dEqs,x +3*h/4,y+(K1*3 + K4*9)/16);

K6 = h*feval(dEqs,x + h,   y+(-3*K1+2*K2+12*K3-12*K4+8*K5)/7);

y = y+(7*K1+32*K3+12*K4+32*K5+7*K6)/90;

x = x+h;

xSol(i) = x; ySol(i,:) = y;

end

A.1.3. Cable Tenssion Function:

m=1000;

g=9.81;

r=30;

D=5 % Rope Angle In Degree

T0=D*pi/180 % Rope Angle In Radian T0=0.0873

T=[-T0:T0/10:T0]

t=[0:0.1:5]; % Time

R=g.*m.*(2*cos(T0)-cos(T)) %Cable tension

Rx=R.*sin(T)

Ry=R.*cos(T)

V=sqrt(2.*g.*r.*(cos(T)-cos(T0))) %Payload Velocity

%g/r=0.327

%TS=dsolve('D2T+(0.327)*T=0','T(0)=0.0873','DT(0)=0')

T1=0.0873*cos(0.572*t)

R1=g.*m.*(2*cos(T0)-cos(T1)) %Cable tension Vs Time

R1x=R1.*sin(T1)

R1y=R1.*cos(T1)

wn=sqrt(g/r)

f=wn/(2*pi)

Per=2*pi/wn

CR=max(R1)

CT=max(T1)

A=subplot(2,1,1);plot(T,R)

grid on

xlabel('time (s)')

ylabel('Fx (N)')

subplot(2,1,2);plot(t,R1)

grid on

xlabel('time (s)')

ylabel('Fy (N)')

Appendix B

Analysis report of the Workbench (Sample)

The project was completed using Ansys Workbench version 14.0 Release

5.1. Units

Table 0-1, Units Defined

Unit System	Metric (m, kg, N, s, V, A) Degrees rad/s Celsius
Angle	Degrees
Rotational Velocity	rad/s
Temperature	Celsius

5.2. Model

5.2.1. Geometry

Table 0-2, Model Geometry

Object Name	*Geometry*
State	Fully Defined
Definition	

Type	DesignModeler
Length Unit	Millimeters
Element Control	Program Controlled
2D Behavior	Plane Stress
Display Style	Body Color
Bounding Box	
Length X	62.061 m
Length Y	60.5 m
Properties	
Volume	6.1483 m³
Mass	48264 kg
Surface Area(approx.)	61.483 m²
Scale Factor Value	1.
Statistics	
Bodies	1
Active Bodies	1
Nodes	13497
Elements	3617
Mesh Metric	None
Basic Geometry Options	
Parameters	Yes
Parameter Key	DS
Attributes	No
Named Selections	No
Material Properties	No
Advanced Geometry Options	
Use Associativity	Yes
Coordinate Systems	No

Reader Mode Saves Updated File	No
Use Instances	Yes
Smart CAD Update	No
Attach File Via Temp File	Yes
Analysis Type	2-D
Decompose Disjoint Faces	No
Enclosure and Symmetry Processing	Yes

Table 0-3, Model (D4, E4, F4) Geometry Parts

Object Name	*Part 1*
State	Meshed
Graphics Properties	
Visible	Yes
Transparency	1
Definition	
Suppressed	No
Stiffness Behavior	Flexible
Coordinate System	Default Coordinate System
Reference Temperature	By Environment
Thickness	0.1 m
Thickness Mode	Manual
Material	
Assignment	Structural Steel
Nonlinear Effects	Yes
Thermal Strain Effects	Yes
Bounding Box	

Length X	62.061 m
Length Y	60.5 m
Properties	
Volume	6.1483 m³
Mass	48264 kg
Centroid X	8.9022 m
Centroid Y	-11.435 m
Centroid Z	0. m
Moment of Inertia Ip1	1.917e+007 kg·m²
Moment of Inertia Ip2	6.7846e+006 kg·m²
Moment of Inertia Ip3	2.5955e+007 kg·m²
Surface Area(approx.)	61.483 m²
Statistics	
Nodes	13497
Elements	3617
Mesh Metric	None

5.2.2. Coordinate Systems

Table 0-4, Model Coordinate Systems

Object Name	*Global Coordinate System*
State	Fully Defined
Definition	
Type	Cartesian
Coordinate System ID	0.
Origin	

Origin X	0. m
Origin Y	0. m
Directional Vectors	
X Axis Data	[1. 0.]
Y Axis Data	[0. 1.]

5.2.3. Mesh

Table 0-5, Model Mesh

Object Name	*Mesh*
State	Solved
Defaults	
Physics Preference	Mechanical
Relevance	0
Sizing	
Use Advanced Size Function	Off
Relevance Center	Coarse
Element Size	Default
Initial Size Seed	Active Assembly
Smoothing	Medium
Transition	Fast
Span Angle Center	Coarse
Minimum Edge Length	2.0187e-002 m
Inflation	

Use Automatic Inflation	None
Inflation Option	Smooth Transition
Transition Ratio	0.272
Maximum Layers	5
Growth Rate	1.2
Inflation Algorithm	Pre
View Advanced Options	No
Patch Conforming Options	
Triangle Surface Mesher	Program Controlled
Advanced	
Shape Checking	Standard Mechanical
Element Midside Nodes	Program Controlled
Number of Retries	Default (4)
Extra Retries For Assembly	Yes
Rigid Body Behavior	Dimensionally Reduced
Mesh Morphing	Disabled
Defeaturing	
Use Sheet Thickness for Pinch	No
Pinch Tolerance	Please Define
Generate Pinch on Refresh	No
Sheet Loop Removal	No
Automatic Mesh Based Defeaturing	On
Defeaturing Tolerance	Default
Statistics	
Nodes	13497
Elements	3617
Mesh Metric	None

5.3. Modal

Table 0-6, Model Analysis

Object Name	Modal (D5)
State	Solved
Definition	
Physics Type	Structural
Analysis Type	Modal
Solver Target	Mechanical APDL
Options	
Environment Temperature	22. °C
Generate Input Only	No

Table 0-7, Modal Initial Condition

Object Name	Initial Condition
State	Fully Defined
Definition	
Pre-Stress Environment	None

Table 0-8, Modal Analysis Settings

Object Name	Analysis Settings
State	Fully Defined

Options	
Max Modes to Find	15
Limit Search to Range	No
Solver Controls	
Damped	No
Solver Type	Program Controlled
Rotordynamics Controls	
Coriolis Effect	Off
Campbell Diagram	Off
Output Controls	
Stress	Yes
Strain	Yes
Nodal Forces	No
Calculate Reactions	No
Store Modal Results	Program Controlled
General Miscellaneous	No
Analysis Data Management	
Future Analysis	MSUP Analyses
Scratch Solver Files Directory	
Save MAPDL db	Yes
Delete Unneeded Files	Yes
Solver Units	Active System
Solver Unit System	mks

Table 0-9, Modal Loads

Object Name	*Fixed Support*

State	Fully Defined
Scope	
Scoping Method	Geometry Selection
Geometry	2 Edges
Definition	
Type	Fixed Support
Suppressed	No

5.3.1. Solution

Table 0-10, Model Modal Solution

Object Name	*Solution (D6)*
State	Solved
Adaptive Mesh Refinement	
Max Refinement Loops	1.
Refinement Depth	2.
Information	
Status	Done

The following bar chart indicates the frequency at each calculated mode.
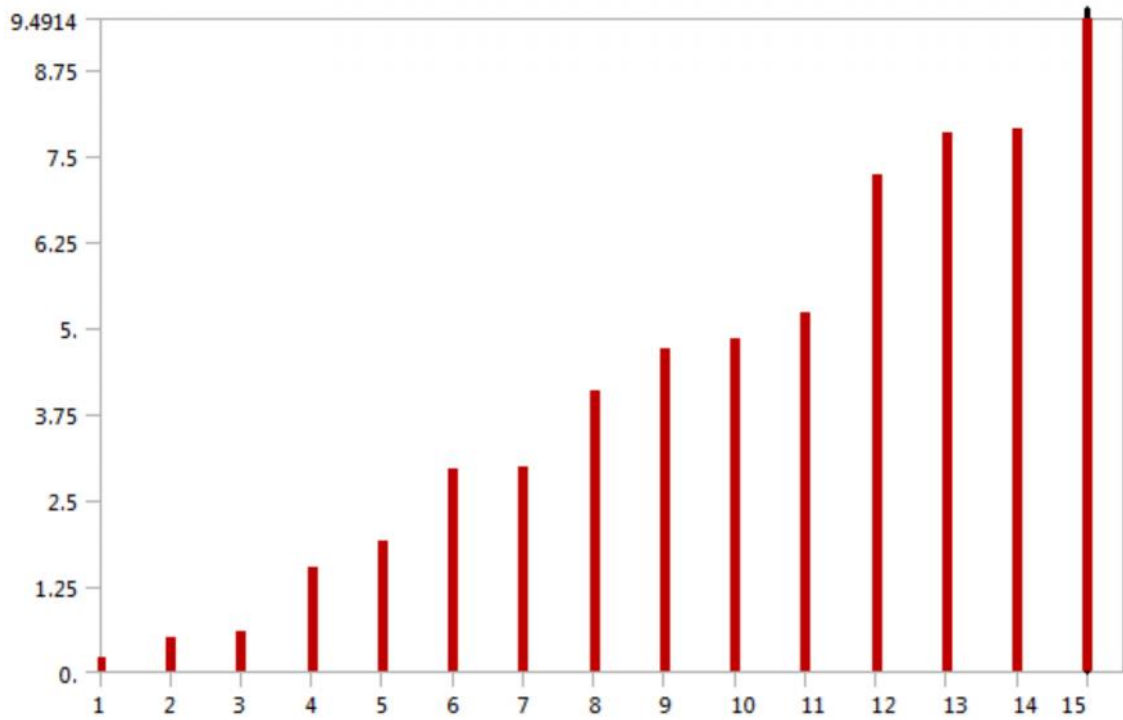
Figure 0-1, Model Modal Solution

Table 0-11, Model Modal Solution

Mode	Frequency [Hz]
1.	0.20287
2.	0.50618
3.	0.59179
4.	1.5128
5.	1.8882
6.	2.9393
7.	2.9805
8.	4.0676
9.	4.676
10.	4.8446

11.	5.2101
12.	7.2248
13.	7.8432
14.	7.8832
15.	9.4914

Table 0-12, Model Modal Solution, Solution Information

Object Name	*Solution Information*
State	Solved
Solution Information	
Solution Output	Solver Output
Newton-Raphson Residuals	0
Update Interval	2.5 s
Display Points	All
FE Connection Visibility	
Activate Visibility	Yes
Display	All FE Connectors
Draw Connections Attached To	All Nodes
Line Color	Connection Type
Visible on Results	No
Line Thickness	Single
Display Type	Lines

Table 0-13, Model Modal Solution Results

Object Name	Total Deformation	Total Deformation 2	Total Deformation 3	Total Deformation 4	Total Deformation 5
State	Solved				
Scope					
Scoping Method	Geometry Selection				
Geometry	All Bodies				
Definition					
Type	Total Deformation				
Mode	1.	2.	3.	4.	5.
Identifier					
Suppressed	No				
Results					
Minimum	0. m				
Maximum	8.7054e-003 m	2.2197e-002 m	2.3535e-002 m	3.0643e-002 m	4.3251e-002 m
Information					
Reported Frequency	0.20287 Hz	0.50618 Hz	0.59179 Hz	1.5128 Hz	1.8882 Hz

Table 0-14, Model Modal Solution Total Deformation

Mode	Frequency [Hz]
1.	0.20287
2.	0.50618
3.	0.59179
4.	1.5128
5.	1.8882
6.	2.9393
7.	2.9805
8.	4.0676

9.	4.676
10.	4.8446
11.	5.2101
12.	7.2248
13.	7.8432
14.	7.8832
15.	9.4914

Table 0-15, Model Modal Solution Total Deformation 2

Mode	Frequency [Hz]
1.	0.20287
2.	0.50618
3.	0.59179
4.	1.5128
5.	1.8882
6.	2.9393
7.	2.9805
8.	4.0676
9.	4.676
10.	4.8446
11.	5.2101
12.	7.2248
13.	7.8432
14.	7.8832
15.	9.4914

Table 0-16, Model Modal Solution Total Deformation 3

Mode	Frequency [Hz]
1.	0.20287
2.	0.50618
3.	0.59179
4.	1.5128
5.	1.8882
6.	2.9393
7.	2.9805
8.	4.0676
9.	4.676
10.	4.8446
11.	5.2101
12.	7.2248
13.	7.8432
14.	7.8832
15.	9.4914

Table 0-17, Model Modal Solution Total Deformation 4

Mode	Frequency [Hz]
1.	0.20287
2.	0.50618
3.	0.59179
4.	1.5128
5.	1.8882

6.	2.9393
7.	2.9805
8.	4.0676
9.	4.676
10.	4.8446
11.	5.2101
12.	7.2248
13.	7.8432
14.	7.8832
15.	9.4914

Table 0-18, Model Modal Solution Total Deformation 5

Mode	Frequency [Hz]
1.	0.20287
2.	0.50618
3.	0.59179
4.	1.5128
5.	1.8882
6.	2.9393
7.	2.9805
8.	4.0676
9.	4.676
10.	4.8446
11.	5.2101
12.	7.2248
13.	7.8432

14.	7.8832
15.	9.4914

5.4. Flexible Dynamic

Table 0-19, Model Analysis

Object Name	*Flexible Dynamic (F5)*
State	Not Solved
Definition	
Physics Type	Structural
Analysis Type	Transient
Solver Target	Mechanical APDL
Options	
Environment Temperature	22. °C
Generate Input Only	No

Table 0-20, Model Flexible Dynamic Initial Conditions

Object Name	*Initial Conditions*
State	Fully Defined

Table 0-21, Model Flexible Dynamic Initial Conditions Initial Condition

Object Name	Modal (None)
State	Fully Defined
Definition	
Pre-Stress Environment	None

Table 0-22, Model Flexible Dynamic Analysis Settings

Object Name	Analysis Settings
State	Fully Defined
Restart Analysis	
Restart Type	Program Controlled
Load Step	1000
Substep	1
Time	19.98 s
Step Controls	
Number Of Steps	1101.
Current Step Number	264.
Step End Time	5.26 s
Auto Time Stepping	On
Define By	Time
Carry Over Time Step	On
Minimum Time Step	2.e-002 s
Maximum Time Step	2.e-002 s
Time Integration	On
Solver Controls	

Solver Type	Program Controlled
Weak Springs	Program Controlled
Large Deflection	On
Restart Controls	
Generate Restart Points	Program Controlled
Retain Files After Full Solve	No
Nonlinear Controls	
Force Convergence	Program Controlled
Moment Convergence	Program Controlled
Displacement Convergence	Program Controlled
Rotation Convergence	Program Controlled
Line Search	Program Controlled
Stabilization	Off
Output Controls	
Stress	Yes
Strain	Yes
Nodal Forces	Yes
Contact Miscellaneous	No
General Miscellaneous	No
Calculate Results At	All Time Points
Max Number of Result Sets	1000.
Damping Controls	
Stiffness Coefficient Define By	Direct Input
Stiffness Coefficient	0.
Numerical Damping	Manual
Numerical Damping Value	0.1
Analysis Data Management	
Future Analysis	None

Scratch Solver Files Directory		
Save MAPDL db	No	
Delete Unneeded Files	Yes	
Nonlinear Solution	Yes	
Solver Units	Active System	
Solver Unit System	mks	

Table 0-23, Model Flexible Dynamic Loads

Object Name	*Fixed Support*	*Force*	*Force 2*	*Force 3*	*Force 4*
State	Fully Defined	Suppressed			
Scope					
Scoping Method	Geometry Selection				
Geometry	2 Edges	1 Edge			
Definition					
Type	Fixed Support	Force			
Suppressed	No	Yes			
Define By		Components			
Coordinate System		Global Coordinate System			
X Component		Tabular Data			
Y Component		Tabular Data			

96
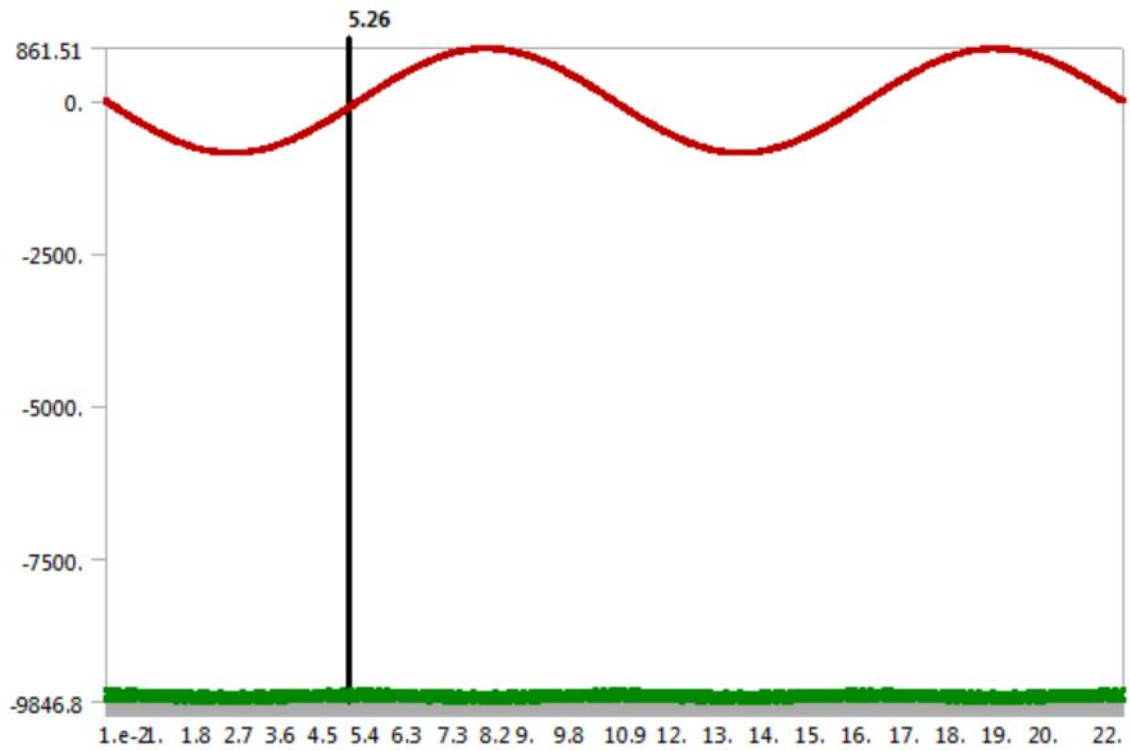
Figure 0-2, Model Flexible Dynamic Force

5.4.1. Solution

Table 0-24, Model Flexible Dynamic Solution

Object Name	Solution (F6)
State	Solve Failed
Adaptive Mesh Refinement	
Max Refinement Loops	1.
Refinement Depth	2.
Information	
Status	Solve Required, Restart Available

97

Table 0-25, Model Flexible Dynamic Solution Information

Object Name	*Solution Information*
State	Solve Failed
Solution Information	
Solution Output	Solver Output
Newton-Raphson Residuals	0
Update Interval	2.5 s
Display Points	All
FE Connection Visibility	
Activate Visibility	Yes
Display	All FE Connectors
Draw Connections Attached To	All Nodes
Line Color	Connection Type
Visible on Results	No
Line Thickness	Single
Display Type	Lines

Table 0-26, Model Flexible Dynamic Solution Results

Object Name	*Total Deformation*	*Y Axis - Directional Deformation*	*X Axis - Directional Deformation*	*Maximum Principal Stress*	*Maximum Principal Elastic Strain*
State	Solved				
Scope					
Scoping Method	Geometry Selection				
Geometry	All Bodies				
Definition					

Type	Total Deformation	Directional Deformation		Maximum Principal Stress	Maximum Principal Elastic Strain
By	Time				
Display Time	2.8 s	Last	7. s	Last	
Calculate Time History	Yes				
Identifier					
Suppressed	No				
Orientation		Y Axis	X Axis		
Coordinate System	Global Coordinate System				
Results					
Minimum	0. m	-1.6926 m	-8.3202e-005 m	0. Pa	3.4812e-008 m/m
Maximum	1.5712 m	7.5022 m	6.4049 m	1.1214e+009 Pa	5.7369e-003 m/m
Minimum Value Over Time					
Minimum	0. m	-10.025 m	-6.4672 m	0. Pa	9.5103e-011 m/m
Maximum	0. m	-3.406e-004 m	-1.5701e-006 m	0. Pa	2.0269e-007 m/m
Maximum Value Over Time					
Minimum	3.4414e-004 m	1.6762e-005 m	3.4632e-006 m	3.1493e+006 Pa	1.5221e-005 m/m
Maximum	12.34 m	11.01 m	6.883 m	2.3702e+009 Pa	1.2189e-002 m/m
Information					
Time	2.8 s	19.98 s	7. s	19.98 s	
Load Step	141	1000	351	1000	
Substep	1				
Iteration Number	283	2051	704	2051	
Integration Point Results					
Display Option				Averaged	
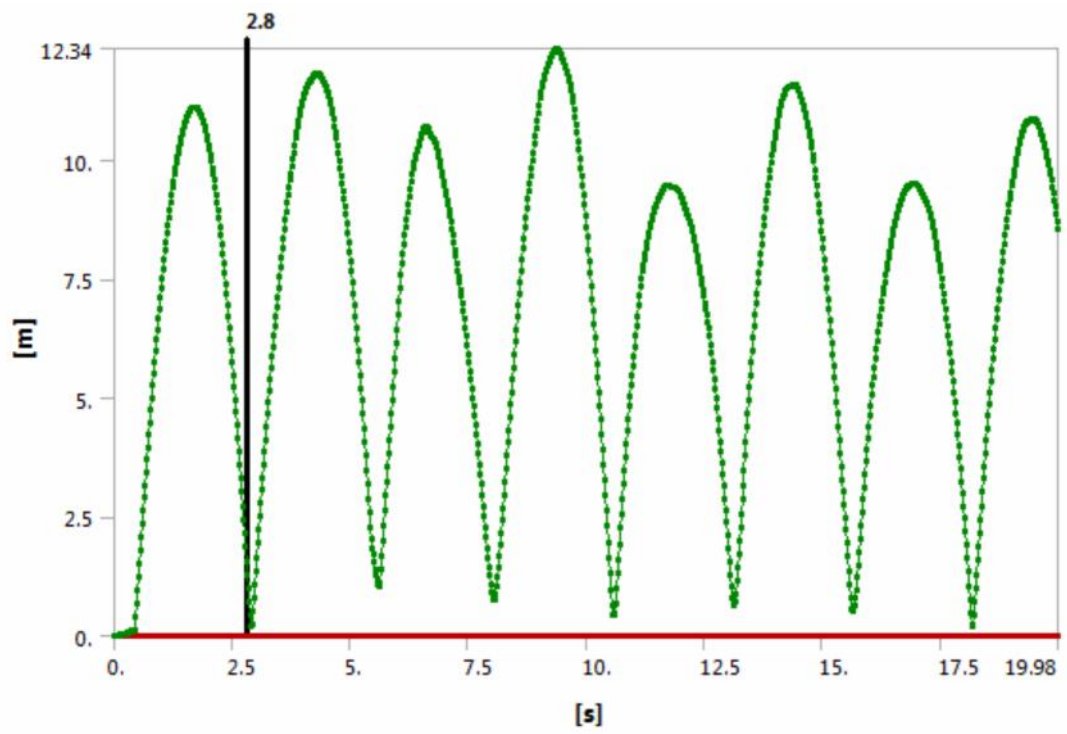
Figure 0-3, Model Total Deformation
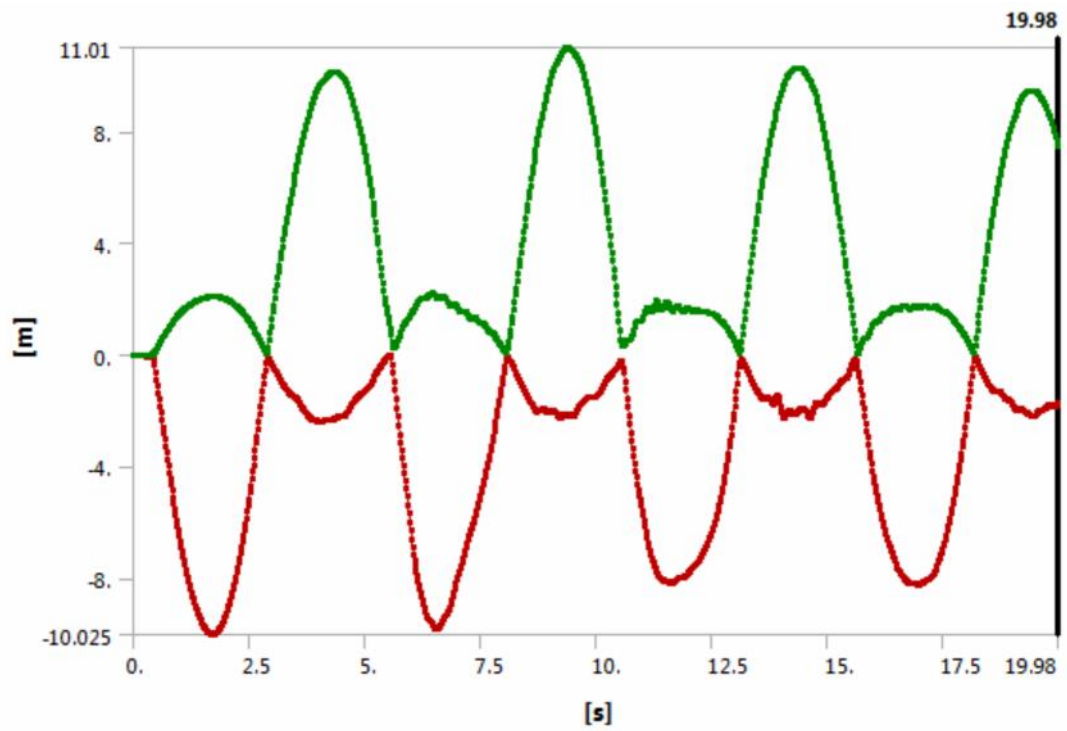
Figure 0-4, Model Y-Axis Directional Deformation
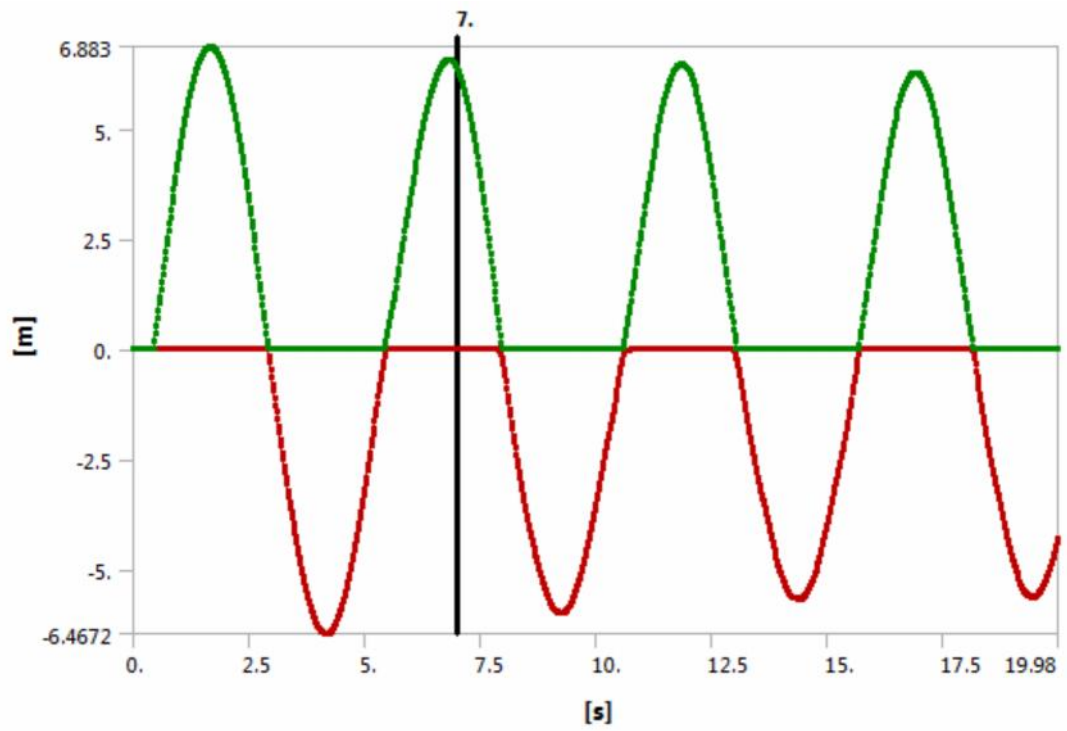
Figure 0-5, Model X-Axis Directional Deformation
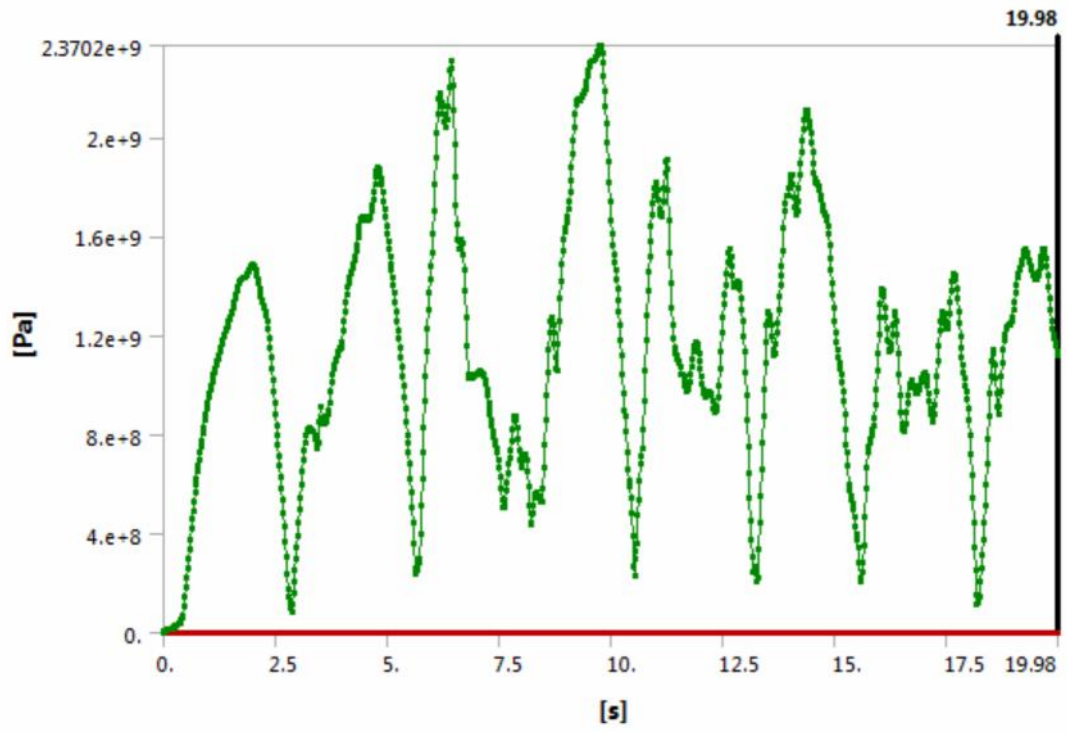
Figure 0-6, Model Maximum Principal Stress
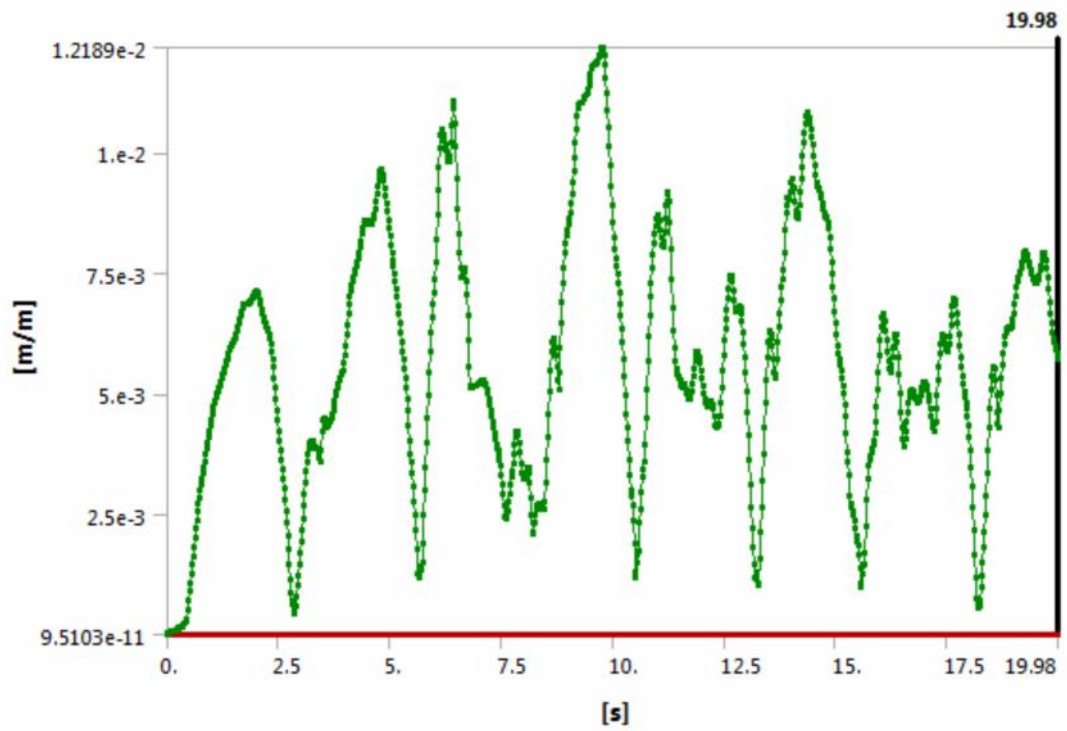
Figure 0-7, Model Maximum Principal Elastic Strain

Table 0-27, Model Flexible Dynamic Solution Probes

Object Name	Deformation Probe	Stress Probe	Force Reaction
State	Solved		
Definition			
Type	Deformation	Stress	Force Reaction
Location Method	Geometry Selection		Boundary Condition
Geometry	1 Face		
Suppressed	No		
Boundary Condition			Fixed Support
Orientation			Global Coordinate System
Options			
Result Selection	Total	Maximum Principal	All
Display Time	End Time		
Spatial Resolution	Use Maximum		
Results			
Total	8.528 m		2.1791e+005 N
Maximum Principal		1.1214e+009 Pa	
X Axis			1.7492e+005 N
Y Axis			-1.2995e+005 N
Maximum Value Over Time			
Total	12.34 m		5.7495e+005 N
Maximum Principal		2.3702e+009 Pa	
X Axis			4.4928e+005 N
Y Axis			5.7032e+005 N
Minimum Value Over Time			
Total	3.4414e-004 m		394.94 N
Maximum Principal		3.1493e+006 Pa	
X Axis			-5.5664e+005 N
Y Axis			-3.6531e+005 N

Information	
Time	19.98 s
Load Step	1000
Substep	1
Iteration Number	2051
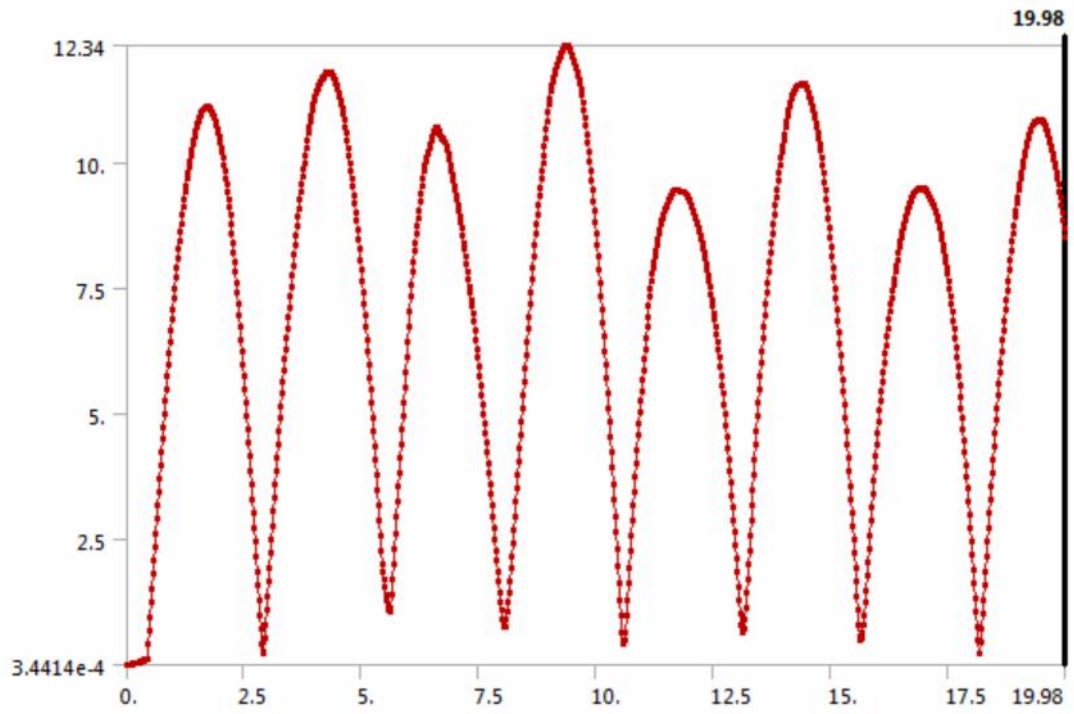
Figure 0-8, Model Deformation Probe
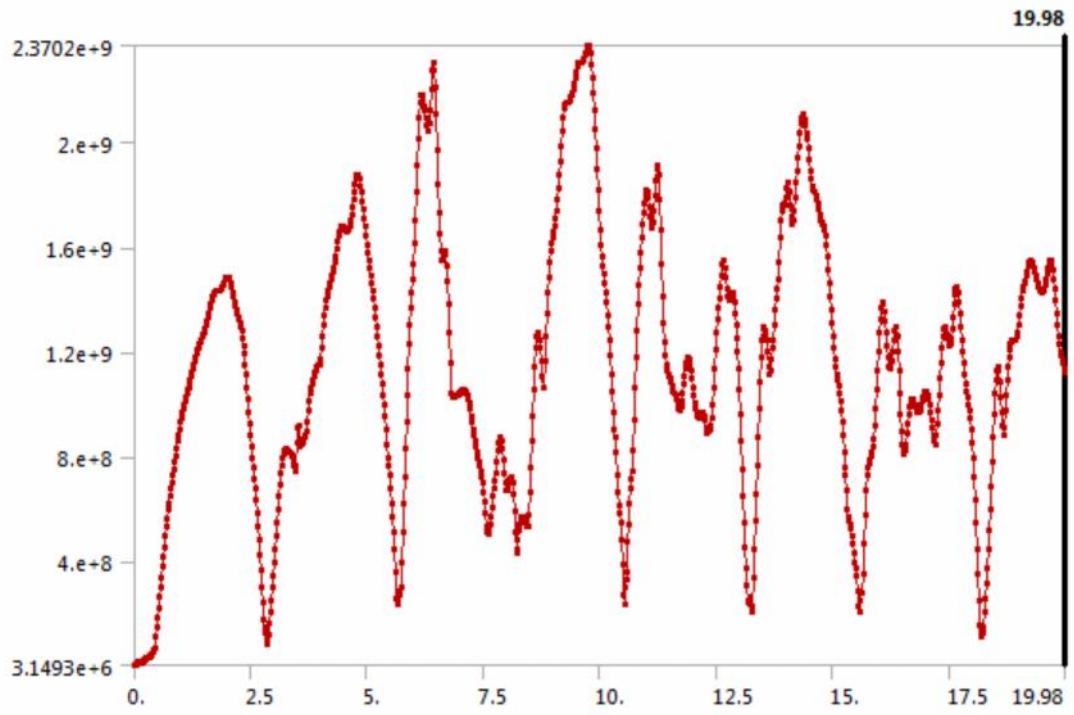
Figure 0-9, Model Stress Probe
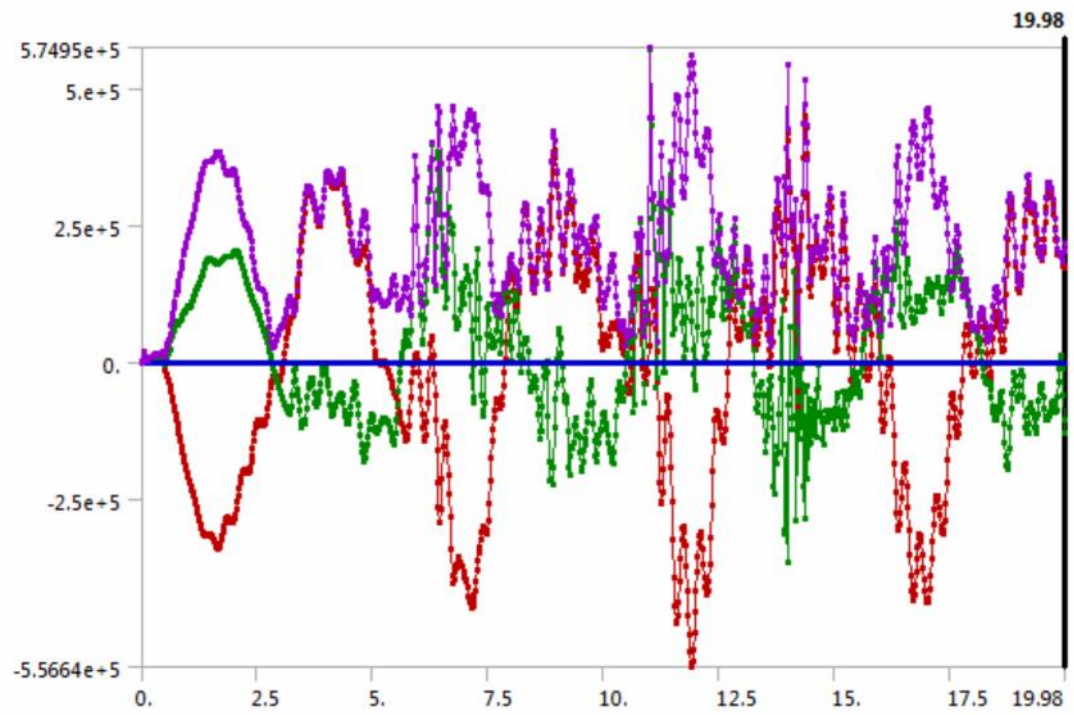
Figure 0-10, Model Force Reaction

5.5. Material Data

5.5.1. Structural Steel

Table 0-28, Structural Steel Constants

Density	7850 kg m^-3
Isotropic Secant Coefficient of Thermal Expansion	1.2e-005 C^-1
Specific Heat	434 J kg^-1 C^-1
Isotropic Thermal Conductivity	60.5 W m^-1 C^-1
Isotropic Resistivity	1.7e-007 ohm m

Table 0-29, Structural Steel Compressive Ultimate Strength

Compressive Ultimate Strength Pa
0

Table 0-30, Structural Steel Compressive Yield Strength

Compressive Yield Strength Pa

2.5e+008

Table 0-31, Structural Steel Tensile Yield Strength

Tensile Yield Strength Pa
2.5e+008

Table 0-32, Structural Steel Tensile Ultimate Strength

Tensile Ultimate Strength Pa
4.6e+008

Table 0-33, Structural Steel Isotropic Secant Coefficient of Thermal Expansion

Reference Temperature C
22

Table 0-34, Structural Steel Alternating Stress Mean Stress

Alternating Stress Pa	Cycles	Mean Stress Pa
3.999e+009	10	0
2.827e+009	20	0
1.896e+009	50	0
1.413e+009	100	0

1.069e+009	200	0
4.41e+008	2000	0
2.62e+008	10000	0
2.14e+008	20000	0
1.38e+008	1.e+005	0
1.14e+008	2.e+005	0
8.62e+007	1.e+006	0

Table 0-35, Structural Steel Strain-Life Parameters

Strength Coefficient Pa	Strength Exponent	Ductility Coefficient	Ductility Exponent	Cyclic Strength Coefficient Pa	Cyclic Strain Hardening Exponent
9.2e+008	-0.106	0.213	-0.47	1.e+009	0.2

Table 0-36, Structural Steel Isotropic Elasticity

Temperature C	Young's Modulus Pa	Poisson's Ratio	Bulk Modulus Pa	Shear Modulus Pa
	2.e+011	0.3	1.6667e+011	7.6923e+010

Appendix C

Configurations of the Tower crane LIEBHERR 132HC

LIEBHERR 132 HC
TOWER CRANE

164 ft (50.0m)

NOTE! See hook height charts inside.

Configuration I
with 132 HC/290 HC Tower
max. 218 ft (66.6m) HUH on concrete foundation
max. 234 ft (71.2m) HUH on undercarriage

Configuration II
with 132 HC/200 HC/290 HC Tower
max. 201 ft (61.3m) HUH on concrete foundation
max. 216 ft (66.0m) HUH on undercarriage

Configuration III
with 132 HC/200 HC Tower
max. 177 ft (53.9m) HUH on concrete foundation
max. 192 ft (58.6m) HUH on undercarriage

Configuration IV
with 132 HC Tower
max. 148 ft (45.1m) HUH on concrete foundation

FREESTANDING
(traveling and stationary)

Morrow Equipment

Configurations   LIEBHERR 132 HC

18'-8" 5.7m
46'-3" 14.1m
13'-5" 4.1m
3'-10" 1.16m
14 x 8' 2" (2.5m) = 114'-7" (35.0m)
Standard 132 HC tower sections
Base tower section
22'-6" 6.85m
8 3/4" 220mm

168'-4" (51.3m) Jib Tip Radius
7'-3" 2.2m
164 ft (50.0m) 4,850 lbs 2 200 kg
148 ft (45.0m) 5,840 lbs 2 650 kg
131 ft (40.0m) 7,055 lbs 3 200 kg
115 ft (35.0m) 8,820 lbs 4 000 kg
98 ft (30.0m) 11,025 lbs 5 000 kg
82 ft (25.0m) 14,110 lbs 6 400 kg

NOTE! See hook height charts below.
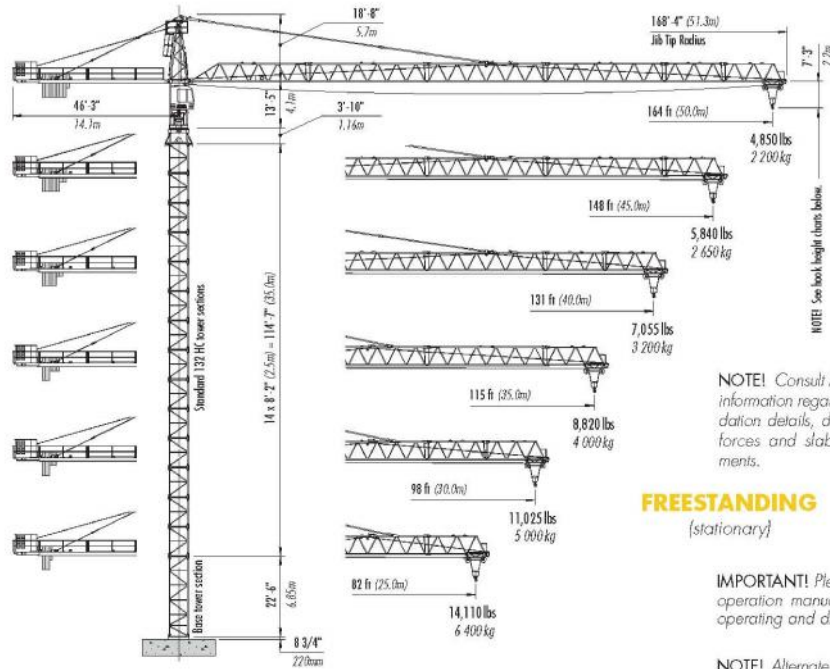
NOTE! *Consult Morrow for specific information regarding alternate foundation details, dimensions, reaction forces and slab opening requirements.*

FREESTANDING
(stationary)

IMPORTANT! *Please consult crane's operation manual before erecting, operating and dismantling crane.*

NOTE! *Alternate tower combinations possible. Contact Morrow for additional information.*

HOOK HEIGHTS

No. of Tower Sections	Tower Configuration I	Hook Height Concrete Foundation ft	m	Hook Height 6m Undercarriage ft	m
0	290HC BTS-40	51.8	15.8	67.0	20.4
1	290HC STS	65.4	19.9	80.6	24.6
2	290HC STS	78.9	24.1	94.2	28.7
3	290HC STS	92.5	28.2	107.8	32.9
4	290HC STS	106.1	32.3	121.4	37.0
5	290HC STS	119.7	36.5	134.9	41.1
6	290HC STS	133.3	40.6	148.5	45.3
7	Transition	146.9	44.8	162.1	49.4
8	132HC BTS-22	169.3	51.6	184.6	56.3
9	132HC STS	177.5	54.1	192.8	58.8
10	132HC STS	185.7	56.6	201.0	61.3
11	132HC STS	193.9	59.1	209.1	63.7
12	132HC STS	202.1	61.6	217.3	66.4
13	132HC STS	210.3	64.1	225.5	68.7
14 [1]	132HC STS	218.4	66.6	233.7	71.2

No. of Tower Sections	Tower Configuration II	Hook Height Concrete Foundation ft	m	Hook Height 6m Undercarriage ft	m
0	290HC BTS-40	51.8	15.8	67.0	20.4
1	200HC STS	65.4	19.9	80.6	24.6
2	200HC STS	78.9	24.1	94.2	28.7
3	200HC STS	92.5	28.2	107.8	32.9
4	200HC STS	106.1	32.3	121.4	37.0
5	200HC STS	119.7	36.5	134.9	41.1
6	200HC STS	133.3	40.6	148.5	45.3
7	200HC STS	146.9	44.8	162.1	49.4
8	200HC STS	160.4	48.9	175.7	53.6
9	200HC STS	174.0	53.0	189.3	57.7
10	200HC STS	187.6	57.2	202.9	61.8
11	Transition	201.2	61.3	216.4	66.0

No. of Tower Sections	Tower Configuration III	Hook Height Concrete Foundation ft	m	Hook Height 6m Undercarriage ft	m
0	200HC BTS-29	40.1	12.2	55.3	16.9
1	200HC STS	53.6	16.4	68.9	21.0
2	200HC STS	67.2	20.5	82.5	25.1
3	Transition	80.8	24.6	96.1	29.3
4	132HC BTS-22	103.3	31.5	118.5	36.1
5	132HC STS	111.5	34.0	126.7	38.6
6	132HC STS	119.7	36.5	134.9	41.1
7	132HC STS	127.8	39.0	143.1	43.6
8	132HC STS	136.0	41.5	151.3	46.1
9	132HC STS	144.2	44.0	159.5	48.6
10	132HC STS	152.4	46.5	167.7	51.1
11	132HC STS	160.6	49.0	175.8	53.6
12	132HC STS	168.8	51.4	184.0	56.1
13 [1]	132HC STS	177.0	53.9	192.2	58.6

No. of Tower Sections	Tower Configuration IV	Hook Height Concrete Foundation ft	m
0	132HC BTS-22	33.2	10.1
1	132HC STS	41.4	12.6
2	132HC STS	49.6	15.1
3	132HC STS	57.8	17.6
4	132HC STS	66.0	20.1
5	132HC STS	74.2	22.6
6	132HC STS	82.4	25.1
7	132HC STS	90.5	27.6
8	132HC STS	98.7	30.1
9	132HC STS	106.9	32.6
10	132HC STS	115.1	35.1
11	132HC STS	123.3	37.6
12	132HC STS	131.5	40.1
13	132HC STS	139.7	42.6
14 [2]	132HC STS	147.8	45.1

[1] Remove top climbing unit from crane prior to operating crane at maximum hook height.
[2] Lower top climbing unit to base of crane prior to operating crane at maximum hook height.

Morrow Equipment Co., L.L.C.

110

46'-3"
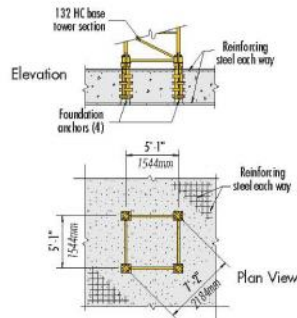14.1m

168'-4"
51.3m

7'-3" (2.2m)
Min. hook position

3'-11"
1.2m

8'-2"
2.5m

6'-0"
1.83m

9 x 8'-2" (2.5m) = 73'-8" (22.5m)

100'-3"
30.56m

16'-5"
5.0m

30'-4" min.
9.25m min.

Hydraulic bottom
climbing unit

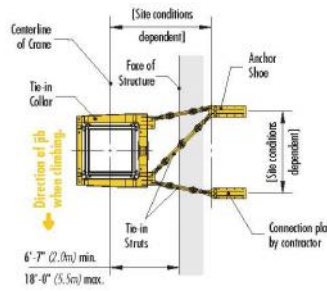**BOTTOM CLIMBING**
with 132 HC Tower Sections
(inside structure)
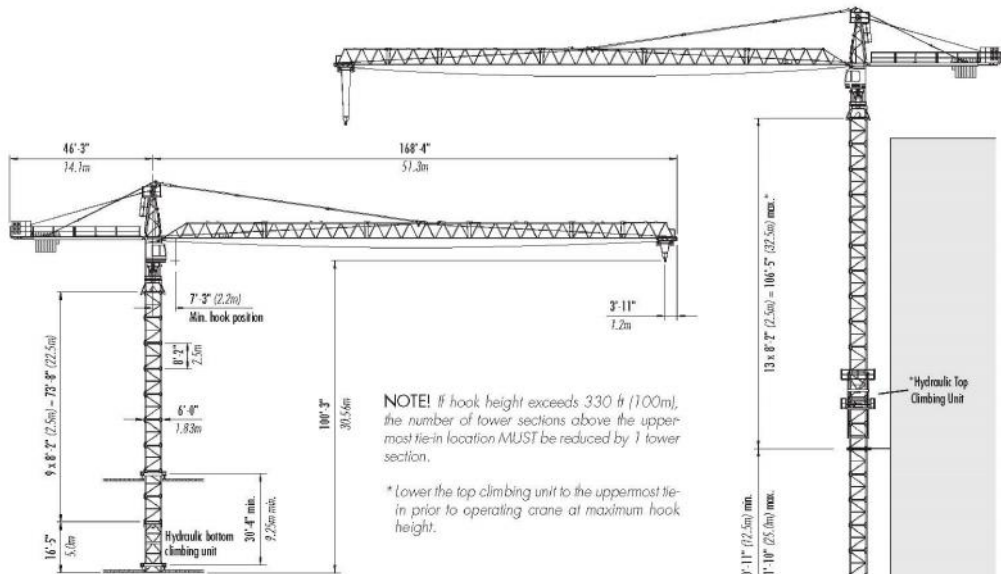
NOTE! *If hook height exceeds 330 ft (100m), the number of tower sections above the uppermost tie-in location MUST be reduced by 1 tower section.*

* *Lower the top climbing unit to the uppermost tie-in prior to operating crane at maximum hook height.*

132 HC base
tower section

Reinforcing
steel each way

Elevation

Foundation
anchors (4)

5'-1"
1544mm

Reinforcing
steel each way

5'-1"
1544mm

7'-2"
2184mm

Plan View

FOUNDATION DETAILS
with 132 HC Base Tower
(concrete slab)

[Site conditions dependent]

Centerline
of Crane

Face of
Structure

Tie-in
Collar

Anchor
Shoe

Direction of jib
when climbing.

[Site conditions dependent]

Tie-in
Struts

Connection plate
by contractor

6'-7" (2.0m) min.
18'-0" (5.5m) max.

TIE-IN ASSEMBLY
(Plan View)

NOTE! *The tie-in assembly shown is an example of a typical installation. Please note, however, that factors determining the installation of tie-in assemblies may vary due to project specific criteria. Contact Morrow for information regarding dimensions, reaction forces, tie-in locations and slab opening requirements.*

13 x 8'-2" (2.5m) = 106'-5" (32.5m) max. *

"Hydraulic Top
Climbing Unit

5 x 8'-2" (2.5m) = 40'-11" (12.5m) min.

10 x 8'-2" (2.5m) = 81'-10" (25.0m) max.

Tie-In
Assembly

1 x 22'-6" (6.85m) + 4 x 8'-2" (2.5m) = 55'-3" (16.85m) min.
1 x 22'-6" (6.85m) + 11 x 8'-2" (2.5m) = 112'-7" (34.35m) max.
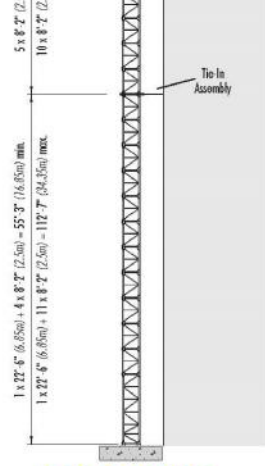
TOP CLIMBING
with 132 HC Tower Sections
(tied to structure)

Morrow Equipment Co., L.L.C.

Radius and Capacities

LIEBHERR Tower Crane Model 132 HC

2-Part Line

Hook Radius	2-Part Line Max Capacity – Radius	ft m	40 12.2	50 15.2	60 18.3	70 21.3	80 24.4	82 25.0	90 27.5	98 30.0	105 32.0	110 33.5	115 35.0	123 37.5	131 40.0	139 42.5	148 45.0	156 47.5	164 50.0
164 ft 50.0m	17,635 lbs – 54.5 ft 8 000 kg – 16.6m	lbs kg	17,635 8 000	17,635 8 000	16,180 7 340	13,710 6 220	11,815 5 360	11,175 5 070	10,010 4 540	9,060 4 110	8,355 3 790	7,825 3 550	7,560 3 430	6,945 3 150	6,415 2 910	5,950 2 700	5,555 2 520	5,180 2 350	4,850 2 200
148 ft 45.0m	17,635 lbs – 56.8 ft 8 000 kg – 17.3m	lbs kg	17,635 8 000	17,635 8 000	16,910 7 670	14,350 6 510	12,370 5 610	11,705 5 310	10,495 4 760	9,500 4 310	8,765 3 975	8,200 3 720	7,935 3 600	7,300 3 310	6,745 3 060	6,285 2 850	5,840 2 650		
131 ft 40.0m	17,635 lbs – 58.7 ft 8 000 kg – 17.9m	lbs kg	17,635 8 000	17,635 8 000	17,550 7 960	14,945 6 780	12,875 5 840	12,190 5 530	10,935 4 960	9,900 4 490	9,125 4 140	8,555 3 880	8,270 3 750	7,630 3 460	7,055 3 200				
115 ft 35.0m	17,635 lbs – 62.0 ft 8 000 kg – 18.9m	lbs kg	17,635 8 000	17,635 8 000	17,635 8 000	15,875 7 200	13,690 6 210	12,960 5 880	11,640 5 280	10,535 4 780	9,735 4 415	9,125 4 140	8,820 4 000						
98 ft 30.0m	17,635 lbs – 64.6 ft 8 000 kg – 19.7m	lbs kg	17,635 8 000	17,635 8 000	17,635 8 000	16,580 7 520	14,285 6 480	13,535 6 140	12,170 5 520	11,025 5 000									
82 ft 25.0m	17,635 lbs – 66.9 ft 8 000 kg – 20.4m	lbs kg	17,635 8 000	17,635 8 000	17,635 8 000	16,930 7 680	14,815 6 720	14,110 6 400											

Morrow Equipment Co., L.L.C.

SPECIFICATIONS

LIEBHERR Tower Crane Model 132 HC

Hoist Speed and Capacity

Hoist Unit	WiW271RX108	2-Part Line				
		Gear	Capacity	Line Speed	Capacity	Line Speed
82 hp (61 kW) AC hoist unit		1	up to 17,635 lbs @ 52 fpm		up to 8 000 kg @ 16 m/min	
3-speed gearbox Electromagnetic gear shifting Eddy current brake		2	up to 9,590 lbs @ 187 fpm		up to 4 350 kg @ 57 m/min	
	LS-164	3	up to 3,745 lbs @ 361 fpm		up to 1 700 kg @ 110 m/min	

NOTE! *Capacities and line speeds indicated will vary depending on the amount of hoist rope installed. This crane model may be equipped with a hoist unit other than that specified in the data above. To verify, check the serial number of the crane and refer to the Liebherr 132 HC Operation Manual for additional information.*

Motor Information

Drive Unit	Horsepower	Kilowatts	Speed	
Trolley (2-part line)	5.4 hp	4.0 kW	39 - 128 - 240 fpm	12 - 39 - 73 m/min
Swing (fluid coupling) *	2 x 6.7 hp	2 x 5.0 kW	0.9 rpm	
Travelling (fluid coupling)	2 x 4 hp	2 x 3.0 kW	82 fpm	25.0 m/min

*NOTE! *Jibs up to and including 131-ft (40.0m) hook reach require only one swing motor; jibs with 148-ft (45.0m) hook reach and longer require two swing motors.*

Power Requirements
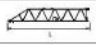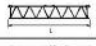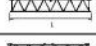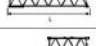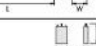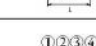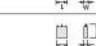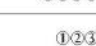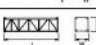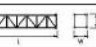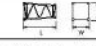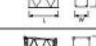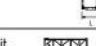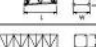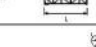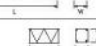
480 V — 3-phase — 60 Hz — 150 Amperes

Specifications subject to change without prior notice. For additional information, contact Morrow Equipment.

Morrow Equipment Co., L.L.C.

Component List   **LIEBHERR**

Description	Dimensions L x W x H	Weight	Description	Dimensions L x W x H	Weight
Tower Top	18'-9" x 4'-9" x 5'-1" / 5.72m x 1.46m x 1.56m	3,030 lbs / 1 375 kg	Jib Section ① #611	33'-7" x 5'-2" x 6'-0" / 10.24m x 1.58m x 1.83m	3,925 lbs / 1 780 kg
Slewing Assembly (Complete) [1]	19'-1" x 8'-8" x 7'-7" / 5.82m x 2.65m x 2.3m	14,500 lbs / 6 575 kg	Jib Section ② #621	33'-10" x 4'-0" x 5'-7" / 10.3m x 1.23m x 1.7m	2,600 lbs / 1 180 kg
Slewing Assembly Upper Part [2]	14'-1" x 8'-8" x 7'-7" / 4.3m x 2.65m x 2.3m	9,450 lbs / 4 285 kg	Jib Section ③ #622	33'-10" x 4'-0" x 5'-7" / 10.3m x 1.23m x 1.7m	3,040 lbs / 1 380 kg
Slewing Assembly Lower Part [3]	5'-0" x 7'-5" x 7'-1" / 1.52m x 2.26m x 2.17m	5,050 lbs / 2 290 kg	Jib Section ④ #631	33'-10" x 4'-0" x 5'-7" / 10.3m x 1.23m x 1.7m	2,095 lbs / 950 kg
Hoist Unit with Frame [4] 82 hp (61 kW)	7'-6" x 13'-6" x 5'-6" / 2.29m x 4.1m x 1.68m	10,580 lbs / 4 800 kg	Jib Section ⑤ #632	17'-5" x 4'-0" x 5'-7" / 5.3m x 1.23m x 1.7m	1,070 lbs / 485 kg
Counterjib [5]	36'-1" x 7'-10" x 4'-5" / 11.0m x 2.4m x 1.34m	5,510 lbs / 2 500 kg	Jib Section ⑥ #641	17'-10" x 4'-7" x 5'-9" / 5.44m x 1.43m x 1.76m	1,115 lbs / 505 kg
Counterweight Block A	3'-11" x 11" x 6'-9" / 1.19m x 0.28m x 2.05m	3,640 lbs / 1 650 kg	Jib Assembly [6] 164-ft (50.0m) ①②③④⑤⑥	165'-4" x 5'-2" x 6'-0" / 50.4m x 1.58m x 1.83m	15,695 lbs / 7 120 kg
Counterweight Block B	3'-11" x 11" x 4'-1" / 1.19m 0.28m x 1.25m	2,205 lbs / 1 000 kg	Jib Assembly [6] 148-ft (45.0m) ①②③④⑥	148'-11" x 5'-2" x 6'-0" / 45.4m x 1.58m x 1.83m	14,640 lbs / 6 640 kg
Base Tower Section 132 HC	22'-6" x 6'-0" x 6'-0" / 6.85m x 1.83m x 1.83m	5,355 lbs / 2 430 kg	Jib Assembly [6] 131-ft (40.0m) ①②③⑤⑥	132'-7" x 5'-2" x 6'-0" / 40.4m x 1.58m x 1.83m	13,670 lbs / 6 200 kg
Long Tower Section 132 HC	32'-10" x 6'-0" x 6'-0" / 10.0m x 1.83m x 1.83m	7,055 lbs / 3 200 kg	Jib Assembly [6] 115-ft (35.0m) ①③④⑥	116'-2" x 5'-2" x 6'-0" / 35.4m x 1.58m x 1.83m	11,685 lbs / 5 300 kg
Standard Tower Section 132 HC	8'-2" x 6'-0" x 6'-0" / 2.5m x 1.83m x 1.83m	2,160 lbs / 980 kg	Jib Assembly [6] 98-ft (30.0m) ①③⑤⑥	99'-9" x 5'-2" x 6'-0" / 30.4m x 1.58m x 1.83m	10,580 lbs / 4 800 kg
Transition Section 200 HC/132 HC	13'-7" x 7'-7" x 7'-7" / 4.14m x 2.3m x 2.3m	5,290 lbs / 2 400 kg	Jib Assembly [6] 82-ft (25.0m) ①③⑥	83'-4" x 5'-2" x 6'-0" / 25.4m x 1.58m x 1.83m	9,500 lbs / 4 310 kg
Base Tower Section 200 HC	29'-0" x 7'-7" x 7'-7" / 8.85m x 2.3m x 2.3m	8,960 lbs / 4 065 kg	Top Climbing Unit w/hydraulics	21'-2" x 6'-11" x 7'-11" / 6.45m x 2.1m x 2.42m	9,900 lbs / 4 490 kg
Standard Tower Section 200 HC	13'-7" x 7'-7" x 7'-7" / 4.14m x 2.3m x 2.3m	4,520 lbs / 2 050 kg	Climbing Collar 132 HC	8'-2" x 7'-8" x 1'-5" / 2.5m x 2.33m x 0.43m	1,765 lbs / 800 kg
Transition Section 290 HC/132 HC	13'-7" x 7'-7" x 7'-7" / 4.14m x 2.3m x 2.3m	5,290 lbs / 2 400 kg	Bottom Climbing Unit w/hydraulics	16'-5" x 6'-0" x 6'-0" / 5.0m x 1.83m x 1.83m	9,390 lbs / 4 260 kg
Base Tower Section 290 HC	40'-9" x 7'-7" x 7'-7" / 12.42m x 2.3m x 2.3m	17,505 lbs / 7 940 kg	Hook Block	1'-7" x 1'-6" x 2'-11" / 0.49m x 0.45m x 0.9m	705 lbs / 320 kg
Standard Tower Section 290 HC	13'-7" x 7'-7" x 7'-7" / 4.14m x 2.3m x 2.3m	5,025 lbs / 2 280 kg	Trolley	5'-11" x 4'-9" x 3'-1" / 1.8m x 1.44m x 0.94m	640 lbs / 290 kg

114